MODELING, SIMULATION, AND STABILITY OF A HYDRAULIC LOAD-SENSING PUMP SYSTEM WITH INVESTIGATION OF A HARD NONLINEARITY IN THE PUMP DISPLACEMENT CONTROL SYSTEM

A Thesis

presented to

the Faculty of the Graduate School

at the University of Missouri-Columbia

In Partial Fulfillment

of the Requirements for the Degree

Master of Science

---

by

ZACHARY DANIEL WAGNER

Dr. Roger Fales, Thesis Supervisor

JULY 2014

The undersigned, appointed by the dean of the graduate school, have examined the thesis entitled

MODELING, SIMULATION, AND STABILITY OF A HYDRAULIC LOAD-SENSING PUMP SYSTEM WITH INVESTIGATION OF A HARD NONLINEARITY IN THE PUMP DISPLACEMENT CONTROL SYSTEM

presented by Zachary Daniel Wagner,

a candidate for the degree of Master of Science,

and hereby certify that, in their opinion, it is worthy of acceptance.

_____

Professor Roger Fales

_____

Professor Noah Manring

_____

Professor Glenn Washer

ACKNOWLEDGEMENTS

I would first like to thank Dr. Roger Fales for his technical guidance and expertise that constructively lead me through every struggle and difficulty I faced in my research. His knowledge and positive attitude always gave me confidence in the path I needed to take and his patience and understanding are characteristics that I will never forget and will apply to my own career wherever it may take me. Thank you, Dr. Fales, for giving me this opportunity to study under you and advance not only in my overall knowledge of engineering, but also in the field of engineering research.

I thank both Dr. Noah Manring and Dr. Glenn Washer for taking the time to serve as members on my thesis committee and for providing constructive criticism that only the most experienced professionals and engineers could offer.

I also want to thank my wonderful fiancé, Jenna, for her unending support and love. Her encouragement and optimism helped me through many tough roadblocks and pushed me to continue and persevere to the end and achieve this goal.

I want to thank my family for all of their consistent support when I seemed to be struggling. Specifically, I thank my father and mother, John and Rosalie Wagner, for teaching me how to be strong and endure through all hardships and for their love and prayers that never stopped no matter what new obstacle I came across. Without them I would not be the man I am today and I would have never had the opportunity to pursue a graduate degree in engineering. Thank you mom and dad, your love and support mean everything to me. I also want to thank my older brother, John, for your understanding and positive attitude and for

always believing in me and somehow always knowing that everything would work out. You were and always will be a great role model to me and an example of a higher level achievement that I can continuously strive towards. I lastly want to thank my best friend, Tyler, for always being there and knowing how to cheer me up. Knowing that I will always be able to count on your friendship, support and help means much more than you could ever know.

Finally, I thank my Lord and Savior Jesus Christ, for without Him I would have nothing and would not have been able to achieve everything that He has allowed me to work towards. Through every trial I have faced in my life, You have never failed me and I know You never will.

TABLE OF CONTENTS

LIST OF FIGURES

LIST OF TABLES

NOMENCLATURE

Abbreviations

FCV	=	Flow Control Valve
LS	=	Load-Sensing
NL	=	Nonlinear
ODE	=	Ordinary Differential Equation
PDFCV	=	Pump Displacement Flow Control Valve
SISO	=	Single Input – Single Output
SS	=	Steady-State
SSR	=	State-Space Representation
TF	=	Transfer Function

Variables

A_A	=	Cross-Sectional Area of PDFCV
A_O	=	Area of the Orifice before Load
A_p	=	Cross-sectional area of a single piston
A_1	=	Cross-sectional Area of Control Actuator
A_2	=	Cross-sectional Area of Bias Actuator
b_m	=	Motor Load Damping Gain

C_c	=	Contraction Coefficient
C_d	=	Discharge Coefficient for sharp – edged orifice
C_i , C_p	=	Swivel Torque Coefficients
d	=	Diameter of PDFCV
J_m	=	Moment of Inertia for Motor Load
k_{spool}	=	Spring Rate for PDFCV
k_1	=	Bias Actuator Spring Rate
K_{AG}	=	Damping Gain for Actuators
K_{SV}	=	Damping Gain for Spool Valve (PDFCV)
K_{SVA}	=	Leakage Area Gain for Spool Valve
L	=	Actuator Moment Arm
M_p	=	Mass of a single piston-slipper assembly
m_{spool}	=	Mass of PDFCV
m_1	=	Mass of Bias Actuator Piston
m_2	=	Mass of Control Actuator Piston
N	=	Total number of pistons within Pump
r	=	Piston pitch radius
V_c	=	Approximate Control Actuator Volume

V_d	=	Volumetric Displacement of Pump
V_L	=	Approximate Load Pressure Volume
V_m	=	Volumetric Displacement of Motor Load
V_{pd}	=	Approximate Pump Discharge Volume
x_p	=	PDFCV Pre-Load Compression Distance
y_{max}	=	Maximum Linear Disp. of Control (and Bias) Actuator
y_p	=	Bias Actuator Pre-Load Distance
α	=	Pump Swash plate Angle
α_{max}	=	Maximum Pump Swash Plate Angle
β	=	Fluid Bulk Modulus
γ	=	Pressure carryover angle
ρ	=	Fluid Density
θ	=	Jet Angle for Flow Forces
ω_p	=	Angular Velocity of Pump shaft

MODELING, SIMULATION, AND STABILITY OF A HYDRAULIC LOAD-SENSING PUMP SYSTEM WITH INVESTIGATION OF A HARD NONLINEARITY IN THE PUMP DISPLACEMENT CONTROL SYSTEM

Zachary Daniel Wagner

Dr. Roger Fales, Thesis Supervisor

ABSTRACT

Certain types of Load-Sensing (LS) pumps utilize a hydro-mechanical control system designed to regulate the pressure difference, or margin pressure, between the inlet and outlet of a flow control valve. With a constant margin pressure, predictable flow control and improved efficiency can be achieved by controlling the orifice area of the flow control valve. Instability due to limit cycles (sustained oscillations) that stem from nonlinearities within the system is a common issue related to hydraulic LS systems. In this work, the stability of the pressure control system was investigated using describing function analysis. Describing function analysis is a method used to approximate a nonlinearity within a nonlinear system and was conducted to predict the existence and stability of limit cycles that occur due to saturation nonlinearities within the mechanical components of the LS system. A combination of linear and nonlinear analysis and modeling was employed to assess the stability of a particular LS pump system.

Among many nonlinearities present in the hydro-mechanical LS system, of particular interest was the saturation inherent in the actuator that is used to displace the pump swash plate and the saturation within the 3-way spool valve that permits flow to

reach the actuator. This saturation nonlinearity was believed to be a problematic source for limit cycles that tend to appear in LS systems. A comprehensive nonlinear model was developed as the foundation for this research as it was used for validation in direct comparison to experimentally acquired data. The nonlinear model proved to be precise and accurate in matching to the experimental test bed response based on the data that was gathered. The acquired data was compared to the NL model simulation through a root mean squared error evaluation and frequency response analysis. The nonlinear model was then used to generate a linearized model necessary for stability analysis. The saturation nonlinearities for two separate mechanical systems were isolated from the rest of the linearized system dynamics to provide a system structure necessary for conducting describing function analysis. Analysis of model characteristics and dynamics was used to make conclusions about the stability of the system.

The results of the describing function analysis demonstrated an accurate diagnosis of the stability of the system through three separate scenarios. Each scenario indicated that describing function analysis can be very useful and certainly is appropriate for predicting the stability for a high-order LS system model such as the one presented in this research. Investigation into the results also revealed the critical importance of following the fundamental assumption of describing function analysis. The linear dynamics used for the hydraulic system must satisfy the filtering hypothesis required for describing functions. A scenario in which the filtering hypothesis was violated was encountered and an adjustment of the model by removing higher frequency dynamics could allow for even more improved results in the future.

CHAPTER 1: INTRODUCTION, BACKGROUND, AND MOTIVATION

1.1. Research Introduction and Motivation

LS pumps are desirable in hydraulic systems and engineering applications that typically require a fluid power source to operate a work cycle for heavy machinery such as excavators or off-highway mobile equipment. These pumps are desirable due to the advantage they provide in terms of improved efficiency. When coupled with a flow control valve, the LS pump attains higher efficiency than other hydraulic architectures by maintaining a constant pressure drop (margin pressure) between pump discharge and the load. Maintaining the orifice area in the flow control valve ultimately allows for the flow within the system to be more predictable and provides greater control over the pump output and efficiency of the pump. This LS capability is achieved through a LS line that acts as "feedback" to the pump displacement flow control valve (PDFCV). The load pressure is "fed back" to assist in displacing the control valve either to increase the swash plate angle of the pump and increase the output pump flow or to prohibit flow from reaching the pump control actuator subsequently reducing the swash plate angle and output flow. This feedback capability allows for the margin pressure to be held constant, but also presents the opportunity for instability and sustained oscillations to be introduced to the system through nonlinearities in the pump displacement control system.

Stability of a dynamic system is always a crucial aspect that needs to be considered and analyzed, especially for hydraulic systems that typically incorporate large loads, high pressures, and very fast dynamics. For this research, the modeling, simulation and stability

analysis of a Rexroth® A10VO Variable-Displacement Axial Piston LS pump was conducted. The analysis was completed with some simplifications through numerical simulations in MATLAB® and Simulink® with the pump being part of a larger hydraulic system. The objectives of this thesis were as follows:

- Successfully characterize and develop a nonlinear (NL) hydro-mechanical LS pump system model
- Accurately simulate the NL model to obtain a stable system response
- Validate the NL model against an experimental test bed and provide error quantification to verify the model is accurately simulating the dynamics of the real LS pump system
- Linearize the NL model to obtain a linearized State-Space Representation (SSR) for the LS system and validate the linearized model through comparison simulations with the NL model
- Restructure the linearized SSR to develop two individual Single Input – Single Output (SISO) transfer functions (TF) based on the two separate saturation cases present within the mechanical components of the LS system
- Utilizing the two newly developed TF's for each saturation case, conduct stability analysis via describing functions to predict the existence of limit cycles within the system response
- Determine through multiple scenarios if describing function analysis is an appropriate method to be applied to hydraulic LS systems that suffer from sustained oscillations

1.2. Research Background in Literature

Previous research has been performed on LS pumps and systems primarily to obtain a better understanding of their level of efficiency, but also to investigate their dynamic characteristics and stability as a result of common and unwanted oscillatory behavior. Research regarding the stability and modeling of LS systems can be traced back to the 1980's with most of the research focusing on transfer function (TF) modeling or linearized models of only specific portions of an overall system instead of the development of a full LS system model [28]. The dynamic efficiency of LS hydraulic systems has been previously examined in different research studies and in one study the efficiency was considered using Bondgraphs. Using the Bondgraph approach and as a result of the complex interaction between the dynamics of the load and the load sensing mechanism that typically produces undesired oscillatory behavior, it was determined that in calculating the overall efficiency of the system, an investigation of the dynamic characteristics was essential to the process [25]. Research on the intriguing dynamics of these LS systems has extended to different approaches such as the investigation of the feasibility of modeling a variable displacement LS pump through Dynamic Neural Networks [2, 29]. Another research study investigated the work cycle efficiency of a variable-displacement pump with LS control. The study compared the variable-displacement pump with LS control to three other hydraulic power system architectures (fixed displacement pump with relief valve, fixed displacement pump with LS unloading valve, and variable displacement pump with pressure compensation) and found the variable displacement pump with LS control attained an 83% efficiency during the work cycle while the other alternatives fell short, with the next highest efficiency only reaching a 43% efficient work cycle [6]. In addition to the

efficiency comparison between the different hydraulic power systems, the same research investigated the stability of a LS system for a paving machine through modeling and analysis using SimHydraulics and identified limit cycle oscillation using phase-portrait analysis and Fourier Transform analysis. The same research also attempted to reduce the instability of the system using an optimal damping orifice. Another research study conducted similar analysis but investigated backstepping control design as a method for possible assistance in stabilizing the system [3].

The stability of LS systems has been a popular area of research due to their nonlinear nature and typical concern of instability, as stated before. Previous research has made an effort to study, largely through linear analysis, the dynamics of LS systems and any unique conditions (such as multiple loads) or methods related to stability as well as identifying criteria related to system parameters to help achieve stability [12,13]. LS systems may be designed with two different pump control options. These two control options are constructed either through the incorporation of electronic LS pump control or the incorporation of hydro-mechanical LS pump control. Linear and NL model simulation based on equations of motion has been researched previously, for the case of electronic LS and not hydro-mechanical feedback as is the focus of this thesis [1, 9]. An area of research for LS systems and pumps that warrants more attention, is the development of a more comprehensive system model that includes dynamics of the pump and additional system components that are coupled. This thesis investigates the model development and stability analysis of a hydro-mechanical LS hydraulic system that includes a load but with a focus on the investigation of the value that describing function analysis can provide in analyzing a saturation nonlinearity present in the pump displacement control system. The

investigation was accomplished by means of NL modeling and simulation, system linearization and TF development, and describing function analysis for stability prediction and characterization.

1.3. Overview of Chapters

An overview of each chapter to follow will be provided in order to offer a brief outline for the reader and to summarize the primary focus of each subsequent chapter for the reader's convenience. Chapter 2 explains the basic operation and function of the LS system/ pump and hydraulic system overall in addition to bringing attention to the main components and points of interest within the system that are specific to this research. Chapter 3 discusses the procedure followed in developing the LS system model with respect to the hydraulic modeling aspects and mechanical system modeling aspects as well as discussing the NL model and linearized model. Chapter 4 addresses the simulation of the developed model as well as the validation of the model using experimental data acquired from the hydraulics laboratory setup. Chapter 4 ends with a comparison of the NL model to the linearized model primarily for verification of the linearized model and to ensure the linearization matched well. Chapter 5 comprehensively discusses all aspects of the method of stability analysis that was incorporated in this research which includes describing function analysis, determination of the linear transfer function necessary for describing function analysis, and further discussion of the stability of the system. Chapter 6 investigates the results that came about from the describing function analysis. Chapter 7 then reviews the key points and comprehensive results that were gathered from this research. Chapter 8 concludes the paper by providing an ending discussion summarizing

all primary objectives that were addressed in this research and the results and interesting discoveries that were obtained or pertained to the original objectives.

CHAPTER 2: EXPLANATION OF LOAD-SENSING PUMP SYSTEM

2.1. Explanation of Hydraulic Load-Sensing Function and Capability

When the term load-sensing is used in relation to a hydraulic system it should be recognized as being analogous to a feedback control system since a LS system is in and of itself, a feedback control system. A hydraulic system with a LS capability indicates that the hydraulic system (or more precisely, the LS pump within the system) is able to sense the highest pressure (or highest pressure among multiple loads) the attached load requires at that certain moment in time. As a result of that sensing capability, the pump output is controlled to only provide the pressure necessary to keep the pressure difference between the load pressure and pump discharge pressure, commonly referred to as the *margin pressure*, constant. It is for this reason that LS systems are commonly desired when dealing with hydraulic systems. Since a hydraulic LS system will only provide the pressure needed within the system and not provide a constant pressure that is above what is necessary, the energy losses within the system are greatly reduced. By maintaining a constant margin pressure and knowing the pressure drop between pump discharge and load, the power output of the hydraulic system can be more efficiently controlled since the main focus of the system shifts from attempting to control the energy losses due to the pressure drop varying, to controlling the area of a flow control valve and predictability of the flow in the system. Although LS systems are greatly desired due to the advantage they provide to hydraulic systems in terms of this improved efficiency, at the same time there is common hesitancy in utilizing these systems as a result of the unstable nature that is jointly connected. The complex dynamics associated with incorporating feedback into the system

and the interaction between the sensed load pressure and pump dynamics often generates instability that is characterized by unwanted oscillatory behavior.

A simple way to think about LS capability is to compare a LS hydraulic system to the well-recognized feedback control loop that consists of a controller, plant, and a sensor located in the feedback line. In a LS system, the instantaneous load pressure is "sensed" or "fed back" to a hydraulic pump within a hydraulic circuit to help control the pump output similar to how an electronic sensor's measurement signal acts as feedback for any type of control system being used to help control a generic dynamic system's output. The only difference between these two control systems is that a LS system basically contains a hydro-mechanical feedback control system and LS port within the pump (the plant in this case) itself instead of having an individual sensor, separate controller, and plant as is shown in a common feedback control loop. A load-sensing pump is actually simply an extension of a pressure-controlled pump [16], with the only difference being that the load pressure within the system indirectly has an effect on and is able to manipulate the pump's displacement (swash plate angle). With respect to hydraulic systems, there are different methods to incorporate LS capability (referring to electronic LS), but for this thesis research whenever a reference is made to LS capability or performance, it will be referring to the hydro-mechanical LS control method being utilized (this will be explained in the following sections) within the system being studied here. Also, please note to avoid any confusion in the remaining entirety of this research, any generic discussion (meaning any discussion that is not within a specific section of study such as pressure dynamics or mechanical system dynamics for example) that mentions "the LS system", "the hydraulic

system", or any mention of a LS system, is referring to the same hydraulic system every time.

2.2. Experimental Setup

This section will present the experimental test setup that was investigated as the focus of this research. The reason for presenting the experimental set up first is because the test bed was used to develop the mathematical model that will be shown later and so an understanding of the actual hydraulic setup is essential to fully understanding the modeling construction described later. Once a general description of the experimental setup and the operation of all the components have been explained, a more detailed breakdown of how the components work together will be provided in the following section.

Figure 1 shows the full experimental test bed and also identifies some of the more key components that need to be noted such as the pump, the tank containing additional oil, the flow control valve (FCV), the flow meter, etc. A Rexroth® A10VO Axial Piston Variable-Displacement pump was generously provided to assist in performing this research and all experimental data that was acquired stemmed from that pump. The rotational speed of the pump was set by a 200 horsepower electric motor as shown in Fig. 2. A better view of the pump can be seen in Fig. 3 where the pump discharge and intake lines have been identified as well as the PDFCV 3-way spool valve. It is difficult to see from the provided figure, but a load-sensing line was fed into the back of the PDFCV to assist in de-stroking (reducing the swash plate angle) the pump as will be shown more clearly in the sections that follow.

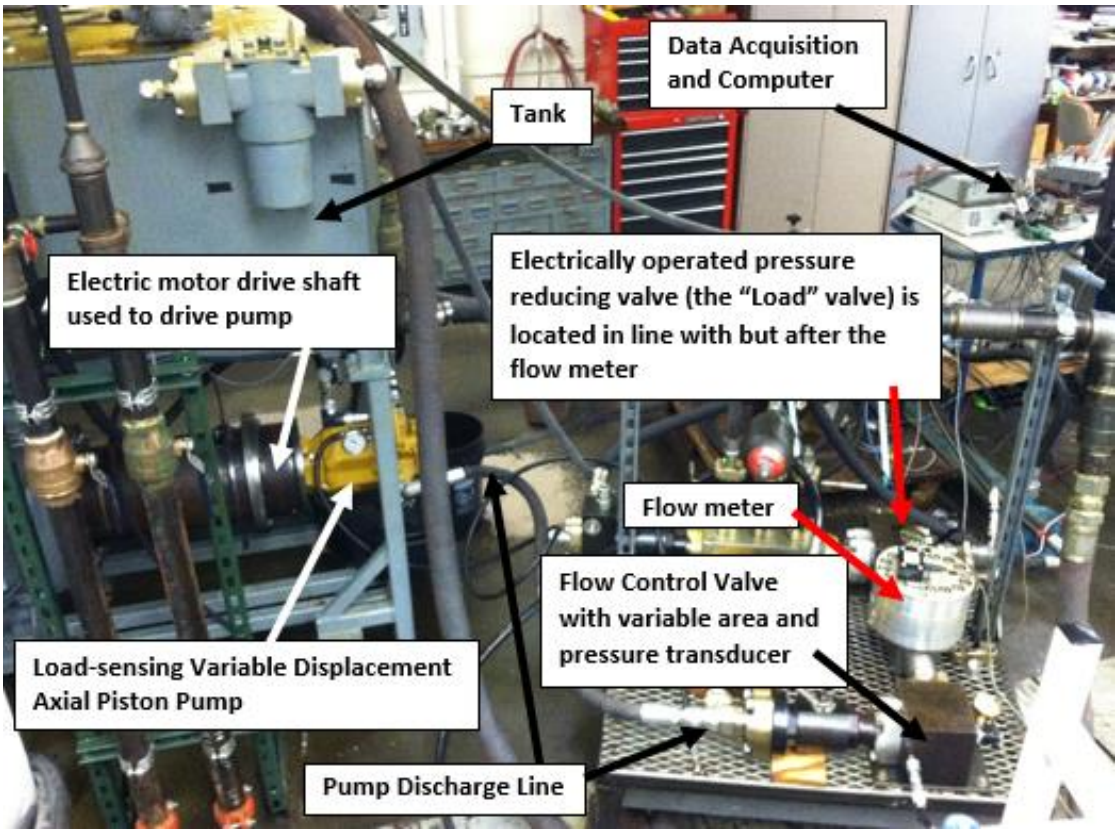

Fig. 1. Full experimental test bed

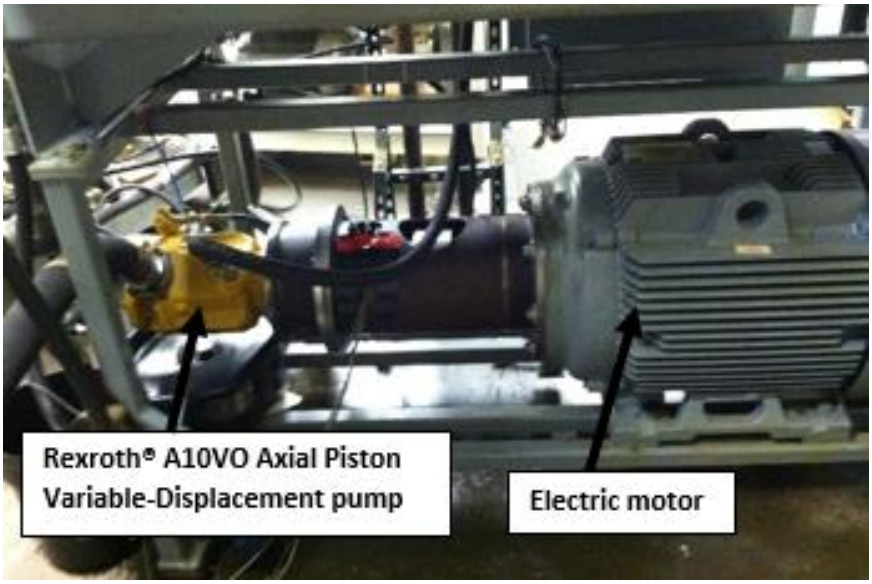

Fig. 2. LS pump and electric motor to set pump speed

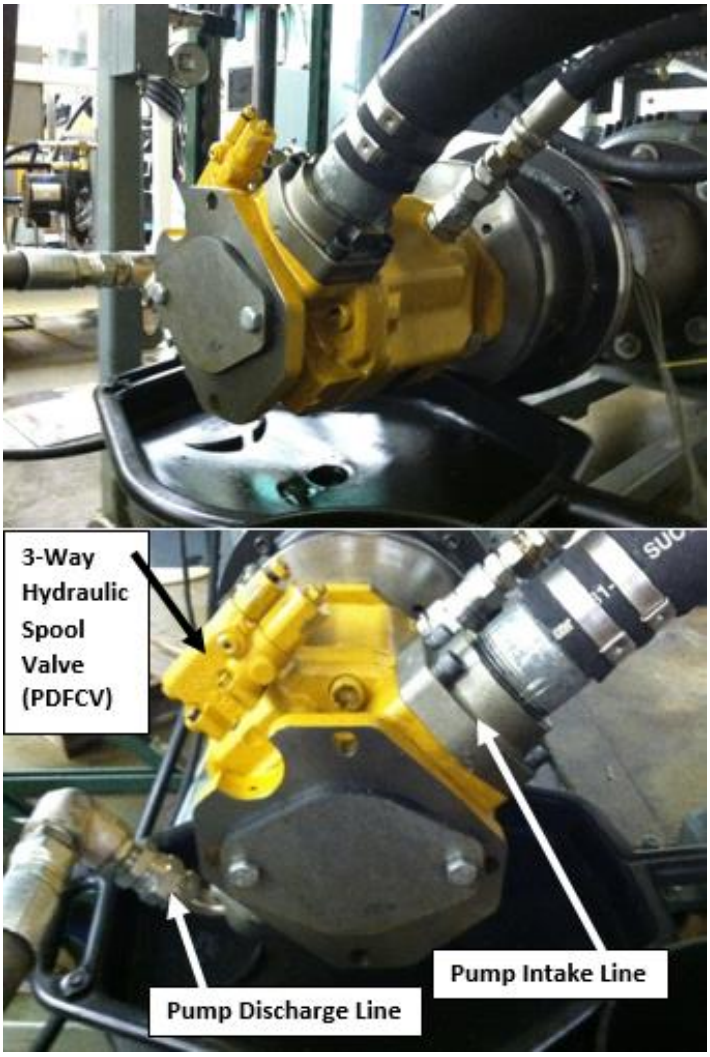

Fig. 3. LS pump and PDFCV (3-way hydraulic spool valve)

Figure 4 shows a closer view of the FCV as well as the flow meter that was in line with the load valve. Lastly, Fig. 5 displays the electrically operated pressure reducing valve that will be referred to as the load valve from here on as well as the load-sensing line that was fed back to the PDFCV and pump. After studying each of the provided figures it should become clear that the experimental test set up was simply a flow loop where the pump,

driven by the electric motor, takes in fluid from the tank and discharges fluid at a certain discharge pressure. The pump discharge flow then continued through the FCV where a pressure transducer was set to record the pump discharge pressure before the load valve. The flow then continued passing through the flow meter to obtain volumetric flow rate data and finally passed through the load valve where an additional pressure transducer was placed to acquire load pressure data. The flow then ultimately continued back to the pump intake port and the beginning of the loop in addition to the PDFCV via the load-sensing port.

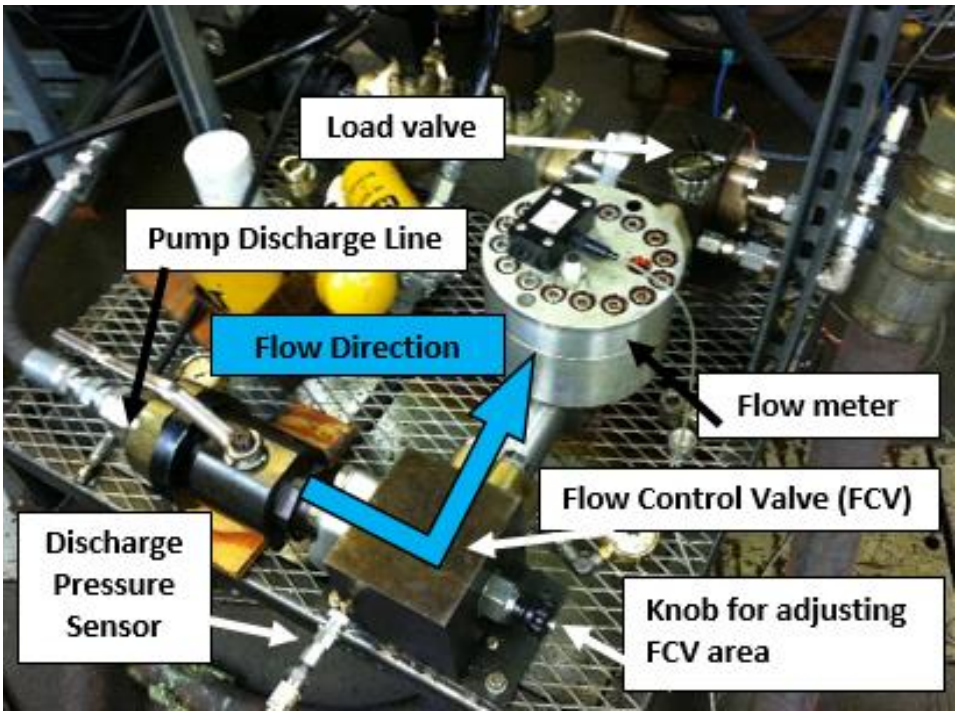

Fig. 4. Flow control valve in line with flow meter and load valve

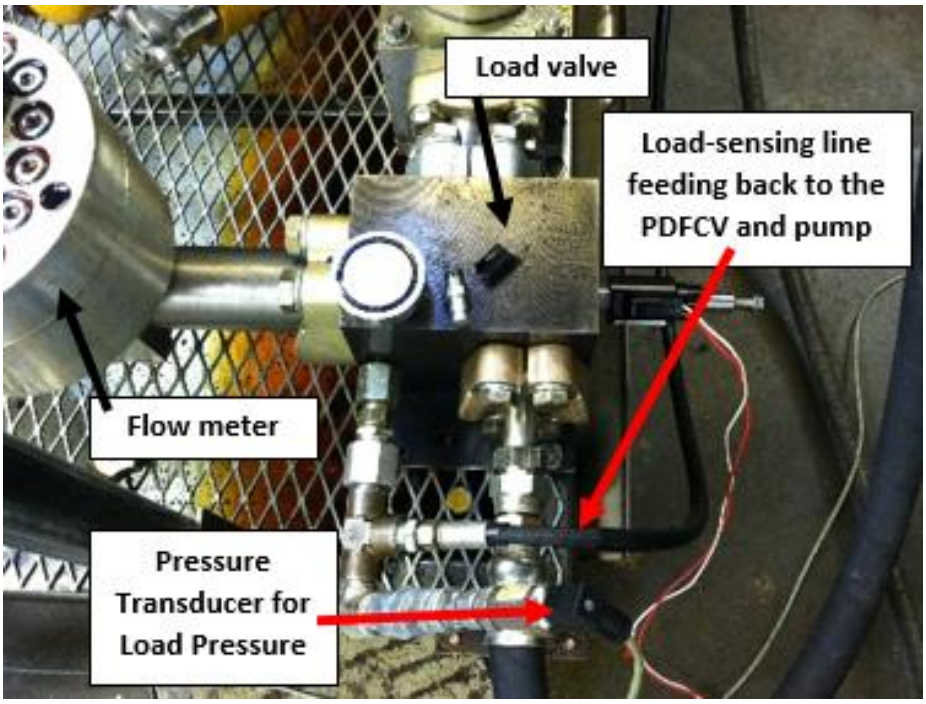

Fig. 5. Electrically operated pressure reducing valve with load-sensing line

2.3. Hydraulic System Components/LS Capability Incorporation

This section will provide additional details on the design and operation of the variable-displacement axial-piston pump, how the LS capability was incorporated into the system, and finally how the load pressure was indirectly able to manipulate the displacement of the pump. The experimental test bed was simplified into a systematic diagram of the complete hydraulic system which can be seen in Fig. 6. The diagram was designed to more easily interpret the operation of the hydraulic system when developing the NL model and to better visualize how each of the system's state variables (defined in Chapter 3) were coupled. Please note that the component labeled "LOAD" in the diagram represents actually two different loads. The "load" for the experimental set up was the electrically operated pressure reducing load valve and for the NL model, a simplified

hydraulic motor model attached to a viscous friction torque and an inertia was initially modeled as a possible load for the system.

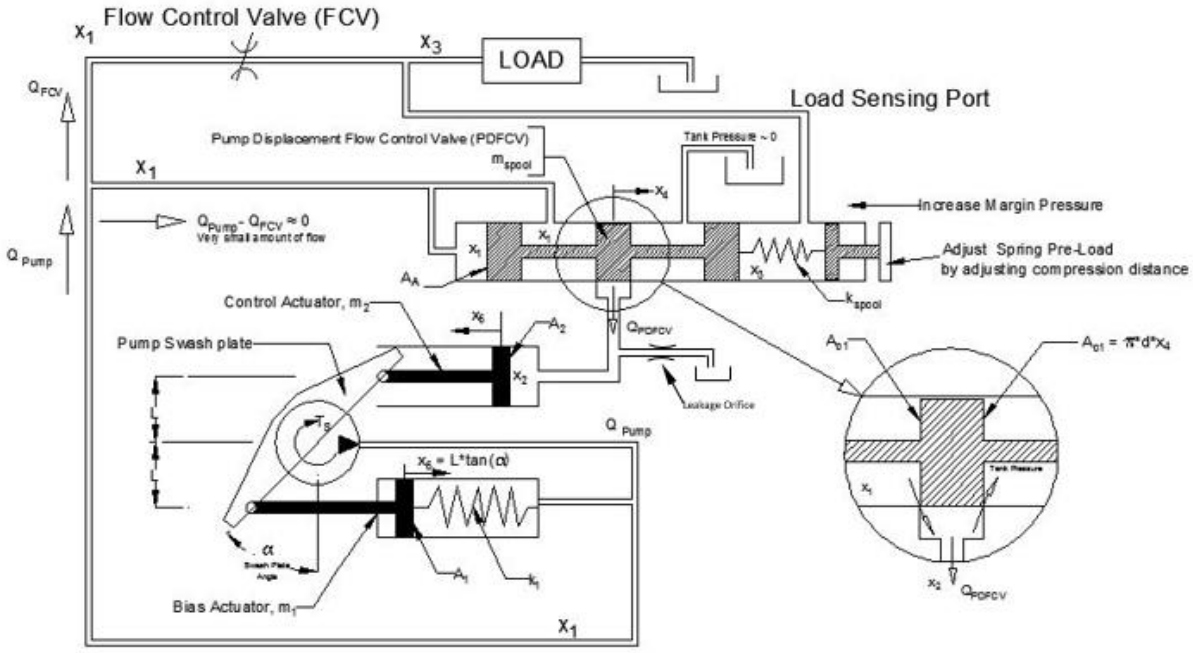

Fig. 6. Simplified theory of operation hydraulic circuit

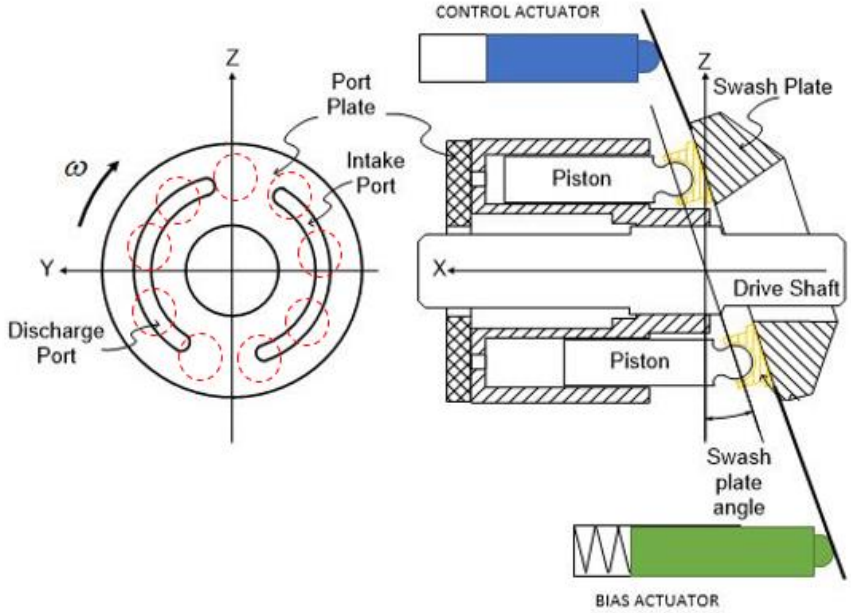

Fig. 7. Simplified schematic for variable displacement axial piston pump

Figure 7 shows a simplified schematic for a variable-displacement axial-piston pump where the circular diagram on the left that is aligned with the Y-Z axes represents a front view of the pump and what is called the port plate. The port plate is fixed (does not rotate) and contains two curved slots, the intake port and the discharge port, which allow for fluid to enter into the pump through the intake port and then permits fluid to discharge from the pump by exiting through the discharge port. Also note that a rotational speed for the pump on this diagram is designated by the variable ω, but that speed is applied to the drive shaft shown on the right diagram that is aligned to the X-Z axes in the figure and not the port plate itself. The diagram on the right displays a simplistic side view of the primary components located within a variable-displacement axial-piston pump. As the drive shaft rotates (rotation is set by an exterior power source, an electric motor in the case of this research) the pistons, identified by the red dashed circles on the port plate, follow a circular path around the port plate with each passing over the intake and discharge ports. The pistons are also allowed to axially translate in and out of their designated pressure chambers and their distance to travel is limited by the angle of the swash plate. As the drive shaft rotates, the pistons rotate, equally spaced from each other and the drive shaft, as well and are forced to follow the profile set by the swash plate. The angle of the swash plate then controls how far each piston can translate within its chamber, ultimately controlling the volume of fluid each piston is able to take into its chamber through the intake port and then discharge through the discharge port. By varying the swash plate angle, the amount of fluid that enters and discharges from each chamber can either be increased by increasing the swash plate angle or decreased by decreasing the swash plate angle. This is what is meant when saying the pump is stroking up (increasing the angle) or de-stroking the pump

(decreasing the angle). It should be fairly clear now as to why this pump design is referred to as an axial-piston variable displacement pump. The axial displacement and direction of the pistons combined with the variable-displacement capability of the swash plate differs from other pump designs that might incorporate fixed-displacement swash plates as well as other design differences. The question now should be how is the swash plate angle increased or decreased? The answer to this question relates to the next topic that is necessary in this discussion and that is the relationship between the control actuator and the LS capability of the system.

The only components in Fig. 7 that still have yet to be mentioned are the control and bias actuators that are located above and below the swash plate, respectively. The reason for this design placement is that these actuators not only help displace the swash plate angle of the pump but also are vital to the LS function of the system, or at least the control actuator is. Additional technical detail will be provided in the model development chapter to follow and so only a basic description on how these components function will be given at this time. To start, the bias actuator typically is displaced from the discharge pressure of the pump in addition to a spring force applied by what is commonly known as the bias spring. The bias actuator applies a force to the swash plate that is a specific perpendicular distance from the swash plate's point of rotation, ultimately applying a torque to the swash plate that tends to increase the swash plate angle and the pump's output (discharge pressure and flow). The control actuator functions the exact same way as the bias actuator except without the use of a spring and tends to de-stroke the pump and reduce the pump's output. The control actuator is forced against the swash plate by receiving

downstream pump discharge flow and pressure that first must pass through the PDFCV as will be shown.

As will be modeled in the next chapter, the PDFCV is a 3-way hydraulic spool valve that is linearly displaced to either allow flow and pressure to reach the control actuator in order to decrease the swash plate angle and pump output or to restrict both flow and pressure from reaching the control actuator and subsequently increase the pump swash plate angle and pump output. The displacement of the PDFCV is determined by the force balance acting on the valve with the forces stemming from the pump discharge pressure, load pressure, and flow through the valve. Referring back to the hydraulic system schematic in Fig. 6, in the upper right corner of the schematic a load sensing port can be seen; this is how the LS capability is incorporated into the dynamics of the system. The pressure that is immediately before the load (indicated by the variable x_3 which will be defined later) is "sensed", or fed back to the PDFCV to be more precise, to act as an additional force on the valve. So as the pump is operating and suddenly the load in the system requires a greater pressure to operate, the load pressure will increase causing the PDFCV valve to translate to a position to the left as shown in Fig. 8 where the flow and pressure in the control actuator (shown by the variable x_2) is actually released to the lower pressure in the tank. This pressure reduction in the control actuator will cause the actuator to stop applying a force to the swash plate and will allow the pump to stroke up and increase its output. Please note that the spool valve within this research was critically-centered and the diagrams depicted in both Fig. 8 and Fig. 9 are exaggerated and do not accurately show the critically-centered nature of the valve that was studied. The critically-centered design

of the valve does affect the mathematical model for flow through the valve, but it does not affect the simplified theory of operation being explained here.

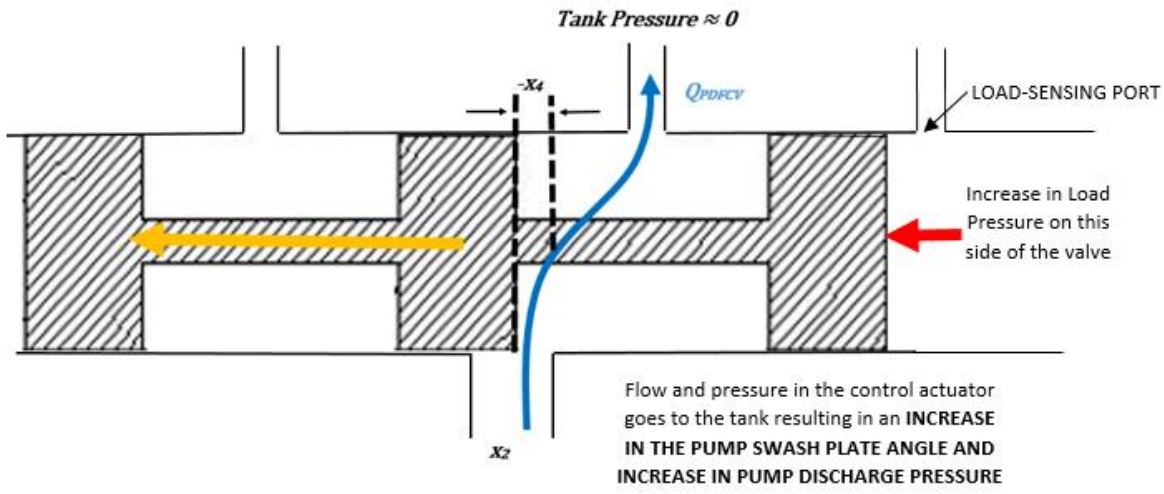

Fig. 8. Negative displacement for PDFCV

Once the desired load pressure is met, the increased pump discharge pressure will act on the PDFCV and the increased force will displace the valve to a position to the right as shown in Fig. 9.

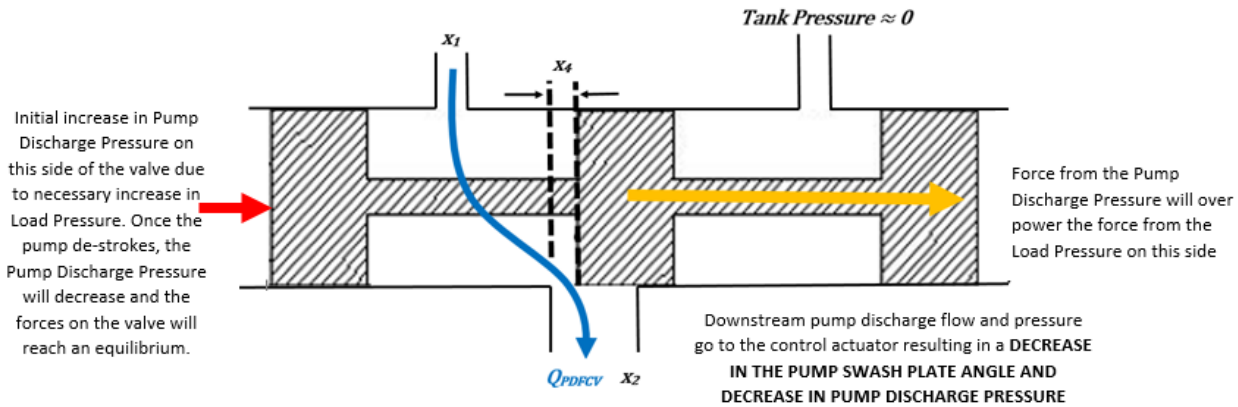

Fig. 9. Positive displacement for PDFCV

At this point, the downstream pump discharge flow and pressure are once again allowed to reach the control actuator which then de-strokes the pump, reduces the pump discharge pressure and allows for the dynamic forces acting on the PDFCV to reach an equilibrium point. This control system is considered hydro-mechanical feedback and LS control (due to the pressure dynamics and mechanical system dynamics that take place in the PDFCV displacement) and results in a more efficient system since the pump is only supplying the exact discharge pressure necessary for the load to operate correctly instead of supplying extraneous amounts of flow, pressure and energy that might not be necessary. As stated before, this control system is considered to be hydro-mechanical due to the coupled nature of the dynamics stemming from the fluid pressures acting on the valve with the dynamics of the PDFCV and the swash plate/actuators. This coupled dynamic system creates a formidable engineering problem to investigate as will be shown in the following chapter on model development. Keep in mind the basic operation of the pump and LS system that was addressed in this section as it will be directly applied in the development of the NL model.

CHAPTER 3: DYNAMIC SYSTEM MODEL DEVELOPMENT

As previously mentioned, a primary research objective for this thesis was to develop a full system model in order to efficiently and accurately analyze the LS hydraulic system's performance and stability. Previous academic research has provided extremely thorough investigation of dynamic models for variable displacement axial piston pumps [10, 26], but these models typically become highly detailed and in some cases provide more focus on the intricate details than what is desired. For this thesis, a NL model based on the equations of motion for each principal part of the hydraulic system was first developed and will be thoroughly shown in the following section. This NL model was then organized into a set of first order ordinary differential equations (ODE) defined by state variables to allow for an easy transition to the second model, a linearized model with a linear State-Space Representation (SSR). The NL model was generated to represent the entire hydraulic system and to allow for simulations to take place over a wide range of operating conditions as opposed to the linear model which would only simulate within a linear range limited by small perturbations from the nominal operating conditions. Each NL equation provided vital information that was necessary to adequately diagnose the dynamic performance of not only the overall system but also the internal parts of the system such as the dynamics associated with the control pressure, the PDFCV, or any of the other components shown in the previous chapter.

Based on the hydraulic system diagram displayed in Fig. 6 and the experimental test setup described in the previous chapter, dynamical equations were developed for the pump discharge pressure dynamics, control pressure dynamics, load pressure dynamics,

PDFCV dynamics, the swash plate's displacement actuator dynamics (which is equivalent to either the bias or control actuator dynamics and to act in place of the rotational dynamics of the swash plate), and a theoretical motor load [18]. Table 1 displays the system dynamics that were evaluated and the order of the ODE corresponding to each system being analyzed. From Table 1, it can be seen that the NL model that was developed for the overall system is 8th order and each individual system will be discussed in the following sections of this chapter.

Table 1. Dynamic system and corresponding ODE order

Dynamic System	***ODE Order***
Time Rate of Change for Pump Discharge Pressure	1st Order
Time Rate of Change for Control Pressure	1st Order
Time Rate of Change for Load Pressure	1st Order
PDFCV Acceleration	2nd Order
Bias or Control Actuator Acceleration	2nd Order
Motor Load Rotational Acceleration	1st Order

For the following sections, in order to provide a more organized presentation of the system model as it is being developed, the following state vector, containing the LS system's state variables that are of interest, is being pre-defined. These state variables are consistent through the entire discussion of the model development.

$$\vec{x} = \begin{bmatrix} x_1 \\ x_2 \\ x_3 \\ x_4 \\ x_5 \\ x_6 \\ x_7 \\ x_8 \end{bmatrix} = \begin{bmatrix} Pump\ Discharge\ Pressure \\ Control\ Pressure \\ Load\ Pressure \\ PDFCV\ Position \\ PDFCV\ Velocity \\ Swash\ plate\ (Bias\ or\ Control) Actuator\ Position \\ Swash\ plate\ (Bias\ or\ Control) Actuator\ Velocity \\ Motor\ Load\ Rotational\ Velocity \end{bmatrix} \quad (1)$$

3.1. Pressure Dynamics

Before investigating the dynamics related specifically to the LS hydraulic system itself, it is necessary to provide background on the general modeling equations being used as the foundation. Once the general equations used for modeling the pressure dynamics within the system are defined, the model equations specific to the LS system will be defined. The orifice equation and the pressure-rise rate equation are two of probably the most well-known and widely used equations in modeling hydraulic systems. These two equations were used as the basis for each dynamical equation needed to define the time rate of change of pressure within the hydraulic realm of the system and can be shown as Eqs. (2) and (3), respectively.

$$Q = A_Q C_d \sqrt{\frac{2}{\rho}(P_1 - P_2)} \quad (2)$$

$$\frac{dP}{dt} = \frac{\beta}{V}\left[Q_{NET} - \frac{dV}{dt}\right] \quad (3)$$

For the first equation shown, the orifice equation, Q represents the volumetric flow rate of the fluid passing through the orifice, A_Q represents the orifice area that the fluid is passing through, C_d represents the discharge coefficient of the orifice, ρ represents the density of

the fluid, P_1 and P_2 respectively represent the pressure of the fluid before and after the orifice. A diagram displaying the parameters within the orifice equation applied to a physical scenario can be seen in Fig. 10 where the fluid is attempting to pass through a sharp-edged orifice. To be specific, the orifice equation is to be used based on the assumption that the flow being considered is steady, incompressible and relates to high-Reynold's-number flow, but exceptions (unsteady flow, slightly compressible flow, low-Reynold's-number flow) are typically made when being utilized to model hydraulic systems and this is normally due to the convenience it provides when quantitatively addressing flow within a system [16, pg. 64]. All analysis within this research involving flow through an orifice was assumed to be a sharp-edged orifice where the discharge coefficient is equal to a value of exactly 0.62, as is common practice in modeling hydraulic systems.

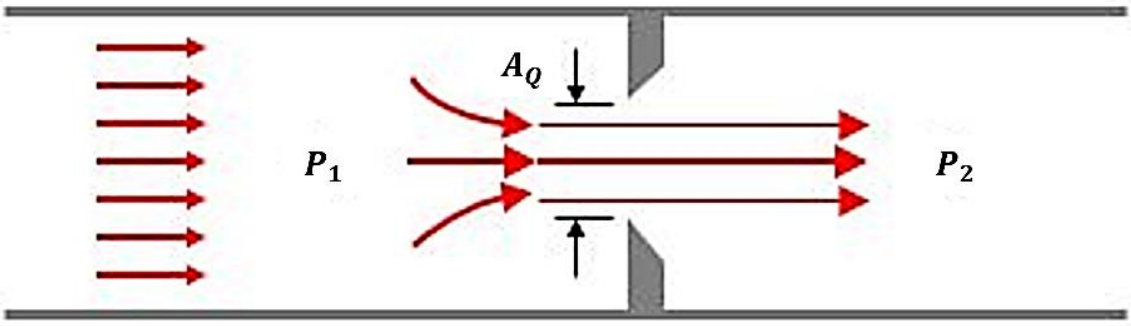

Fig. 10. Diagram for sharp-edged orifice

For the second equation, the pressure-rise rate equation, β represents the bulk modulus of the fluid, V represents the general volume of fluid being considered, Q_{NET} represents the net flow in or out of the control volume and lastly the two terms, $\frac{dP}{dt}$ and $\frac{dV}{dt}$, respectively

represent the time rate of change of pressure and volume. The pressure-rise rate equation defines the time rate of change of pressure within a defined control volume and by studying the equation it should be noted that the change in pressure of a fluid within a control volume is a function of both the net flow in or out of the control volume as well as the volumetric time rate of change of the control volume itself. A simple diagram can be seen in Fig. 11 where a scenario is displayed in which the pressure within a control volume is dynamically changing due to flow entering the control volume as well as the volume changing due to a piston being displaced.

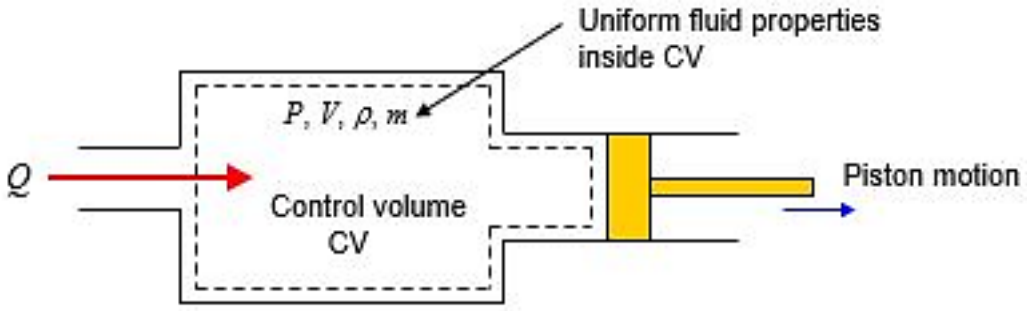

Fig. 11. Diagram for pressure-rise rate scenario

Please take note that the orifice equation is a basic algebraic equation and the pressure-rise rate equation is a first-order ODE defining the first time derivative of a generic pressure.

3.1.1. Pump Discharge Pressure

Now that the general equations used for the modeling of the pressure dynamics within the system have been defined, the first dynamic model to be discussed will be in relation to the pump discharge pressure. The dynamic model for the pump discharge pressure defines the time rate of change of the output pressure that the pump provides. This can mathematically be defined as

$$f_1 = \dot{x_1} = \frac{\beta}{V_{pd}}\left[Q_{Pump} - Q_{FCV} - A_1 x_7\right] \tag{4}$$

where Q_{Pump} represents the pump discharge flow that can be defined as

$$Q_{Pump} = V_d \omega_p \frac{\alpha}{\alpha_{max}} \tag{5}$$

and Q_{FCV} represents the flow through the FCV located right before the load and can be defined as

$$Q_{FCV} = A_O C_d \sqrt{\frac{2}{\rho}(x_1 - x_3)}\ . \tag{6}$$

Eq. (4) takes into account the difference between the pump discharge flow and the flow through the FCV as well as the volumetric change in the bias actuator shown by the $A_1 x_7$ term.

Recall earlier in Chapter 2, when discussing the advantage of a LS system when keeping the margin pressure constant, the main focus in improving the efficiency of the system rests on controlling the variable area of the FCV. It should be more apparent now when looking at Eq. (6) that the margin pressure is defined by the $x_1 - x_3$ term and if this term is a constant value the only variable allowed to change is A_O, the area of the orifice. By then controlling that area, predictable flow is produced along with opportunity for better management of the pump's power output. It should be noticed that the swash plate angle, α, was not defined as a state variable and so it became necessary to define the pump discharge flow in terms of the desired state variables since the NL model is a coupled system. It was with this thought in mind that the decision to model the swash plate rotational dynamics in terms of the linear dynamics of the actuators was made. Both

actuators were equidistant from the swash plate's point of rotation and so using basic trigonometry the algebraic expression for defining the swash plate angle in terms of the displacement of an actuator was identified to be

$$\alpha = (\tan^{-1}(\frac{y_{max} - x_6}{L})) \tag{7}$$

Another important decision that was made when developing the model was the decision to simplify the expression needed to define the volume of fluid being analyzed within each pressure dynamics equation. Typically the volume (the V that appears in the $\frac{\beta}{V}$ term of each pressure-rise rate equation) would be defined in terms of state variables as well since there is chance for slight variation in the volume during the system's operation, but the initial idea was to keep the model simple and add detail if necessary during the model validation stage which proved to be unnecessary. Instead of modeling each volume as a function of state variables, it was decided to define the variables as constant values for each pressure-rise rate equation and estimate their numerical value through model validation with experimental data.

3.1.2. Control Pressure

The second NL dynamic model was used to define the time rate of change of pressure within the control actuator. The control pressure dynamics were mathematically defined by

$$f_2 = \dot{x_2} = \frac{\beta}{V_c}[Q_{PDFCV} - A_2 x_7] \tag{8}$$

where Q_{PDFCV} represents the flow through the critically-centered PDFCV and is dependent on the position, x_4, of the valve itself and the $A_2 x_7$ term defines the volumetric change

within the control actuator chamber. The flow through the valve is defined for two different operating conditions and can be mathematically defined as

$$Q_{PDFCV} = \begin{cases} C_d \pi d x_4 \sqrt{\frac{2}{\rho}(x_1 - x_2)} - C_d K_{SVA} \sqrt{\frac{2}{\rho}(x_2 - P_{Tank})} & x_4 > x_{null} \\ -(C_d \pi d x_4 + C_d K_{SVA}) \sqrt{\frac{2}{\rho}(x_2 - P_{Tank})} & x_4 < x_{null} \end{cases} \quad (9)$$

Referring back to Fig. 9 in Chapter 2, the first case for the PDFCV flow is when the valve position is positively displaced to the right and is greater than the null valve position, x_{null} (this position is defined by the pre-load that is applied by a spring on the LS port side of the valve and dictates the position of the valve that restricts flow both to the control actuator and the tank), the downstream pump discharge flow and pressure are allowed to reach the control actuator and reduce the pump swash plate angle. Referring back to Fig. 8, the second case for the flow is when the valve position is negatively displaced to the left and is less than the null valve position, the control pressure within the control actuator is then released to the tank allowing for the force from the bias actuator to overpower the force from control actuator and increase the pump swash plate angle. Note that in both these cases the variable K_{SVA} shows up in the flow equation. This variable represents a circumferential leakage area that is represented as an orifice and is present in either flow scenario. This leakage provides damping within the physical system and can assist in improving the performance of the system response.

3.1.3. Load Pressure

The load pressure dynamics were included in the NL model to anticipate the inclusion of different load types. For the general NL model and initial simulation, as was

stated before, a theoretical hydraulic motor model was included and coupled to the load pressure dynamic model being presented. The load pressure dynamics were modeled as

$$f_3 = \dot{x_3} = \frac{\beta}{V_L}[Q_{FCV} - V_m x_8] \tag{10}$$

where the flow through the FCV is the same as was previously defined and the $V_m x_8$ term represents the volumetric displacement provided by the motor model.

3.2. Mechanical System Dynamics

Due to the hydro-mechanical nature of the system, the modeling of the mechanical system dynamics in addition to the pressure dynamics is necessary in defining a complete LS system model. Recalling the basic operation of the LS system as defined in Chapter 2, the system is considered hydro-mechanical due to the pressures that are coupled with and that act within the mechanical systems of the PDFCV and the variable-displacement axial-piston pump. Similar to the process that was followed for defining the dynamic pressure model equations for the LS system, the same method will be applied for investigation of the mechanical systems operating within the LS system by first addressing the foundational equation for each mechanical system.

The governing equation used for modeling the mechanical systems is the universally recognized Newton's Second Law of Motion defined as

$$\sum F = m\ddot{z} \tag{11}$$

where the term on the left hand side of the equation represents the sum of the forces acting on a body, m represents the mass of the body the forces are being applied to, and $\ddot{z}$ represents both the acceleration and second time derivative of the position, z, of the body.

3.2.1. Pump Displacement Flow Control Valve Dynamics

Using Newton's Second Law of Motion and the free body diagram of the PDFCV shown in Fig. 12, the following second order ODE can be developed to describe the acceleration of the valve with displacement to the right being considered positive

$$m_{spool}\ddot{x_4} = x_1 A_A - x_3 A_A - (x_p + x_4)k_{spool} - K_{SV}x_5 + F_f \tag{12}$$

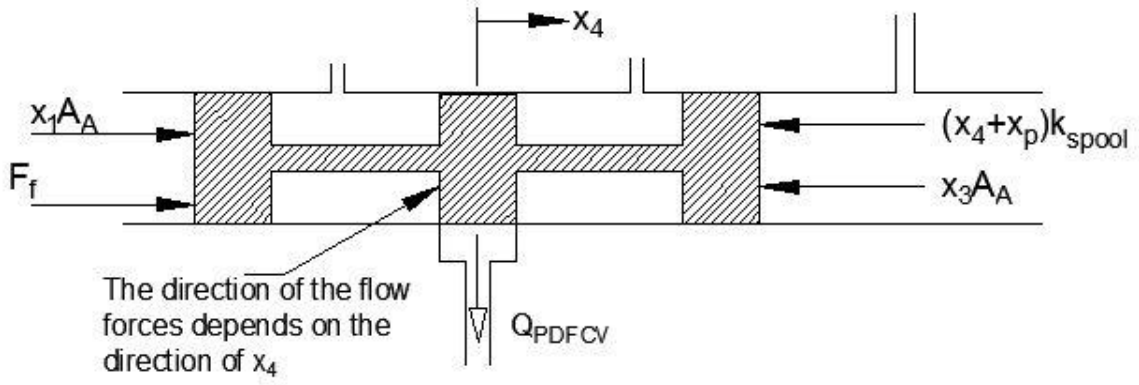

Fig. 12. Free body diagram for PDFCV

The valve is a single rigid body and on the right side of the valve appears the forces that are generated from the spring pre-load and force in addition to the force that occurs from the load pressure being fed back to the valve. It should be noted here that in addition to this valve, a pressure-relief valve was also present within the hydraulic control valve system shown in Fig. 3. This pressure relief valve was neglected due to the assumption that the dynamics or stability of the relief valve would not affect the dynamics of the other systems being modeled unless the maximum relief pressure was approached, which was never a scenario within this research. On the left side appears the force occurring from the pump discharge pressure as well as the F_f term which represents the flow forces or the force that the body of fluid flowing through the valve exerts on the valve. The flow force contains

both transient terms and static terms and are is derived by applying Reynold's Transport Theorem to the control volumes defined within the valve [16, 17, 19]. The transient portion of the flow force consists of two terms with one term defining the effect that the time rate of change of pressure has on the flow force and the second term defining how the time rate of change of the valve position, or the velocity in other words, affects the flow force. Typically in the past, the transient terms have been neglected for certain cases and only the static term has been kept for modeling flow forces that act on a spool valve. Previous but more recent research, [17,19], has indicated though that neglecting the transient portion of the flow force model could be costly due to the transient term having a magnitude equal to that of its' static counterpart for systems operating at high frequencies. It is clear from previous research that the flow force transient term can greatly influence the dynamics of the valve being modeled in certain scenarios, but it was decided early in this research that initially a model with only the static term of the flow force, shown by Eq. (13), would be incorporated and analyzed to see if it was adequate for defining the flow force acting on the PDFCV. Model validation simulations that will be shown later, prove that for the scope of this thesis and research, the static flow force alone was acceptable for analysis of this model. For future research, incorporation of the transient flow force terms would be another intriguing aspect to be investigated and added to the model development.

$$F_f = \begin{cases} -\frac{2C_d^2 \pi d x_4 (x_1 - x_2)}{C_c} \cos(\theta) & x_4 > x_{null} \\ -\frac{2C_d^2 \pi d x_4 (x_2 - P_{Tank})}{C_c} \cos(\theta) & x_4 < x_{null} \end{cases} \tag{13}$$

Recall that the forces on the valve determine the position of the valve and the position of the valve effects the pump output by either allowing flow to reach the control actuator to

reduce the pump swash plate angle or to restrict flow from reaching the actuator and instead allowing the control pressure to go to the tank and having the bias actuator increase the pump swash plate angle. As the dynamics play out and ideally the forces balance on the valve, a second order response for the valve is to be expected but previous research has indicated, as stated before, that with the load pressure feedback on the valve, instability and oscillations tend to occur due to the system's attempt to control the output of the pump when achieving the desired load pressure in the system. In anticipation of the linear model to be developed later, the second order ODE defined for the PDFCV dynamics was organized into a coupled system of two first order ODE's where the velocity of the valve is defined as

$$f_4 = \dot{x_4} = x_5 \tag{14}$$

and the acceleration of the valve is defined as

$$f_5 = \dot{x_5} = \frac{1}{m_{spool}}\left[x_1 A_A - x_3 A_A - \left(x_p + x_4\right)k_{spool} - K_{SV}x_5 - F_f\right]. \tag{15}$$

3.2.2. LS Pump Swash plate/Actuator System Dynamics

Similar to the model developed for the PDFCV, a second order ODE was developed for the pump swash plate/actuator system dynamics according to the free body diagram shown in Fig. 13. Dynamic variable-displacement pump models have been developed in previous research, [26], and are typically described through a set of highly nonlinear and complex equations that incorporate many detailed parameters and for this research a highly detailed approach was not desired as will be shown later. There are different approaches that could have been taken when modeling the swash plate and actuator system and the

important thing to note is that the actuators and the swash plate are a system together and as a result can be modeled as one system, not individually. For example, modeling the dynamics as a summation of the moments acting on the swash plate could have been another approach but to avoid dealing with the inertia approximation for the swash plate, the dynamics were defined by applying a summation of the linear forces acting on the control actuator and any torque acting on the swash plate was then redefined as a force acting on the actuator. For the type of pump that was studied, the vertical distance from the swash plate's point of rotation to the center of the actuator, defined as *L* in the free body diagram, was the same for both the control and bias actuators.

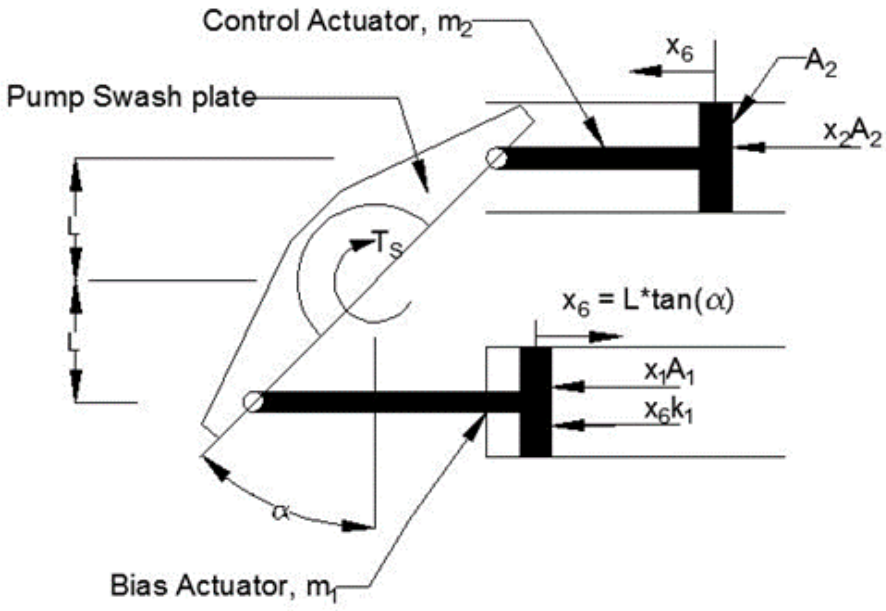

Fig. 13. Free body diagram of pump swash plate/actuator system

This resulted in a case where by finding an approximate system mass, the forces acting on the system (the swash plate, control actuator, and bias actuator) could be seen as acting on a single rigid body and so only one dynamic model needed to be developed since the displacement, velocity, and acceleration of one actuator resulted in the exact same set of

dynamics for the other actuator and vice versa. Once all forces were summed together and equated to the summed mass of both the bias and control actuators multiplied by the acceleration of the control (or bias) actuator, with positive displacement being to the left for the control actuator and right for the bias actuator, the model for the pump's mechanical dynamics were defined as

$$(m_1 + m_2)\ddot{x_6} = x_2A_2 - x_1A_1 - (y_p + x_6)k_1 - K_{AG}x_7 - \frac{T_S}{L}. \quad (16)$$

The $\frac{T_S}{L}$ term is a force but actually is in terms of torque, sometimes referred to as the swivel torque, being applied to the swash plate and as described before. This torque was simply divided by the moment arm distance to an actuator to be redefined as a translational force acting on an actuator. It is fairly intuitive to see how the external forces that are generated by either the control pressure or pump discharge pressure acting on each actuator appear in Eq. (16), but the swivel torque is not as intuitive and must be defined to explain its significance. As can be imagined, the torque acting on the swash plate is a complicated value to define and is a result of the forces of the internal components of the pump. Due to this fact and the importance of taking into account the forces acting on the swash plate when designing the mechanical components within (bearings, housings, etc.) there has been extensive research regarding the moments and forces that act on the swash plate of a variable displacement axial piston pump [20, 21, 30]. For the role that the torque plays within the scope of this research, a more simplified expression was desired to work into the model. The swivel torque acting on the swash plate can be confidently approximated as

$$T_S = C_i\alpha - C_p x_1 = C_i\left(tan^{-1}\left(\frac{y_{max}-x_6}{L}\right)\right) - C_p x_1 \tag{17}$$

where

$$C_i = \frac{NM_p r^2\omega^2}{2} \tag{18}$$

and

$$C_p = \frac{NA_p r\gamma}{2\pi} \quad . \tag{19}$$

In order to understand how the swivel torque is generated and exerted on the swash plate, first recall from Chapter 2, the theory of operation for a variable-displacement axial-piston pump. A brief review is that these pumps typically have either 7 or 9 pistons (an odd number of pistons is typically desired to minimize what is known as the flow ripple amplitude, more information can be found on this topic [16, pg. 282-283]) that are allowed to translate in and out of their respective pressure chambers but are limited in travel by the angle of the swash plate. As these pistons rotate within the pump and follow the angled profile of the swash plate while also taking in fluid through the intake port and expelling fluid through the discharge port, the pistons experience a pressure within each chamber. The pistons moving within the pump are each having a force applied to them but at the same time are exerting a force on the swash plate which results in a torque being applied to the swash plate.

As stated earlier, Eq. (17) is a reliable approximation for the torque where C_i and C_p are variables that take into account the number of pistons operating within the pump, the mass, radius and area of each piston-slipper assembly, the rotational speed of the pump, and the pressure carryover angle [16, pg.285-286]. The first term in Eq. (17) is positive

and defines how the inertia of the piston-slipper assemblies acts to increase the swash plate angle as each assembly revolves within the pump. The second term helps define the torque that results from the fluctuating pressure profile (described by the pressure carryover angle) that each piston experiences through the transition from a lower pressure at intake to a higher pressure at discharge. This second term is also negative which indicates that it actually helps to de-stroke the pump alongside the control actuator. Also, it can be seen that the second term is multiplied by x_1, the pump discharge pressure, and the first term is only multiplied by the swash plate angle. As a result of this, the second term will typically end up being much larger when the pump is operating at higher pressures. The second order ODE was then re-organized into a coupled system of two first order ODE's where the velocity is defined as

$$f_6 = \dot{x_6} = x_7 \tag{20}$$

and the acceleration is defined as

$$f_7 = \dot{x_7} = \frac{1}{(m_1+m_2)}\left[x_2A_2 - x_1A_1 - (y_p + x_6)k_1 - K_{AG}x_7 - \frac{T_S}{L}\right] . \tag{21}$$

Lastly, for this section, the load initially defined for the NL model simulation was a hydraulic motor model consisting of a viscous friction torque and an inertia. The basic mathematical model for this was

$$f_8 = \dot{x_8} = \frac{1}{J_m}[x_3V_m - b_m x_8] \quad . \tag{22}$$

3.3. Coupled NL System

This section will provide the complete, analytical NL model as one set of eight NL equations in terms of the pre-defined state variables for the reader's convenience. A

presentation of all NL equations (without the inclusion of Q_{PDFCV} and F_f due to their values being dependent on valve position) also is advantageous in identifying how each equation is coupled to one or multiple equations and presents the format necessary for system linearization. The analytical model provided here was then programmed into Simulink® for simulation. The full, analytical NL system model, Eq. (4)-(22) with each NL equation identified as functions f_1 through f_8 can be shown as:

$$f_1 = \dot{x_1} = \frac{\beta}{V_{pd}}\left[V_d\omega_p\frac{(tan^{-1}\left(\frac{y_{max}-x_6}{L}\right))}{\alpha_{max}} - A_O C_d\sqrt{\frac{2}{\rho}(x_1-x_3)} - A_1 x_7\right]$$

$$f_2 = \dot{x_2} = \frac{\beta}{V_c}[Q_{PDFCV} - A_2 x_7]$$

$$f_3 = \dot{x_3} = \frac{\beta}{V_L}\left[A_O C_d\sqrt{\frac{2}{\rho}(x_1-x_3)} - V_m x_8\right]$$

$$f_4 = \dot{x_4} = x_5$$

$$f_5 = \dot{x_5} = \frac{1}{m_{spool}}\left[x_1 A_A - x_3 A_A - (x_p + x_4)k_{spool} - K_{SV}x_5 - F_f\right]$$

$$f_6 = \dot{x_6} = x_7$$

$$f_7 = \dot{x_7} = \frac{1}{(m_1+m_2)}\left[x_2 A_2 - x_1 A_1 - (y_p + x_6)k_1 - K_{AG}x_7 - \left[\frac{\left(\frac{NM_p r^2\omega^2}{2}\right)(tan^{-1}\left(\frac{y_{max}-x_6}{L}\right)) - \left(\frac{NA_p r\gamma}{2\pi}\right)x_1}{L}\right]\right]$$

$$f_8 = \dot{x_8} = \frac{1}{J_m}[x_3 V_m - b_m x_8]$$

3.4. Linear Model Development

A linear model was generated by performing a linearization on the aforementioned non-linear model equations. The primary importance of the linear model was that it provided the gateway necessary to characterize the stability of the system via describing function analysis, using an extension of the Nyquist Stability Criterion [7]. A linearized model was necessary since it allowed for the saturation nonlinearity to be separated from the rest of the model and also allowed for the remaining dynamics (with other nonlinearities) to be simplified as a linear portion and reduced down to a single TF (Single Input Single Output) as shown by the example block diagram displayed in Fig. 14. The separation of the nonlinear and linear portions of the model will be discussed in more detail later in regards to an application of describing function analysis.

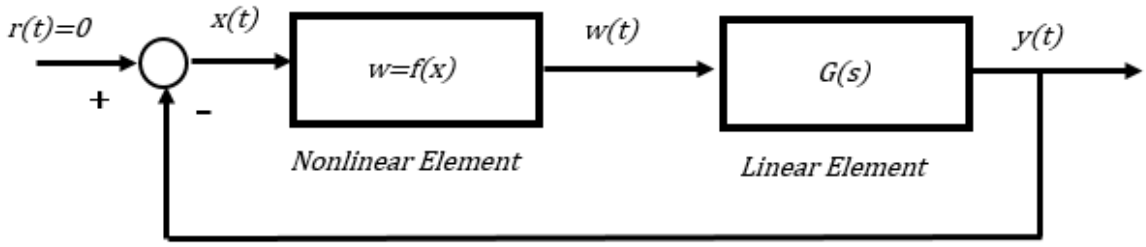

Fig. 14. Nonlinear system represented by separate nonlinear and linear elements

As stated before, a linearization was performed on the system of nonlinear equations in order to obtain a linear model for use in stability analysis for the overall system. For organization and simplification when comparing to the nonlinear model performance, the linearization was formatted according to an SSR as shown in Eq. (23) where A_{sys}, B, C, and D are matrices with sizes 8x8, 8x1, 8x8, and 8x1, respectively. It should be noted that for

the simulations used for the comparison of the nonlinear and linear models, there were no inputs to the system. Simulations were performed with dynamic stimulation coming from the initial conditions for each equation to verify the accuracy of the linearization.

$$\begin{aligned} \dot{\vec{x}} &= A_{sys}\vec{x} + B\vec{u} \\ \vec{y} &= C\vec{x} + D\vec{u} \end{aligned} \tag{23}$$

The linearization was accomplished through the use of the well-known Taylor series expansion and applying a first-order Taylor series approximation. This provided a linear approximation for each state variable with respect to each NL function, f. Each partial derivative was then organized according to the Jacobian matrix that can be seen in Eq. (24). All partial derivatives that were calculated can be found in Appendix B.

$$A_{sys} = \begin{bmatrix} \frac{\delta f_1}{\delta x_1} & \frac{\delta f_1}{\delta x_2} & \frac{\delta f_1}{\delta x_3} & \frac{\delta f_1}{\delta x_4} & \frac{\delta f_1}{\delta x_5} & \frac{\delta f_1}{\delta x_6} & \frac{\delta f_1}{\delta x_7} & \frac{\delta f_1}{\delta x_8} \\ \frac{\delta f_2}{\delta x_1} & \frac{\delta f_2}{\delta x_2} & \frac{\delta f_2}{\delta x_3} & \frac{\delta f_2}{\delta x_4} & \frac{\delta f_2}{\delta x_5} & \frac{\delta f_2}{\delta x_6} & \frac{\delta f_2}{\delta x_7} & \frac{\delta f_2}{\delta x_8} \\ \frac{\delta f_3}{\delta x_1} & \frac{\delta f_3}{\delta x_2} & \frac{\delta f_3}{\delta x_3} & \frac{\delta f_3}{\delta x_4} & \frac{\delta f_3}{\delta x_5} & \frac{\delta f_3}{\delta x_6} & \frac{\delta f_3}{\delta x_7} & \frac{\delta f_3}{\delta x_8} \\ \frac{\delta f_4}{\delta x_1} & \frac{\delta f_4}{\delta x_2} & \frac{\delta f_4}{\delta x_3} & \frac{\delta f_4}{\delta x_4} & \frac{\delta f_4}{\delta x_5} & \frac{\delta f_4}{\delta x_6} & \frac{\delta f_4}{\delta x_7} & \frac{\delta f_4}{\delta x_8} \\ \frac{\delta f_5}{\delta x_1} & \frac{\delta f_5}{\delta x_2} & \frac{\delta f_5}{\delta x_3} & \frac{\delta f_5}{\delta x_4} & \frac{\delta f_5}{\delta x_5} & \frac{\delta f_5}{\delta x_6} & \frac{\delta f_5}{\delta x_7} & \frac{\delta f_5}{\delta x_8} \\ \frac{\delta f_6}{\delta x_1} & \frac{\delta f_6}{\delta x_2} & \frac{\delta f_6}{\delta x_3} & \frac{\delta f_6}{\delta x_4} & \frac{\delta f_6}{\delta x_5} & \frac{\delta f_6}{\delta x_6} & \frac{\delta f_6}{\delta x_7} & \frac{\delta f_6}{\delta x_8} \\ \frac{\delta f_7}{\delta x_1} & \frac{\delta f_7}{\delta x_2} & \frac{\delta f_7}{\delta x_3} & \frac{\delta f_7}{\delta x_4} & \frac{\delta f_7}{\delta x_5} & \frac{\delta f_7}{\delta x_6} & \frac{\delta f_7}{\delta x_7} & \frac{\delta f_7}{\delta x_8} \\ \frac{\delta f_8}{\delta x_1} & \frac{\delta f_8}{\delta x_2} & \frac{\delta f_8}{\delta x_3} & \frac{\delta f_8}{\delta x_4} & \frac{\delta f_8}{\delta x_5} & \frac{\delta f_8}{\delta x_6} & \frac{\delta f_8}{\delta x_7} & \frac{\delta f_8}{\delta x_8} \end{bmatrix} \tag{24}$$

The *B*, *C*, and *D* matrices used in the NL to linear model comparison were organized so that all states appeared in the output vector, *y*, and no inputs were applied to the system since the desired response was prompted from state initial conditions.

CHAPTER 4: MODEL SIMULATION AND VALIDATION

4.1. Non-Linear Model Simulation and Validation

The NL model was the first to be simulated using Simulink®. Coupled subsystems were generated that represented each individual differential equation and together, formed the entire LS hydraulic system as shown in Fig. 15. Figure 15 shows a simplified Simulink® model (this model does not show all the details needed to correctly simulate) that is being provided to strictly exhibit the input and output of each subsystem and not to provide the full model that was actually used. Each colored subsystem represents an individual model for a specific component within the system (each analytical model that was shown previously). Again please note that this model is simplified to only show the input/output relationship within the basic model structure and within each subsystem there exists additional block diagrams used to solve each individual equation (examples of the block diagrams within the subsystems can be found in Appendix D). The stable NL model simulation results can be seen in Fig. 16 through Fig. 20 which display the dynamic responses of all 8 state variables in addition to the time responses for both the swash plate angle and the margin pressure. For these simulations, all state initial conditions were set to 0 except for the PDFCV position, x_4, which was set to the x_{null} position. Also please note that for initial NL model simulations and simulations used to compare the NL model to the linearized model, numerical values were used for certain parameters that differed from those used in the model validation simulations to be shown later. All parameters that were used for the stable NL model simulations and NL and linear model comparison simulations

can be seen in Appendix C. The reason for this difference in the values that were used was for initial modeling, a stable response was desired and the values displayed in the table in Appendix C provided a clean response and verified that the model was working appropriately. Values were changed later for the model validation simulations in order to improve the model response and match the model to the experimental data.

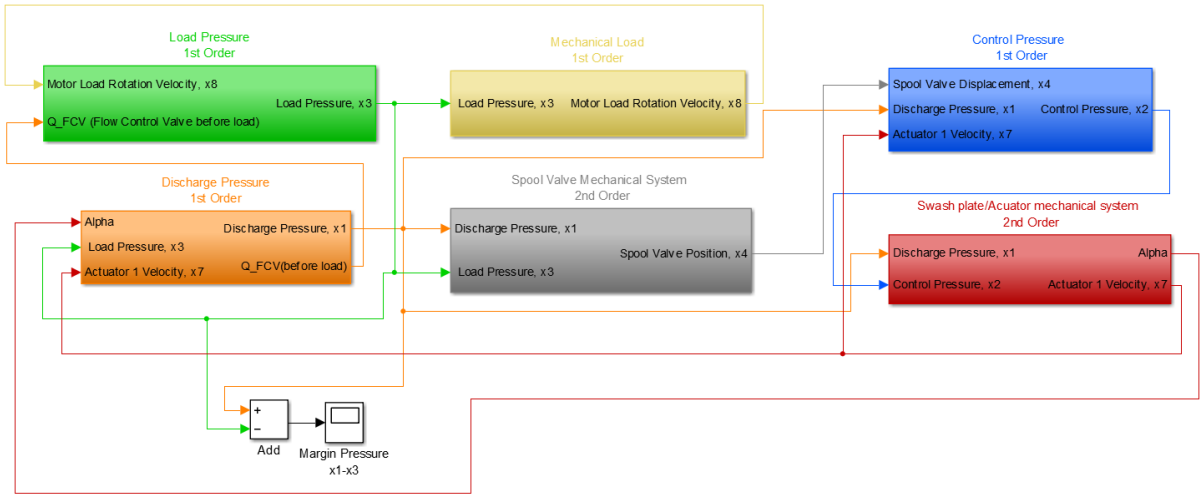

Fig. 15. Basic Simulink® model structure used for simulation of NL model

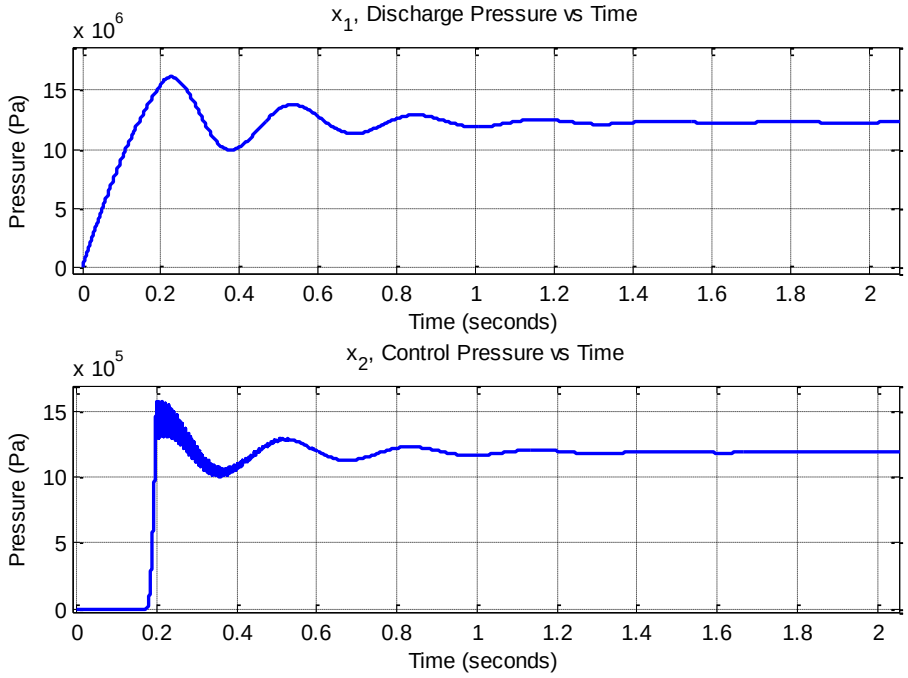

Fig. 16. Stable NL model simulation for discharge and control pressure

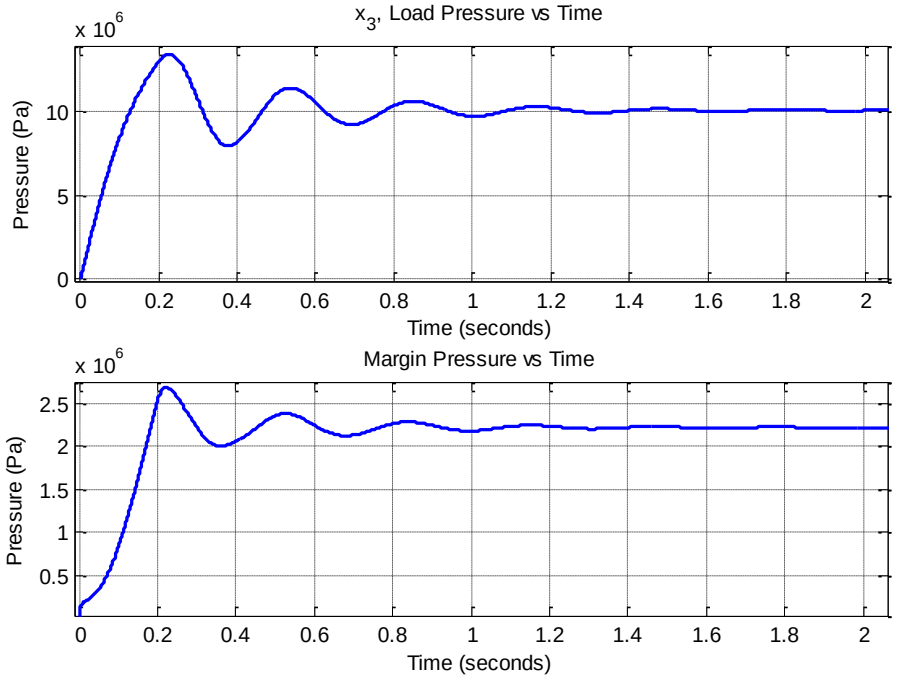

Fig. 17. Stable NL model simulation for load and margin pressure

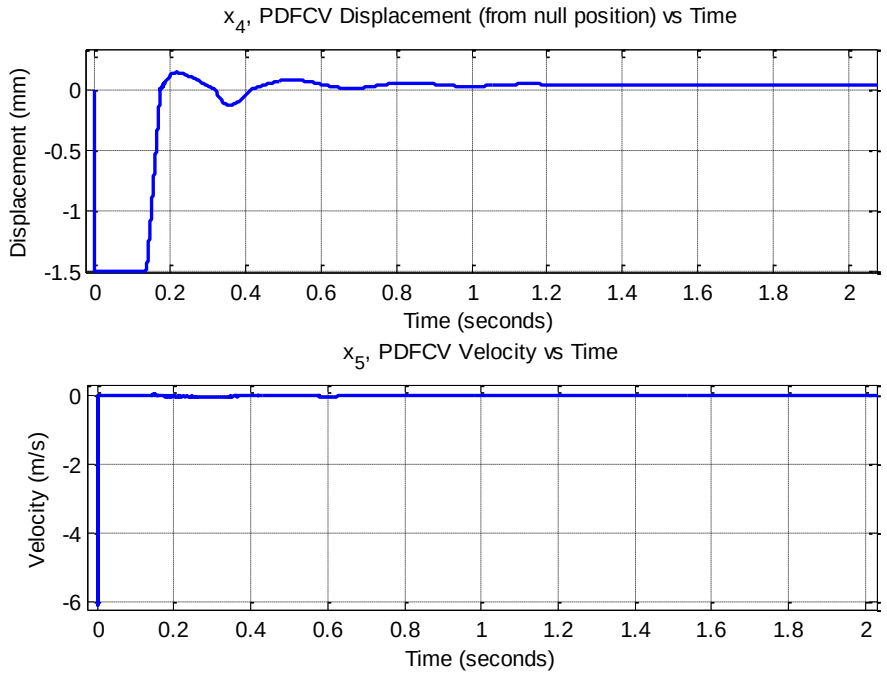

Fig. 18. Stable NL model simulation for PDFCV displacement and velocity

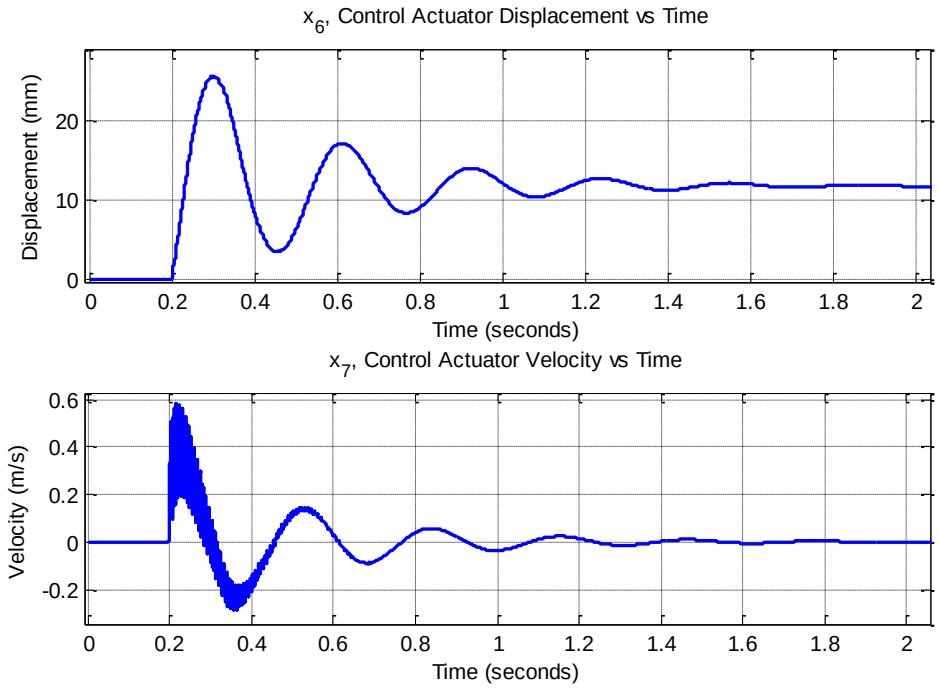

Fig. 19. Stable NL model simulation for control actuator displacement and velocity

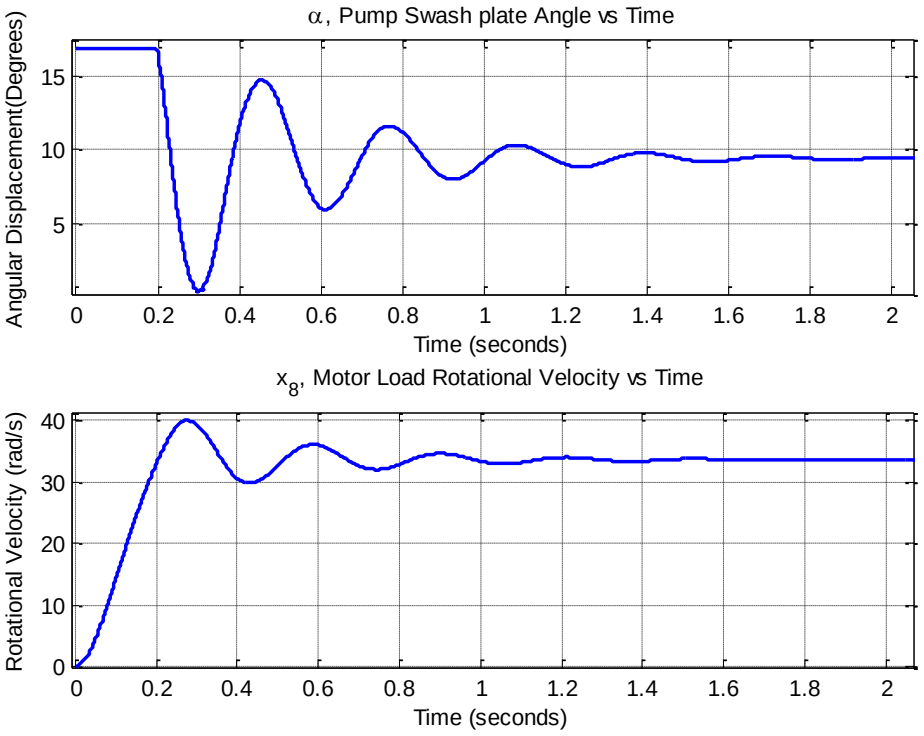

Fig. 20. Stable NL model simulation for swash plate angle and load rotational velocity

Once the NL model was simulated and verified to be stable, experimental data was acquired via hydraulic lab experimental testing in order to properly validate the NL model and ensure that the model was accurate when simulating. The experimental set up that was tested matched exactly to the system components that were shown earlier in the paper for the NL model development. The only difference between the experimental components and the components used to develop the NL model was the load that was being tested. As was mentioned in Chapter 2, for the NL model, the load was represented as a simplified hydraulic motor model. For the experimental testing, an electrically operated pressure reducing valve ("load" valve) was incorporated to simulate a pressure drop for an attached load. In order to properly compare the experimental data and simulation model, the

dynamics defining the simplified hydraulic motor model and load pressure were removed from the NL model and the load pressure data that was experimentally acquired was used as an input to the NL model.

Two types of testing were conducted to validate the model. In both types of testing, a certain rotational speed was selected (250, 500, 750, 1000 rpm) and held constant for the pump as well as the area of the FCV in order to sustain a constant flow rate (ranging from 5 lpm to 100 lpm depending on the pump speed being tested) within the system. The first type of testing conducted was dynamic testing where the setting of the load valve (not the FCV) was adjusted in "steps" approximately every two seconds for a total of two minutes per test to obtain a series of both increasing and decreasing dynamic pressure steps for both the load pressure and pump discharge pressure. Knowing that a LS system works to maintain a constant margin pressure and to only supply the pump discharge pressure necessary to support the highest load pressure needed at that moment within the system, it should be clear that when the load valve setting was adjusted the load pressure changed as well. As a result of the changing load pressure and in order to maintain a constant margin pressure, the pump discharge pressure then responded with a pressure change also as expected. As stated before, the load pressure data that was experimentally acquired was used as the input to the NL model. The resulting experimental pump discharge pressure data was then used as output data to compare to the simulation model's pump discharge pressure output. Table 2 displays the numerical values used in the model validation simulations and Fig. 21 displays the validation of the NL model using the full experimental dynamic testing approach for a pump speed of 500 rpm and a flow rate of 20 lpm. Figure 22 shows the comparison between the experimental flow rate and the model simulated flow

rate that was maintained within the system. The significant decrease in flow that occurs in the middle of the plot is directly related to the pump reaching its maximum operating pressure and as a result the flow was reduced. Please note that the values displayed in Table 2 were varied by trial and error in order to best match the model simulation response to the experimental data and some values may require refinement for future work. For example the bulk modulus listed at 2.8 GPa is believed to be a slightly overestimated value for the oil that was used within the experimental test bed and the density value was assumed to be 85% of the density of water.

Table 2. Parameters and numerical values used for model validation simulations

Model Parameter	*Numerical Value*	*Unit (Metric)*
Spool Valve Diameter	0.007	m
Spring Rate for Bias Spring	4,671.5	N/m
Spring Rate for PDFCV Spring	16,800	N/m
Control Actuator Diameter	0.02965	m
Bias Actuator Diameter	0.01398	m
Piston /Slipper Area	4.15×10^{-4}	m^2
Piston Pitch Radius	0.0469	m
PDFCV Mass	0.005	kg
Control Actuator Mass	0.3452	kg
Bias Actuator Mass	0.1452	kg
Piston Mass	0.1605	kg
Moment Arm Distance for Actuator	.087	m
Maximum Swash plate Angle	16.83 (0.2937)	deg (rad)
Pump Speed	(250,500,750,1000)	rpm
Number of Pistons within pump	9	
Fluid Bulk Modulus (Oil)	2.8×10^{9}	Pa
Fluid Density (Oil)	850	kg/m^3
Pump Discharge Pressure Volume	0.01	m^3
Control Pressure Discharge Volume	0.0005	m^3
Pressure Carryover Angle	20 (0.3491)	deg (rad)
FCV Area	Varied by test	m^2
Discharge Coefficient	0.62	
Contraction Coefficient	0.61	
Jet Angle for Flow Forces	69 (1.2043)	deg (rad)
Pump Volumetric Displacement	1.5915×10^{-5} ($\approx$100)	m^3/rad (cc/rev)
Spool Valve Leakage Area	2.474×10^{-6}	m^2
Actuator Viscous Damping Coefficient	1	N-s/m
PDFCV Viscous Damping Coefficient	1	N-s/m
Desired Margin Pressure	2.9×10^{6}	Pa
Maximum Actuator Displacement	0.0263	m
PDFCV Spring Pre-Load Distance	0.00538	m

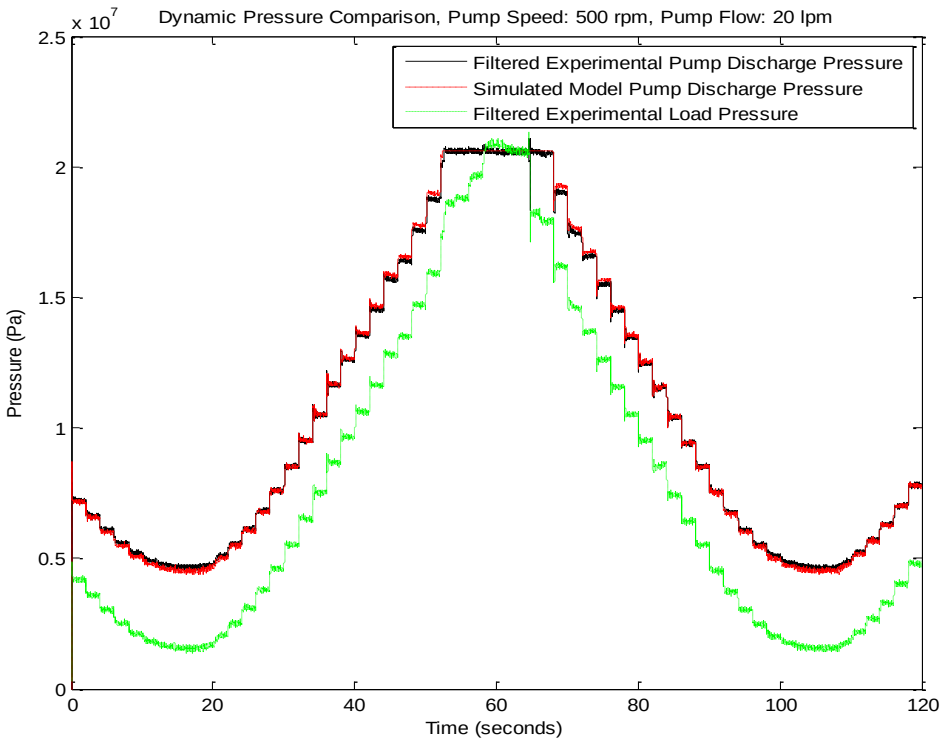

Fig. 21. Dynamic testing pump discharge pressure comparison for 500 rpm/20 lpm

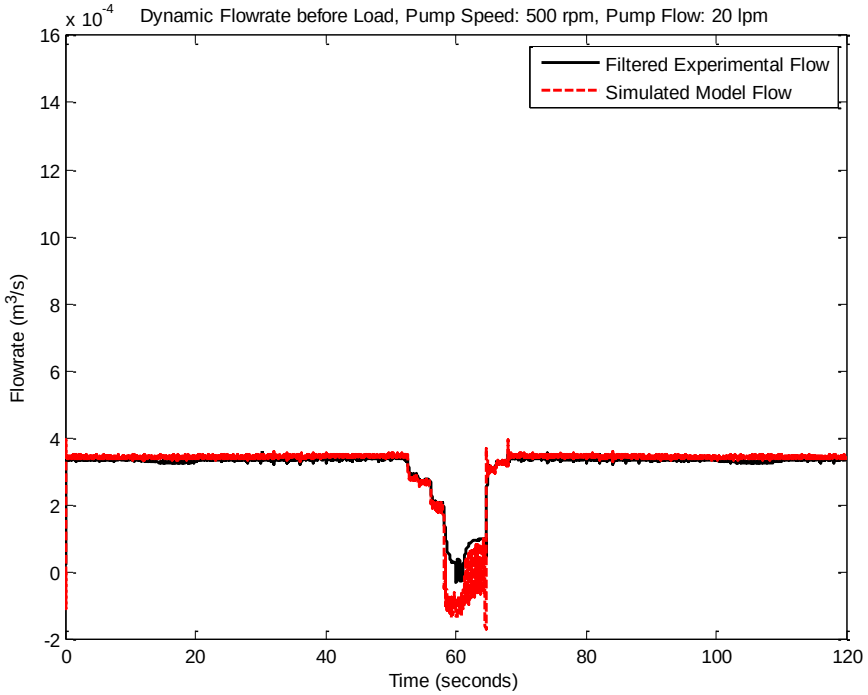

Fig. 22. Dynamic testing flow rate comparison for 500 rpm/20 lpm

Figure 23 displays a magnified section of Fig. 22 to provide a better view of the NL model matching to the dynamic testing experimental data. It is clear from the comparison of the simulated pump discharge pressure and experimentally acquired pump discharge pressure, that the mathematical model successfully and accurately simulates the real LS system being tested. Although the model does match up well, it can be seen for pressures greater than 13MPa or so, the simulated data begins to offset slightly from the experimental data. The reason for this is the margin pressure within the experimental system actually began to decrease from its prescribed setting of 2.9MPa to as low as 2.6 MPa for some tests while the simulated model kept the margin pressure constantly set to 2.9MPa. The pump within the experimental test bed may have had additional leakage that was not incorporated into the NL model being simulated such that the real system may have been unable to continuously maintain the desired margin pressure.

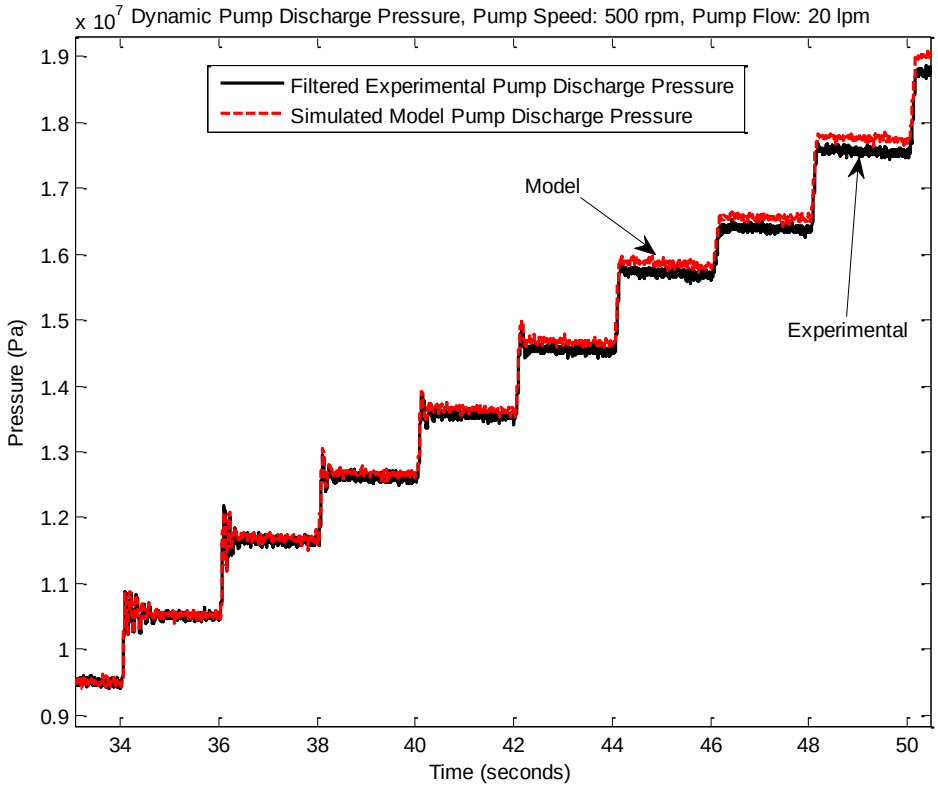

Fig. 23. Magnified view of Fig. 22 - Dynamic testing pump discharge pressure comparison

Figure 24 shows a further magnified view of a single pressure step response within Fig. 23. Due to the noise within the experimental data, it is slightly difficult to see the exact nature of the pressure response other than there is some slight oscillation about the 10.5 MPa point, but it is certainly clear that the simulated response matches very well in terms of matching the overshoot, transient response, and average steady-state value of the experimental data. Figure 25 is simply an additional example of how well the model matched the experimental data. In this case a decreasing pressure step response is displayed for 750 rpm at 20 lpm and indicates an even more active transient response. Even with the

increased activity within the transient portion of the response, it is still clear that the model matches very well to the general response indicated by experimental data.

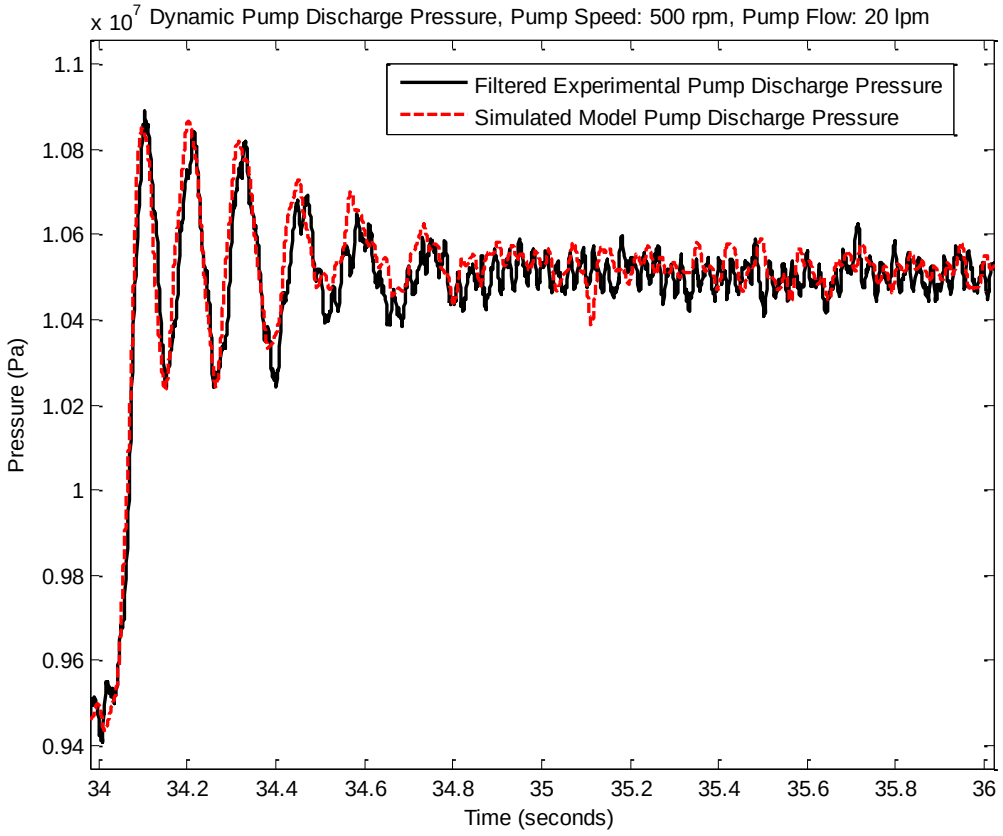

Fig. 24. Single pump discharge pressure step response for dynamic testing at 500 rpm/20 lpm

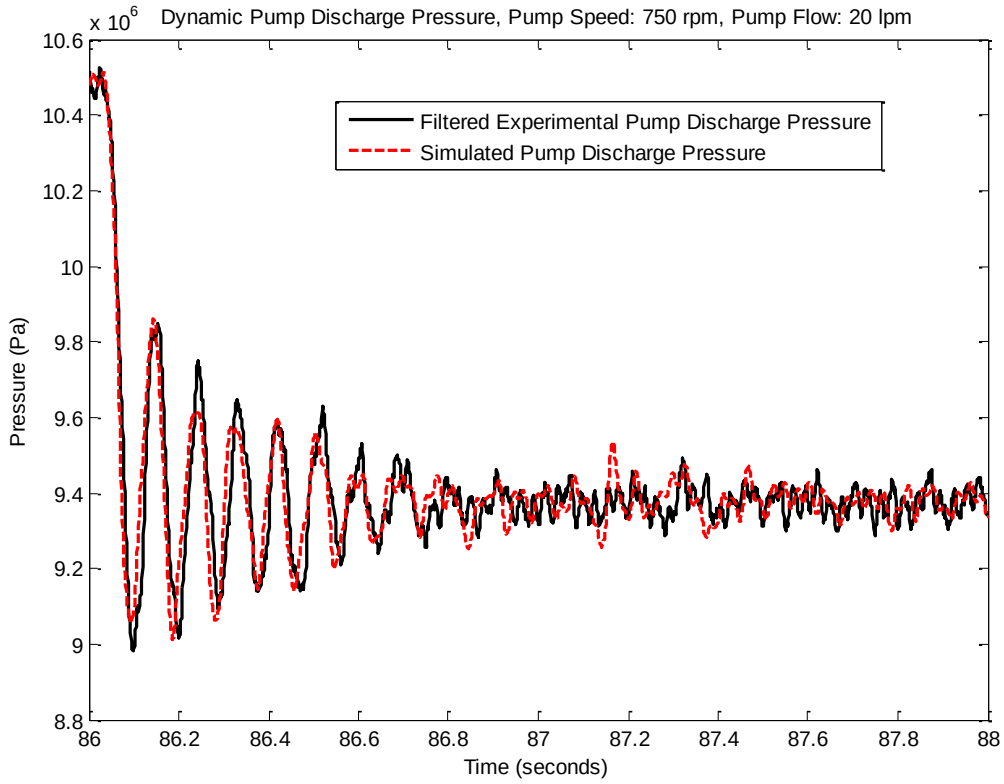

Fig. 25. Single pump discharge pressure step response for dynamic testing at 750 rpm/20 lpm

The second type of experimental testing that was conducted was considered quasi-steady state testing. In this type of testing the setting of the load valve was slowly but continuously adjusted so that the load pressure was varied similar to the previous experiment except with removal of the dynamic steps and instead obtaining a steady and fairly linear pressure response both increasing and decreasing. Figure 26 displays the comparison of the nonlinear model results with the experimental quasi-steady state testing approach for again a pump speed of 500 rpm and a flow rate of 20 lpm. As was the case for the dynamic testing, the results appear the same for the quasi-steady state test. The simulated NL model

seemed to match very well to the experimental data that was obtained across all pressures.

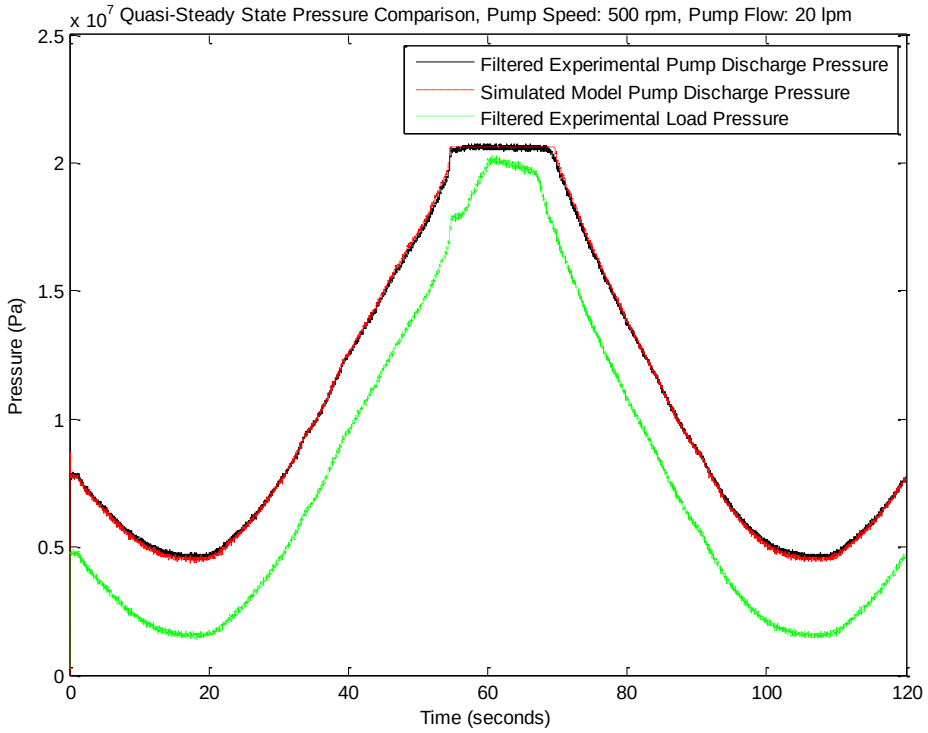

Fig. 26. Quasi-steady state testing for 500 rpm/ 20 lpm

Figure 27 then shows a magnified view of the same quasi-steady state experimental test for a pump speed of 500 rpm and flow at 20 lpm. The results again show in more detail the accuracy and validity of the model. Similar to what was happening in the dynamic testing though, the simulated response slowly begins to offset slightly from the experimental data around the 13MPa mark due to the decrease in margin pressure in the experimental test bed. Figure 28 shows the final magnified view of the quasi-steady state test and again verifies how well the model matches the experimental data.

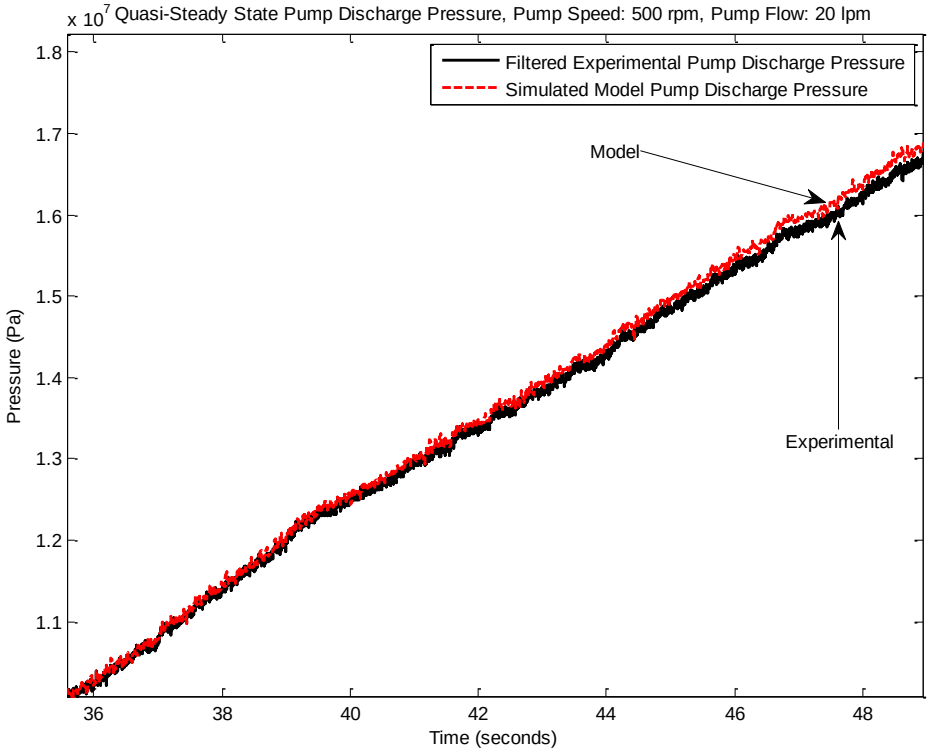

Fig. 27. Magnified view of Fig. 26 – quasi- steady state testing for 500 rpm/ 20 lpm

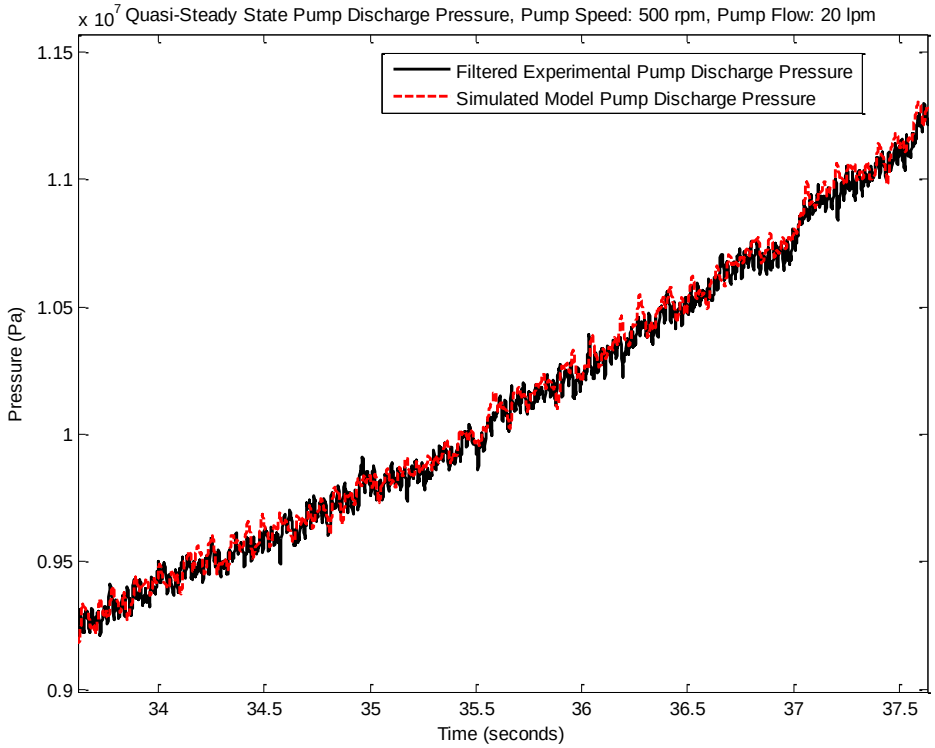

Fig. 28. Detailed view of model validation quasi-steady state testing for 500 rpm/ 20 lpm

Approximately sixty experimental tests were conducted overall (including both dynamic and quasi-steady state) with each test output matching closely to the previously shown figures in this section. Due to the extensive amount of data that was gathered in addition to the model simulation data, only twenty-six tests were used to thoroughly compare the model and experimental data and provide error quantification. For each of the twenty-six tests the root-mean-squared-error (RMSE) was calculated using

$$RMSE = \sqrt{\frac{\sum(w-\hat{w})^2}{n}} \tag{25}$$

where w represents the experimental data, $\hat{w}$ represents the model simulation data, and n represents the total number of data points being compared. In order to calculate this RMSE,

each individual test was segmented into thirty sets of data (two seconds of data for each set consisting of exactly two thousand and one data points). Within each two second set of data, the model and experimental data for that specific period of time were compared to calculate the RMSE. The first fifteen sets of data define the increasing portion of the experiment and the last fifteen sets of data define the decreasing portion of the experiment. There were two main reasons for organizing the data this way. The first was due to the different sampling rates (using a variable-step solver in Simulink® caused the model data to initially vary in step size) in between the experimental and model data. By organizing the data into these thirty, equally-sized sets and down sampling the model data to match the experimental data precisely in terms of the number of points, a direct, consistent and accurate comparison of each data point could be completed. The second reason was that this organization provided a reduction in the overall data needing to be analyzed and focused on the most important and interesting portions of each experimental test.

The mean, maximum, and minimum RMSE values for the first fifteen sets of data and last fifteen sets of data were tabulated for each of the twenty-six experiments that were chosen for comparison and can be seen in Table 3. The *I* and *D* displayed within Table 3 stand for the *INCREASING* and *DECREASING* portions of the experiment and respectively represent the first fifteen and last fifteen sets of data analyzed for each experiment. As stated earlier, for each comparison between the model and the experimental data, it was noticed that at the lowest pressures during the testing and pressures above approximately 13 MPa, the model and the experimental data matched well in terms of overshoot and frequency of oscillation but were just slightly offset due to the difference in margin pressure between the experimental test bed and the model. This can be seen in Fig. 29

where an example of the RMSE values for dynamic testing at 750 rpm and 20 lpm are provided in relation to their corresponding data set (keep in mind each data set contains a two second pressure step time response). The maximum RMSE always occurred at pressures above 13MPa (data sets 11-19) due to the offset caused by the difference in margin pressure between the model and the experimental test bed. The RMSE proved to be a valid method for quantifying error at lower pressures when the model and experimental data were reaching approximately the same steady-state value, but at the higher pressures when there was an offset between the steady state values of the model and experimental data, the RMSE did not provide the accuracy that was desired when quantifying the error. This is due to the RMSE taking into account only the difference between each numerical data point and as a result even though the model was matching the experimental data well in terms of the shape of the dynamic response, the RMSE method still resulted in calculations of increased error due to the large difference in numerical values. Although it is correct that the error reflect this pressure offset between the model and experimental data since it does indicate error within the model, it inappropriately diagnoses the effectiveness of the model across the entire pressure range of the LS system. In order to counteract this scenario where the RMSE was indicating extreme error at higher pressures, another method was utilized in addition to the RMSE being calculated.

Table 3. Root mean squared error for model validation simulations

	Pump Speed (RPM)	*Flow (LPM)*	*RMSE (KPa)*					
			MEAN		*MAX*		*MIN*	
			I	*D*	*I*	*D*	*I*	*D*
DYNAMIC	250	5	132.8	133.9	250.2	222.9	87.9	95.4
		15	102.7	102.7	190.4	173.4	61.9	64.4
		20	100.9	100.0	210.3	186.2	52.2	51.5
	500	15	120.0	124.6	239.3	237.3	73.1	79.6
		20	100.8	102.6	205.7	200.1	51.1	55.0
		25	96.3	93.4	206.0	195.3	49.0	44.8
	750	20	115.8	111.39	272.1	246.0	59. 9	60.7
		25	105.4	101.9	238.6	237.2	47.4	44.5
		50	130.9	112.7	324.6	300.3	37.0	32.6
	1000	20	124.4	125.3	280.3	273.2	63.9	66.5
		25	112.9	114.4	283.6	263.3	47.5	53.9
		50	121.4	114.9	298.1	288.9	44.9	40.3
		80	170.8	154.2	398.8	381.6	37.5	37.0
QUASI-STEADY STATE	250	5	122.0	138.3	216.2	263.2	81.6	94.1
		15	93.2	106.6	176.1	214.8	53.5	57.1
		20	90.2	100.8	186.7	220.5	42.5	49.8
	500	15	115.2	126.6	238.2	294.8	67.2	68.9
		20	91.0	104.2	173.6	223.9	51.3	51.9
		25	89.2	100.5	188.2	229.1	40.1	39.1
	750	20	108.6	116.0	246.8	305.9	51.6	52.5
		25	93.4	105.9	214.5	216.7	44.6	40.1
		50	113.6	116.8	282.9	314.6	35.6	34.5
	1000	20	109.4	127.9	227.2	309.2	62.9	60.7
		25	102.1	115.4	243.9	294.0	42.5	45.6
		50	111.8	121.1	279.5	312.7	38.5	36.8
		80	153.8	160.2	369.9	425.5	36.6	40.2

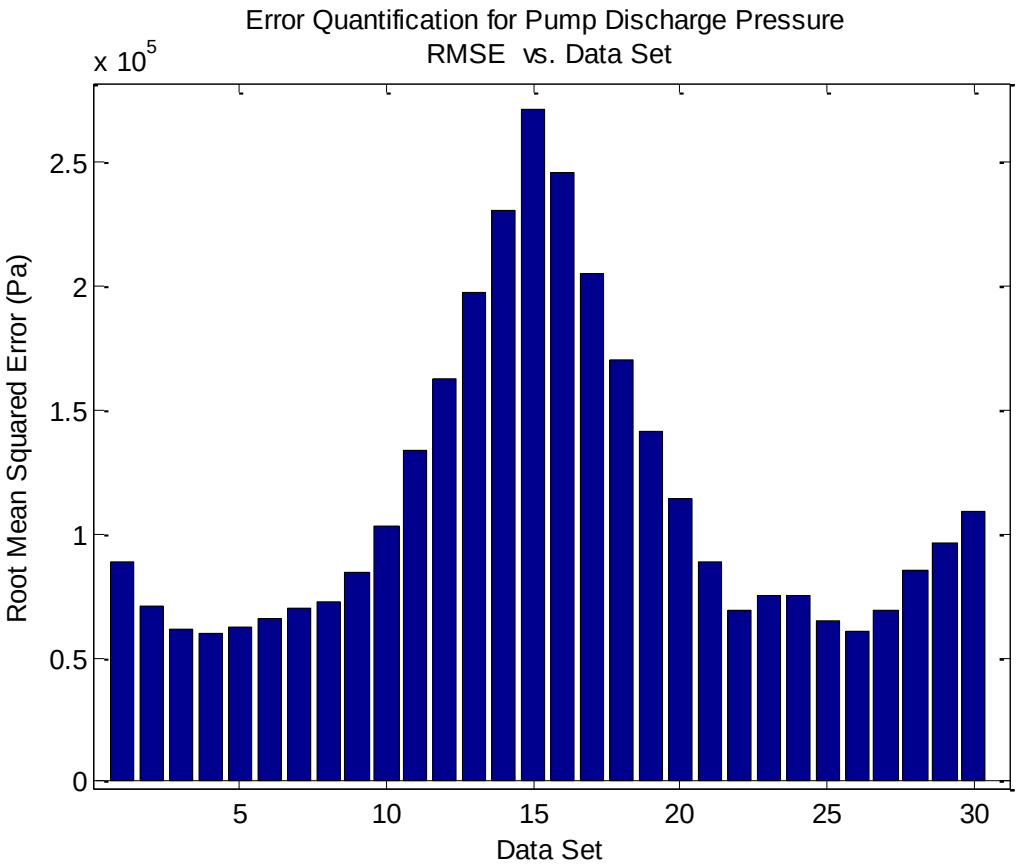

Fig. 29. RMSE plotted against data sets for dynamic testing at 750 rpm/ 20 lpm

The Fast Fourier Transform, or FFT for short, was implemented within MATLAB® to analyze the data within the frequency domain. This method provided the means necessary to show that the resonant frequencies within the simulated model data matched well to the experimental data even though there was offset between the steady state values of the time response data. Two examples are provided where the time response data that is shown clearly indicates there is a steady state offset between the data sets. As stated previously, this offset caused the model error to be unreliably quantified with a high RMSE value even though the other characteristics defining the responses matched well. The first example shown in Fig. 30 represents data set 16 in Fig. 29 which is the dynamic time

response data acquired at a pump speed of 750 rpm and a flow rate of 20 lpm. The experimental data reached a steady state value of approximately 18.8 MPa and the model simulated to a steady state value of approximately 19.1 MPa. This time response data was then analyzed within the frequency domain using the FFT and the resulting frequency response can be seen in Fig. 31 where it is clear that the frequency response of the model matches almost seamlessly to that of the experimental data. The same process was then completed for a second experimental dynamic test scenario shown in Fig. 32 to prove the consistency and validity of the results. This test was conducted at a pump speed of 500 rpm and a flow rate of 20 lpm and featured a slightly different transient response compared to that which was shown in the first case but the frequency response results proved to be just as consistent as seen in Fig. 33.

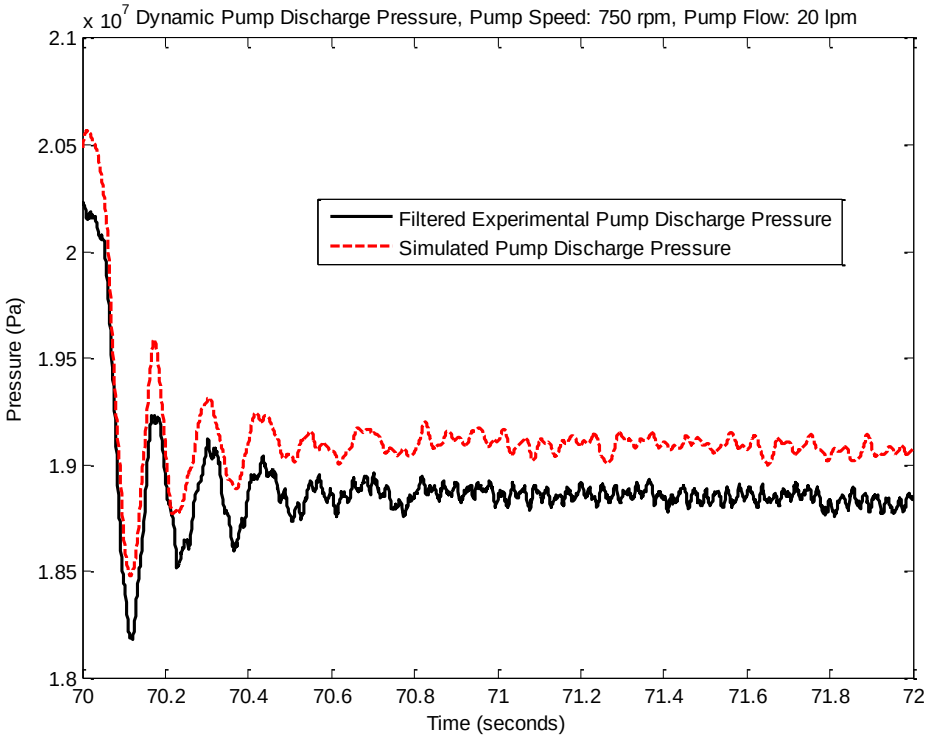

Fig. 30. Offset pressure step response between model and experimental data for dynamic testing data set 16 at 750 rpm/ 20 lpm

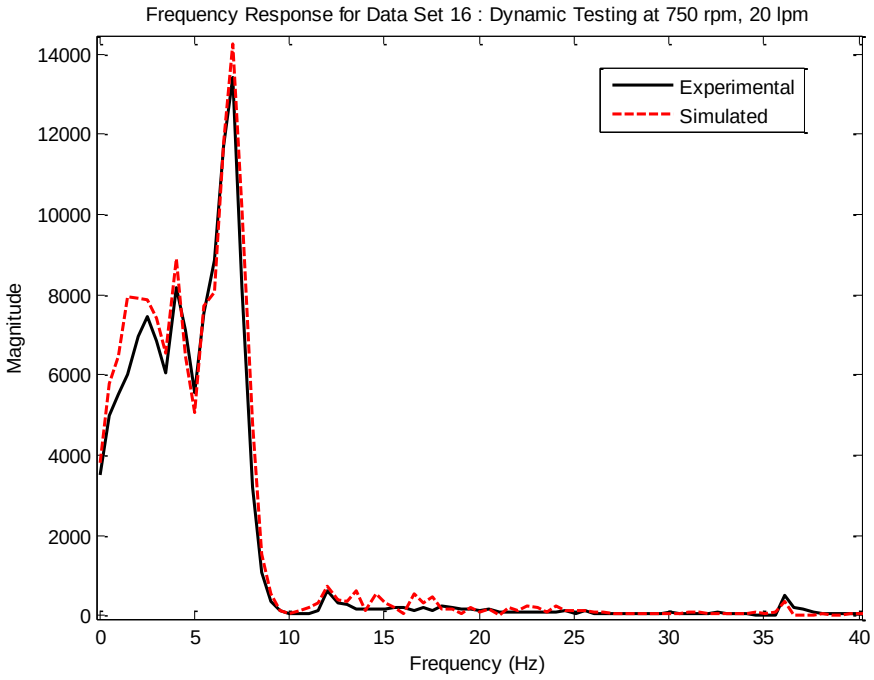

Fig. 31. Frequency response for data set 16 in Fig. 30

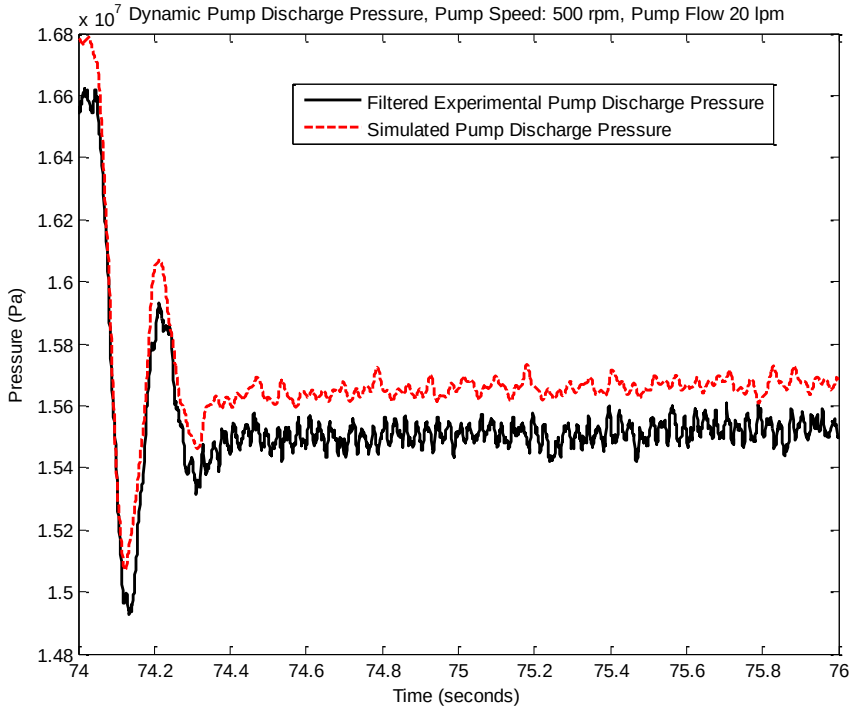

Fig. 32. Offset pressure step response between model and experimental data for dynamic testing data set 18 at 500 rpm/ 20 lpm

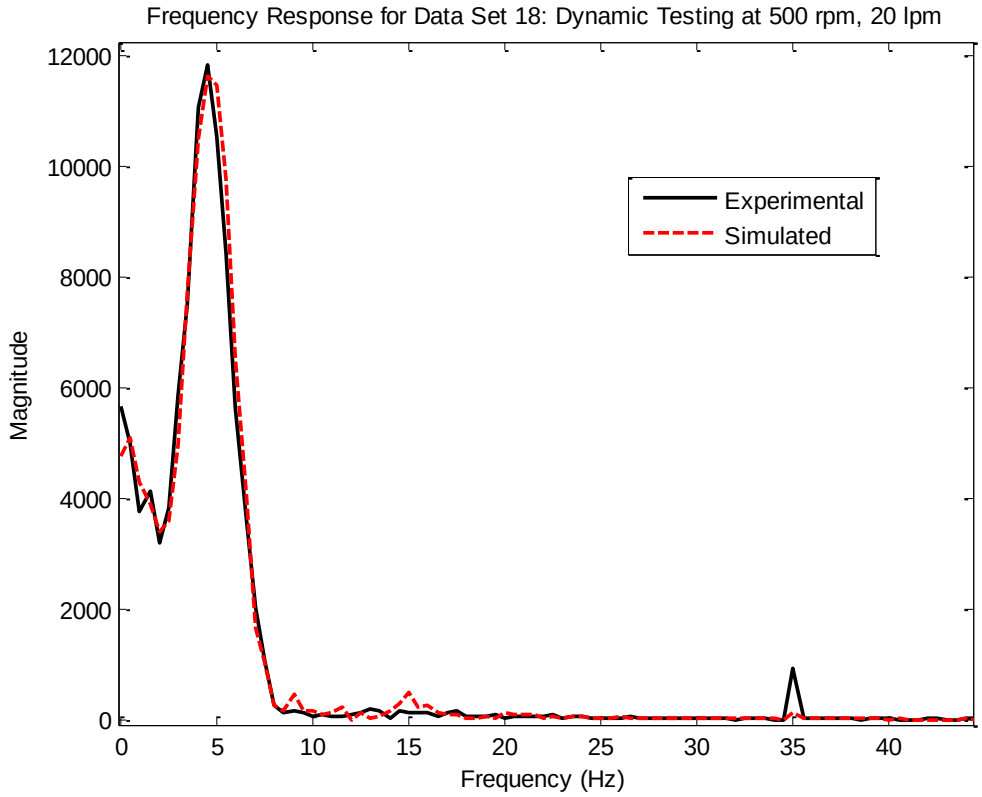

Fig. 33. Frequency response for data set 18 in Fig. 32

4.2. Linear and Non-Linear Model Comparison

The stable NL model was then compared to the linearized model using Simulink® to verify that the models matched adequately and that the linearized model was correct and stable. The performance of both the nonlinear and linear models was evaluated by comparing the dynamic response of each state as it varied with time. Three main points of comparison were checked for the dynamic response of each state variable. These three points consisted of: 1. Does the initial slope of the response match almost exactly for both models? 2. Does the transient portion of the response match adequately for both models? and 3. Do both models reach a similar SS value with no signs of oscillation or instability?

A common difficulty of simulating a linearized model is the identification of nominal operating points and initial conditions for each state that appears in the linearized system. The operating point for each state helps define the stability of the linear system (by identifying the eigenvalues of the A_{sys} matrix) and this is where the nonlinear model was extremely beneficial. For this problem, the nonlinear model was simulated using the previously mentioned and formulated Simulink® model. The nonlinear model was simulated twice where the first stable simulation was conducted for 5 seconds with the initial state conditions all being equal to 0 (except for the PDFCV which was in the null position due to a spring force pre-load) allowing for the hydraulic system to fully stabilize and reach steady-state (SS). MATLAB® code was then written to take an average of a large number of the last data points (the number of data points averaged depended on when the system clearly arrived at SS to ensure that an accurate SS value was obtained) for each state. These averaged values then acted as the nominal operating points for the linear model. In order for the model comparison between linear and nonlinear to match up, the nonlinear model was then simulated a second time but this time with the initial conditions set as the previously stored SS values (from the first simulation) with a small perturbation (~$1/1000^{th}$ of the SS value) being added to each value. The small perturbation values alone then acted as the initial conditions for the linear simulation [24]. The minuteness of the perturbed value ensured that the linear model would stay within the linear range of the nominal operating point for each state in the system. Comparison simulations were completed and provided outputs for each state variable in addition to the margin pressure and swash plate angle which can be seen in Fig. 34 through Fig. 37. The transient responses do slightly differ for a few states but this is believed to be from other nonlinear effects that

the linearized model did not account for. For this reason, the linearized model was adjusted through trial-and-error in order to obtain a response that matched well to the NL model response. The main adjustment that was made was the incorporation of the leakage, K_{SVA}, within the $\frac{\partial f_5}{\partial x_1}$ and $\frac{\partial f_5}{\partial x_2}$ terms of the linearization (partial derivatives can be found in Appendix B). The incorporation of the leakage within these terms was not inherently obvious and future research should investigate if the inclusion of the leakage within these terms is even appropriate or logical (leakage showing up in the flow force terms may be the key). More appropriate or other correct adjustments could possibly be made instead to better match the linearized model to the NL model. Also refinement of the linearized model for the operating point, $x4_o < x_{null}$, may be necessary for future research due to the leakage possibly being inappropriately accounted for within the linearization.

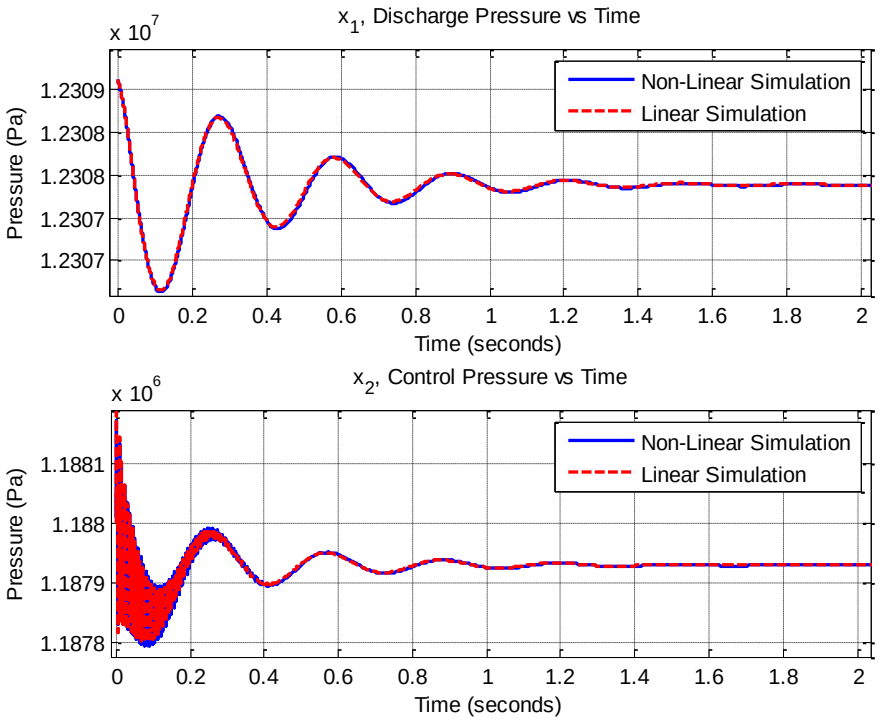

Fig. 34. NL and linear model comparison for discharge and control pressure

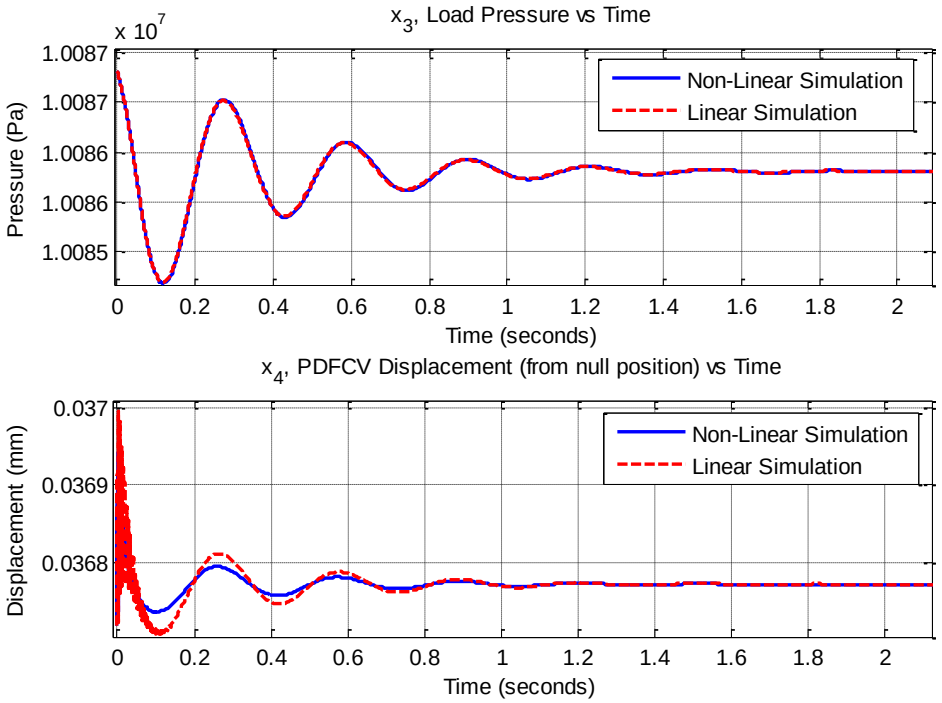

Fig. 35. NL and linear model comparison for load pressure and PDFCV displacement

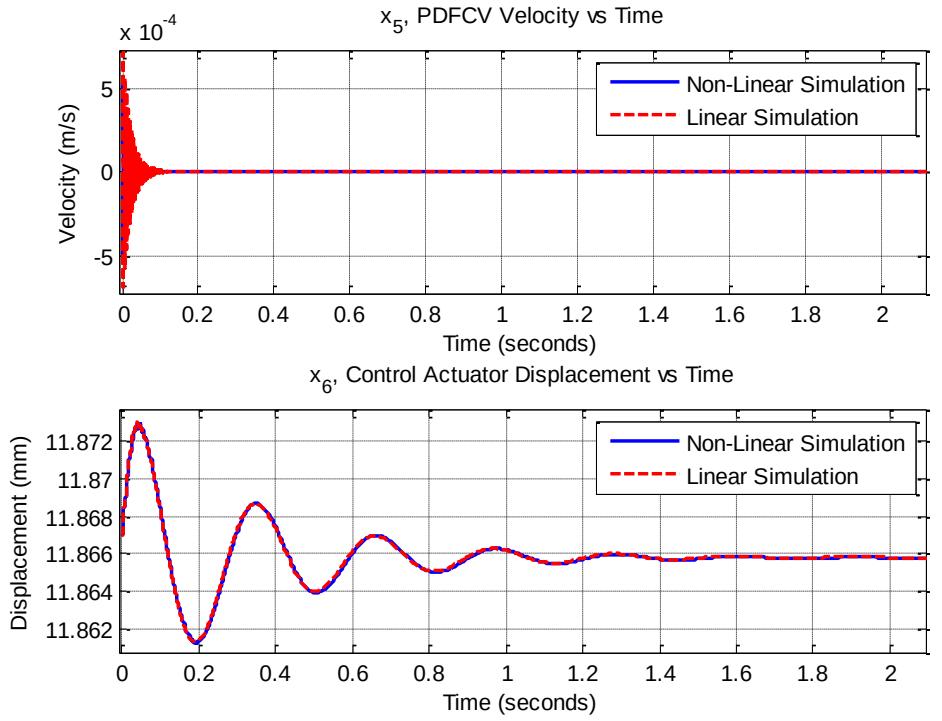

Fig. 36. NL and linear model comparison for PDFCV velocity and actuator displacement

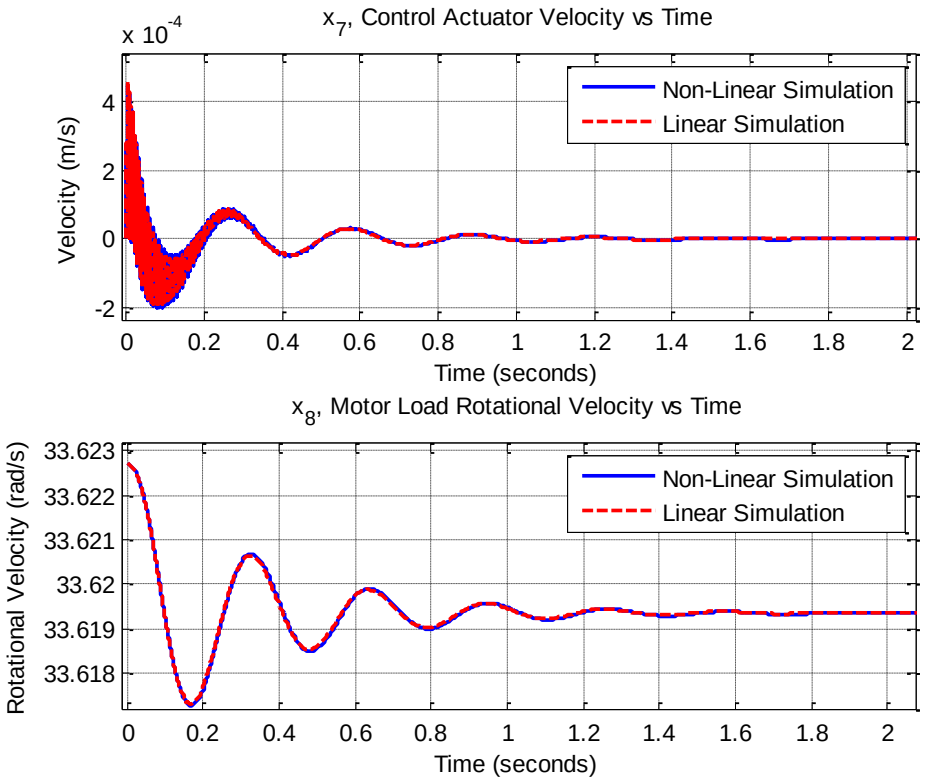

Fig. 37. NL and linear model comparison for actuator velocity and load rotational velocity

CHAPTER 5: METHOD OF ANALYSIS FOR STABILITY DIAGNOSIS

5.1. Background on Describing Function Analysis

Describing function analysis was a graphical method used to assist in analyzing the stability of the nonlinear model for this research. By separating the "hard" nonlinearities, such as saturation for this LS system, in a nonlinear system from the linear portion of the dynamics, a describing function can be identified to approximate the nonlinearity and not only predict the existence of limit cycles within the system but also provide insight into the parameters that characterize the limit cycles (i.e., the amplitude and frequency of oscillation). The primary reason for investigating the stability of this system using describing functions (since the same objective can be accomplished other ways, one for example would be simply using a valid nonlinear model like the one previously displayed in this thesis) is for the purpose of improvement and convenience during the system design stage. Using describing function analysis could greatly improve the efficiency of the design stage of a LS system or pump since ideally it would be possible to quickly change design parameters and then predict and identify the stability of the proposed system by simply addressing the system in the frequency domain (specifically the system's Nyquist diagram) as opposed to the computationally intensive scenario of running countless trial-and-error nonlinear simulations or other time-consuming alternatives.

Before diving into the analytical aspects of describing function analysis, the primary assumptions as applied to the NL system under investigation will first be considered due to their importance in the final results to be shown later. There are four

conditions that the NL system being analyzed, must satisfy in order for the basic version of the describing function method to be generated [27]. The first assumption is that only one NL element is present in the system. Two different options are available in order to follow this condition with the first being the option to lump several nonlinearities together (such as two in parallel) into a single NL element or the second option being to select a primary nonlinearity and neglect the others, which for this analysis was the case. Only one nonlinearity was selected and analyzed and the presence (if other nonlinearities were present) of any other nonlinearities was neglected. The second assumption is well known and is actually due to the describing function method being an extension of the Nyquist criterion which is limited to only apply to linear time-invariant systems (autonomous systems). The third assumption is the most vital (at least in reference to the results of this research) and fundamental. In fact, it is referred to as the fundamental assumption of the describing function method and basically defines that a describing function is only an approximation for a NL element that after having a sinusoidal input applied, provides an output that contains both low and high frequency harmonics. The approximation is a result of the assumption that only the fundamental component of the output response of the NL element needs to be accounted for and any higher-frequency harmonics within the output are allowed to be neglected. As a result of assuming only the fundamental component needs to be taking into account, the linear element, coming after the NL element as shown in Fig. 38, must act as a low-pass filter. The fourth and final assumption, stating that the nonlinearity is odd, describes the symmetry between the input and output of the NL element and is used for simplicity when applying the Fourier expansion for development of the describing function.

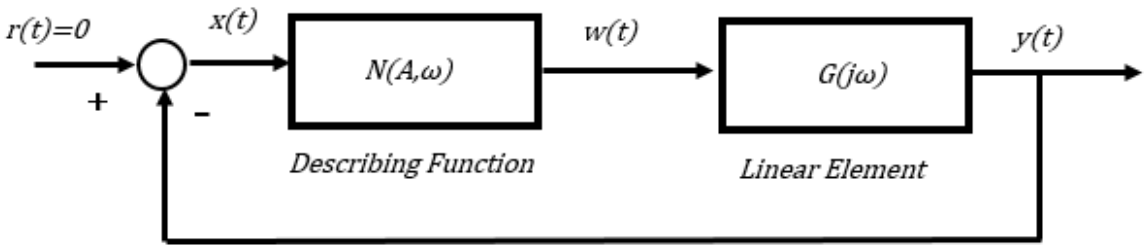

Fig. 38. Nonlinear system approximated by describing function and linear element

Fig. 38, which was just addressed, shows a nonlinear system that is very much like Fig. 14 that was shown previously. Note that negative feedback is assumed in Fig. 38 which is typical of feedback control system analysis. The difference here should be noted, that the NL element is now being approximated by a describing function where it is assumed that self-sustained oscillations of amplitude A and frequency ω exist within the system. For clarification without providing the full, basic derivation here (summarized derivation can be found in Appendix A) a describing function of the nonlinear element as defined by Slotine and Li, is "the complex ratio of the fundamental component of the nonlinear element by the input sinusoid…". With this in mind, each variable in Fig. 38 can then be defined as follows:

$$\begin{aligned} x(t) &= A\sin(\omega t) = -y \\ w &= N(A,\omega)x \\ y &= G(j\omega) \end{aligned} \tag{26}$$

resulting in the equation

$$y = G(j\omega)N(A,\omega)(-y) \tag{27}$$

and, since $y \neq 0$, Eq. (27), simplifies to

$$G(j\omega) = -\frac{1}{N(A,\omega)} \tag{28}$$

From this equation it can be seen that an unknown amplitude and frequency corresponding to the limit cycles present in the system will act as a solution [27]. If a solution is not present, this indicates that there are no limit cycles in the system. An analytical form of the describing function must be defined for each nonlinearity in order to solve Eq. (28). For saturation the corresponding describing function is defined as

$$N(A) = \frac{2k}{\pi}\left[\sin^{-1}\frac{a}{A} + \frac{a}{A}\sqrt{1-\frac{a^2}{A^2}}\right], \tag{29}$$

where a represents the range of the linearity, k represents the slope of the linearity, and A indicates the amplitude of the sinusoidal input (derivation provided in Appendix A). Here it should be noted that the saturation describing function is only a function of the amplitude and not of the frequency so when graphically defined in the complex plane, the function will only appear along the real axis. Typically, due to the difficulty of finding an analytical solution to Eq. (28), a graphical method of identifying the solution is opted for by creating a Nyquist plot of $G(j\omega)$ and then plotting $-\frac{1}{N(A,\omega)}$ on the same complex plane to locate any intersections between the two curves [11, 22, 23, 27] and other previous studies have utilized this or a similar application of describing function analysis as an approach to various hydraulic systems but with different nonlinearities in focus [8, 14]. The amplitude and frequency that correspond to any intersections then act as the solutions to Eq. (28). Multiple intersections are possible, indicating that multiple solutions do exist but are dependent on the initial conditions in the system. In addition to identifying intersections within the complex plane and limit cycles within the system, the stability of the identified

limit cycles can be determined as well. The stability of a limit cycle is determined by encirclements within the complex plane [27, pg.184-186]. A limit cycle is stable if an intersection is identified within the complex plane and the describing function in the direction of increasing amplitude from the point of intersection is NOT encircled by $G(j\omega)$. If the describing function in the direction of increasing magnitude from the point of intersection IS encircled by $G(j\omega)$ then the limit cycle is unstable.

Two cases of saturation were possible for the given LS system and so two describing functions, one for control actuator saturation and one for PDFCV saturation, were necessary in order to appropriately investigate each case. Both saturation describing functions can be seen in Fig. 39 and Fig. 40 where they are plotted against varying amplitude of the sinusoidal input. These plots were used to back calculate the amplitude of the oscillation that was predicted by the inverse of the describing function in the complex plane. Also, please note that these plots will change based on the range of linearity and slope of linearity that is specific to the system under investigation. The plots provided are not universal and should be checked before attempting to back calculate a predicted amplitude.

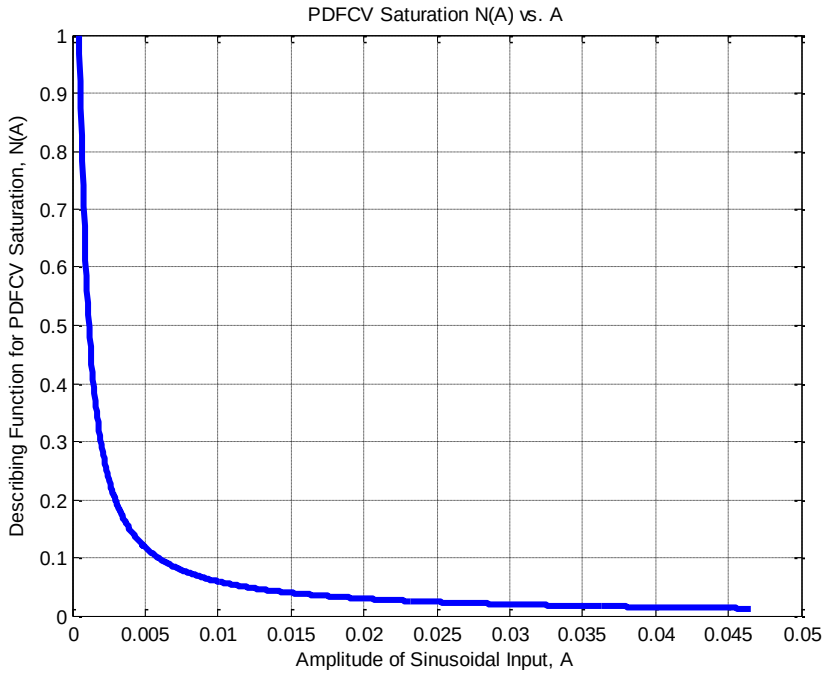

Fig. 39. Describing function for PDFCV saturation

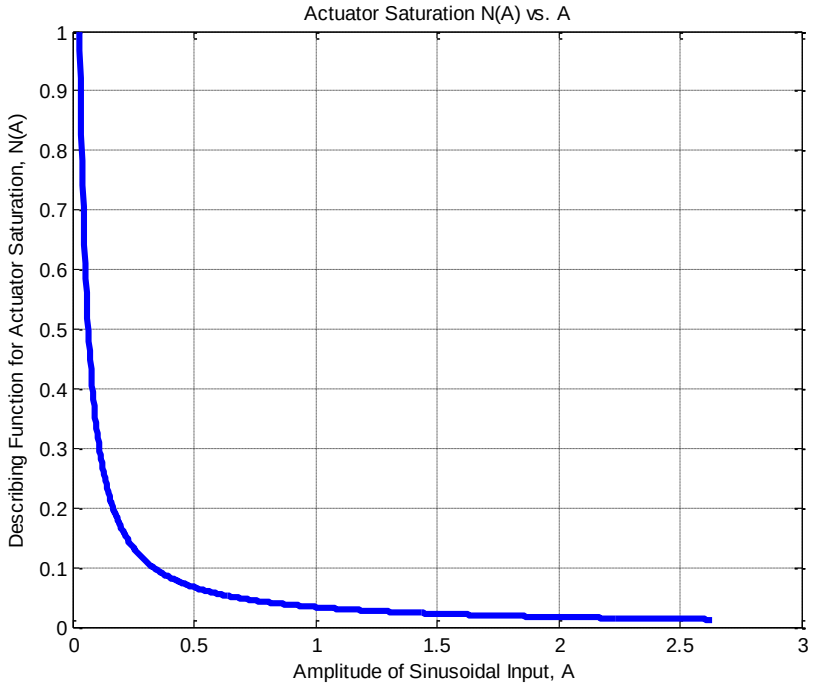

Fig. 40. Describing function for control actuator saturation

5.2. Determination of Linear Element, *G(s)*

Once the linearization was complete and the describing functions for the saturation nonlinearity cases were identified, an acceptable linear element denoted as *G(s)*, that accurately and correctly represented the dynamics of the hydraulic system was necessary in order to conduct the stability analysis. As stated before for saturation, the primary components affected were mainly limited to the two mechanical systems, the PDFCV and the control actuator that displaces the pump swash plate. From test simulations it seemed apparent that both systems were equally susceptible to saturation and as a result *G(s)* needed to be determined for both cases. Following along with Fig. 38 that was displayed earlier, either the actuator displacement or the PDFCV displacement (depending on the saturation case being considered), needed to act as both the input and output for the linear element and as a result *G(s)* needed to be a SISO TF. *G(s)* was generated by first properly redefining the correct input and output for the linearized system through a restructuring of the A_{sys}, B, and C matrices, which will be more thoroughly explained later, and then finding the corresponding transfer function through MATLAB®. *G(s)* is dependent upon the values used in A_{sys} and so the nominal operating points chosen will change A_{sys} and subsequently alter *G(s)*. Here the TF *G(s)* will be presented for the stable system that was simulated. For the PDFCV saturation case, *G(s)*, in zero/pole/gain form with both the input and output being equal to x_4, was calculated to be

$$\frac{-2.655e09\,(s+311.3)(s^2+19.87s+578.8)(s^2-223.4s+1.112e05)}{(s+85.52)(s-15.85)(s^2+35.65s+379.9)(s^2-67.05s+7.721e05)(s^2+200s+2.545e07)} \tag{30}$$

For the control actuator saturation case, *G(s)*, again in zero/pole/gain form with both the input and output being equal to x_6, was calculated to be

$$\frac{3.883e05\ (s-4471)\ (s^2+14.72s+500.1)(s^2+5377s+4.968e07)}{(s+91.71)\ (s-0.172)\ (s^2+19.95s+113.5)(s^2+34.25s+7.729e05)(s^2+92.54s+2.543e07)} \quad (31)$$

Take note that Eq. (30) and Eq. (31) are both SISO transfer functions where *s* represents the Laplace variable and the 8th order polynomial on the bottom is due to the system being 8th order overall.

In order to obtain these transfer functions the following process was conducted and will be explained. For this example the control actuator saturation will be the desired case. Initially, all NL equations containing x_6 (depending on the saturation case to be analyzed the same could be done for x_4 in the case of the PDFCV), Eq. (4) and (21) were identified within the system model as is shown.

$$f_1 = \dot{x_1} = \frac{\beta}{V_{pd}}\left[V_d\omega_p\frac{(tan^{-1}\left(\frac{y_{max}-x_6}{L}\right))}{\alpha_{max}} - A_O C_d\sqrt{\frac{2}{\rho}(x_1-x_3)} - A_1 x_7\right]$$

$$f_7 = \dot{x_7} = \frac{1}{(m_1+m_2)}\left[x_2A_2 - x_1A_1 - (y_p+x_6)k_1 - K_{AG}x_7 - \left[\frac{\left(\frac{NM_p r^2\omega^2}{2}\right)(tan^{-1}\left(\frac{y_{max}-x_6}{L}\right)) - \left(\frac{NA_p r\gamma}{2\pi}\right)x_1}{L}\right]\right]$$

Once the appropriate NL equations were identified the partial derivatives that were dependent on x_6 were reorganized within the SSR. The previously shown A_{sys} matrix remained the same except for any partial derivative that contained x_6 was then placed in the *B* matrix to act as an input and a 0 was then used to fill in the previous position of that partial derivative within the A_{sys} matrix. The *C* matrix was then restructured to only have x_6 as an output instead of all states and the *D* matrix was reduced to a single scalar value of 0 as a result of the system having a single output. This restructuring provided a linear system where the single input and single output were both x_6 which was necessary since x_6

was a state computed in the model and dependent on other states as well as the state interfacing with (passing through) the saturation nonlinearity. This process is displayed below for the reader's convenience. The transfer function relating the output x_6 to the input x_6 was found in MATLAB® according to the equation

$$C\left(sI - A_{sys}\right)^{-1}B + D = G(s) \tag{32}$$

where A_{sys}, B, C, and D are defined in Fig. 41 and I represents the identity matrix.

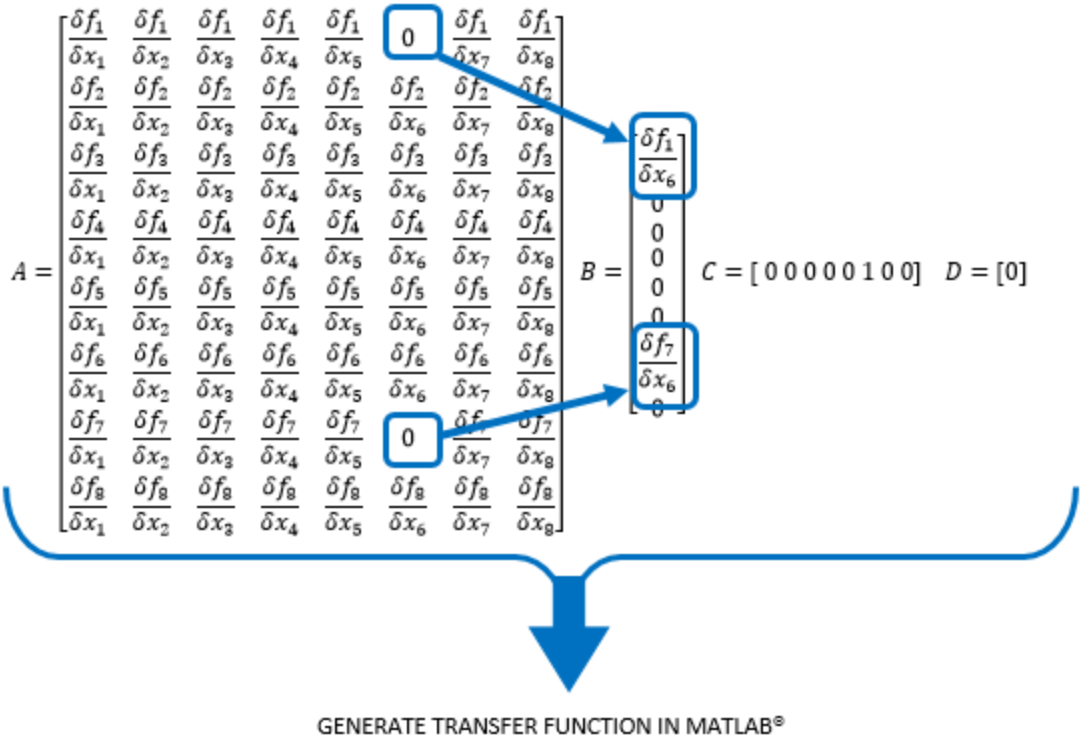

Fig. 41. State-space manipulation for determination of *G(s)*

Also it is important to note that the LS system that was analyzed was a positive feedback system (i.e. x_6 for example was not subtracted from a reference signal as in a feedback control system). This meant that the describing function result shown previously still applied to this LS system except the linear element, $G(j\omega)$, was multiplied by -1 to

account for positive feedback rather than negative feedback that was used in the standard derivation of describing function/Nyquist stability in Eq.(28) and subsequent equations. When applying describing function analysis to approximate a nonlinearity, it is assumed that a negative feedback system, Fig. 38, is being taken into account which is not the case for this LS system.

CHAPTER 6: STABILITY ANALYSIS RESULTS

6.1. Describing Function Analysis Results

The basic description and development of describing function analysis was addressed in the previous chapter and this chapter will address the process that was followed and the results that were obtained specific to the application of describing function analysis to the LS system. Recall previously from Chapter 5, the process for identifying the existence of limit cycles within the system requires both the Nyquist plot of $G(j\omega)$ and *-1/N(A)* (the negative inverse of the describing function for a saturation nonlinearity) to be analyzed within the same complex plane. The analysis then comes down to searching for any intersections between $G(j\omega)$ and *-1/N(A)* since an intersection indicates a possible solution to Eq. (28) and the existence of limit cycles. Before identifying any possible instability (existence of limit cycles), it is important to note that the linearization used for this application of describing function analysis was not based on the numerical values used in the model validation simulations (when the model was simulated against the experimental data) since this analysis involved additional dynamics (load pressure and a theoretical motor load). Although this stability analysis was not analyzed under the same exact conditions as what was estimated in the experimental test bed, the analysis still provided results that revealed the capabilities of describing function analysis when applied to a LS system model.

The stability analysis was conducted according to three different scenarios. Starting with Scenario 1, describing function analysis was applied to the stable models (corresponding to the stable dynamic responses shown prior in Fig. 34 through Fig. 37) to

ensure that no intersection would occur since logically there should be no intersection due to the non-existence of limit cycles. The analysis was conducted for both actuator saturation and PDFCV saturation with the expectation that both would result in zero intersections in the complex plane. This result occurred for the actuator saturation where no intersection was identified, as shown in Fig. 42. Unfortunately, when PDFCV saturation was analyzed, a single intersection was encountered as shown in Fig. 43 indicating a false prediction of limit cycle. This result reduced confidence in the application of describing function analysis for this system.

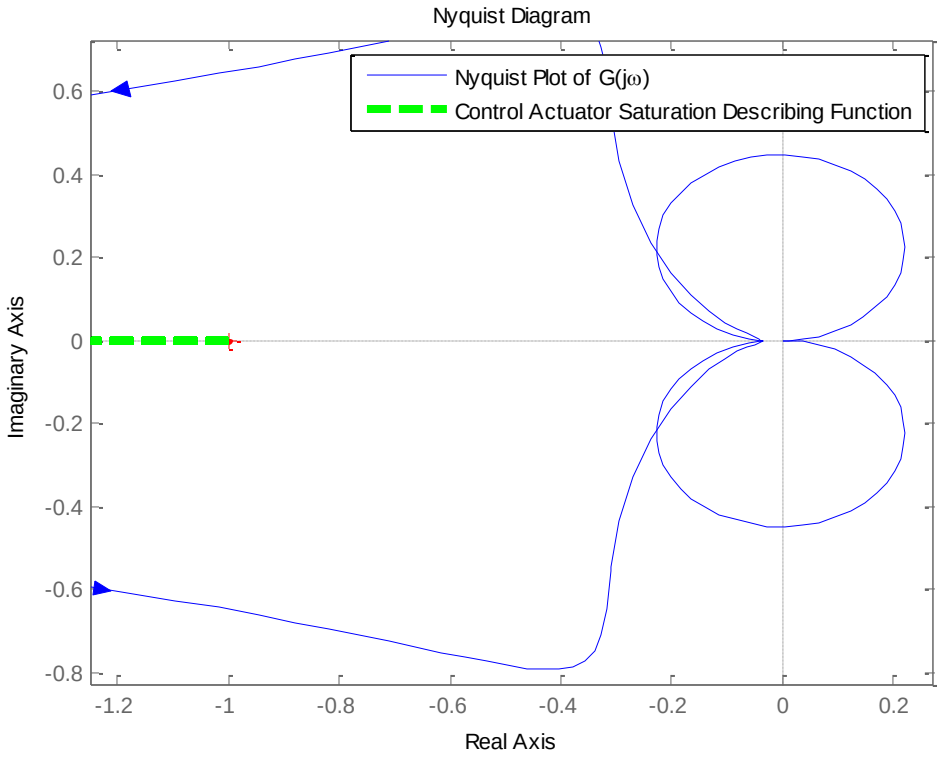

Fig. 42. Scenario 1 - Correct identification by describing function of no existence of limit cycles using actuator saturation case for stable system response

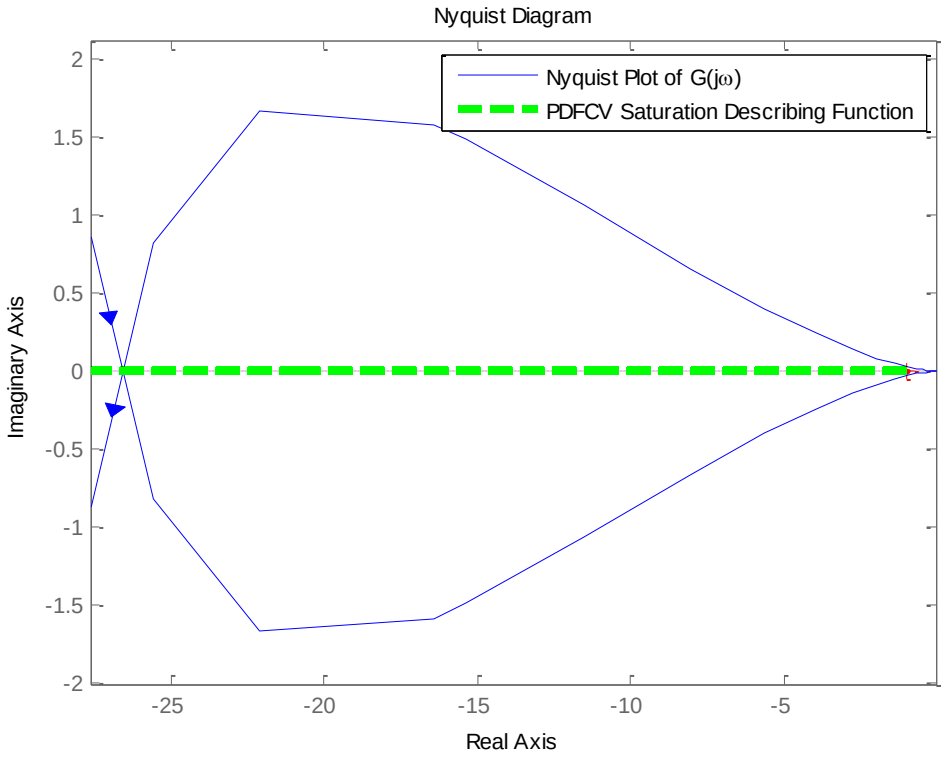

Fig. 43. Scenario 1 - Incorrect identification by describing function of existence of limit cycles using PDFCV saturation case for stable system response

Scenario 2 involved a simulation in which oscillations were induced due to saturation of only the control actuator displacement. Analysis was then conducted in order to further test the capability of the describing function analysis in identifying limit cycles and the characterizing parameters (amplitude and frequency) that correspond to the limit cycles. In order to induce limit cycles within the system, the cross-sectional area of the control actuator piston was reduced to approximately 34% of the original area that was used when the system was stable. After analyzing the system, the procedure explained previously for describing function analysis was conducted. A single intersection resulted, shown in Fig. 44, indicating a stable limit cycle was present. The limit cycle was considered

stable due to there being no encirclements of the describing function in the direction of increasing amplitude (to the left along the real axis) from the point of intersection. The amplitude and frequency associated with the intersection predicted the amplitude and frequency of the limit cycle taking place within the system. It is important to note again that describing function analysis is only an approximation of the nonlinearity. Therefore, in this case for example, the frequency and amplitude at the intersection were estimated to be approximately 44Hz (278 rad/s shown in the plot) and 19 mm, respectively. Both the NL simulation of the LS system and a linear simulation (note this is not the same linear simulation of the linearized SSR shown previously in Chapter 4) of *G(s)* in series with a saturation nonlinearity indicated an approximate frequency very close to the value that was predicted via the describing function as shown by Fig. 45 and Fig. 46, respectively. Note that due to saturation within the NL simulation, there were two oscillations taking place at different frequencies. The saturated oscillation had a frequency estimated to be around 20 Hz while the higher frequency oscillation taking place was estimated to be around 40-50 Hz (closer to the predicted frequency). The predicted amplitude was difficult to verify for two reasons. The first was that the saturation within the NL simulation was possibly prohibiting the oscillations from reaching their full amplitude. The oddly natured and saturated oscillations that result gave a false indication of the amplitude of the response. The second reason was that the linear simulation also did not provide an exact verification of the predicted amplitude. This was due to the structure of the simulation and the saturation nonlinearity again affecting the TF output. For these two reasons, the frequency predicted by the describing function analysis was the parameter of greatest interest within the presented results.

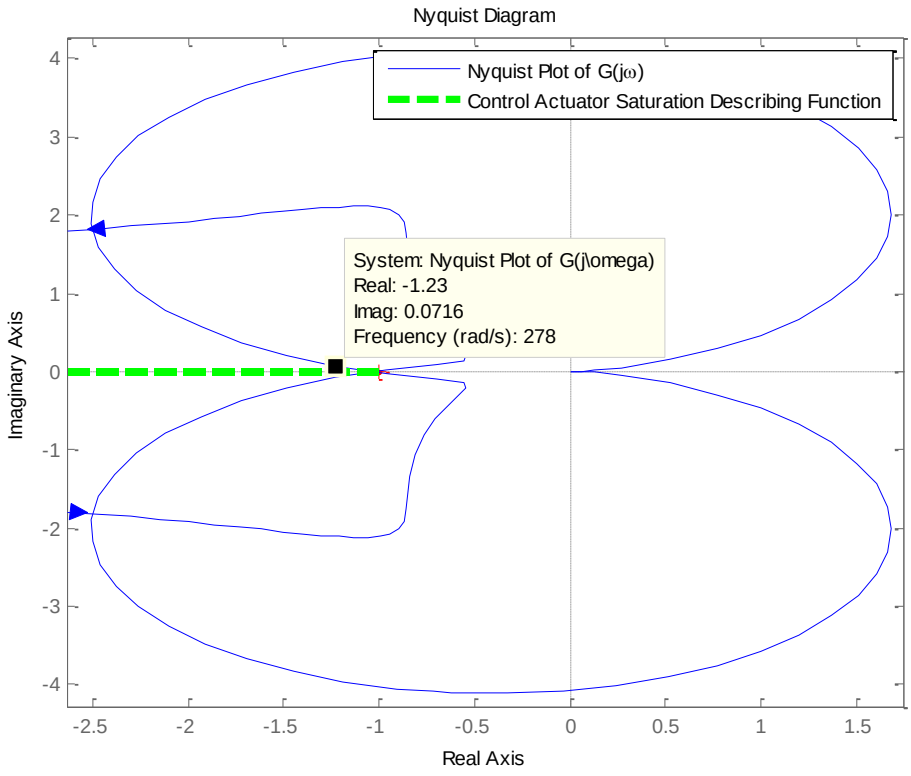

Fig. 44. Scenario 2 - Correct prediction and characterization of limit cycles using the describing function control actuator saturation case

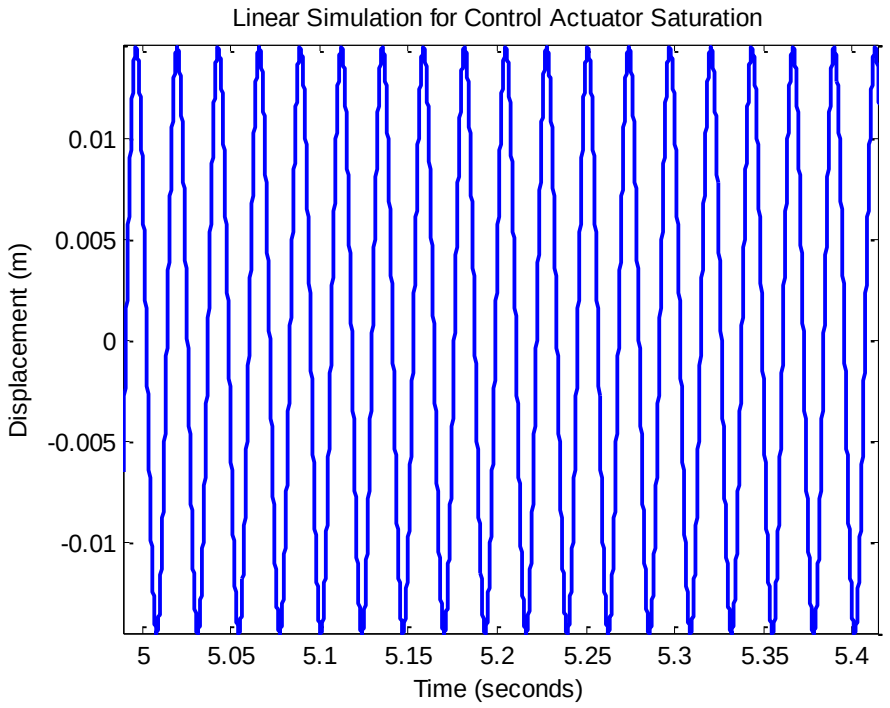

Fig. 45. Scenario 2 - Linear simulation verification of describing function prediction in Fig. 44

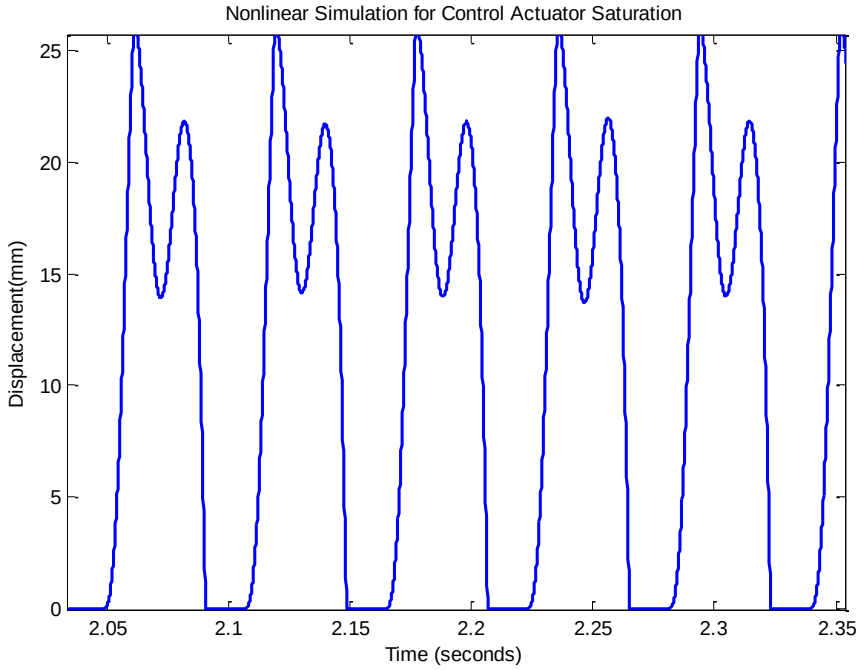

Fig. 46. Scenario 2 - NL simulation verification of describing function prediction in Fig. 44

A third and final scenario was tested where in order to introduce limit cycles into the system this time the cross-sectional area of the bias actuator piston was reduced to approximately 50% of the original area that was used when the system was stable. When this scenario was analyzed, it was realized that both the control actuator and the PDFCV were saturating. Since there were two components with saturation, it was unclear as to which was causing the limit cycle behavior within the response. The first case to be considered was the saturation of the control actuator. When describing function analysis was applied, a single intersection, indicating a stable limit cycle (same reasoning as in Scenario 2), was discovered in the complex plane as shown in Fig. 47. The predicted frequency and amplitude respectively were 3Hz (17.1 rad/s) and 80 mm. The amplitude prediction was completely unfeasible but the predicted frequency was validated against both a NL and linear simulation as in the previous two scenarios.

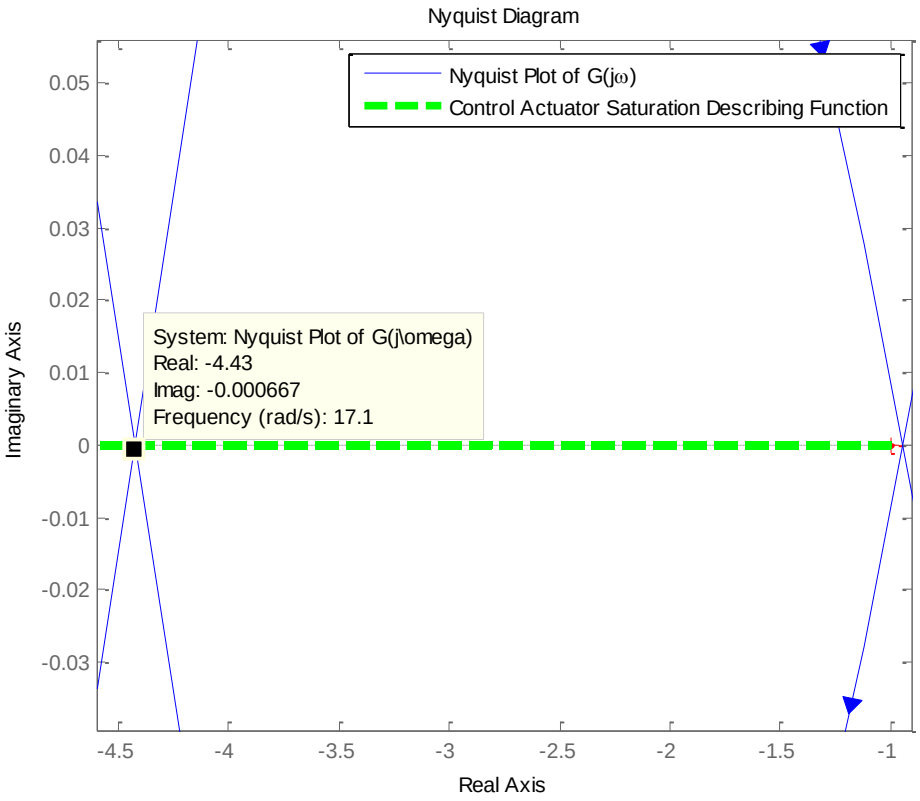

Fig. 47. Scenario 3 - Correct describing function prediction of existence of limit cycles using control actuator saturation case

Figure 48 displays the NL simulation for control actuator displacement where it is clear that the actuator was saturating on both the upper and lower bounds. The frequency indicated by the NL simulation was approximately 3 to 4 Hz which matched almost exactly to the frequency predicted by the describing function analysis.

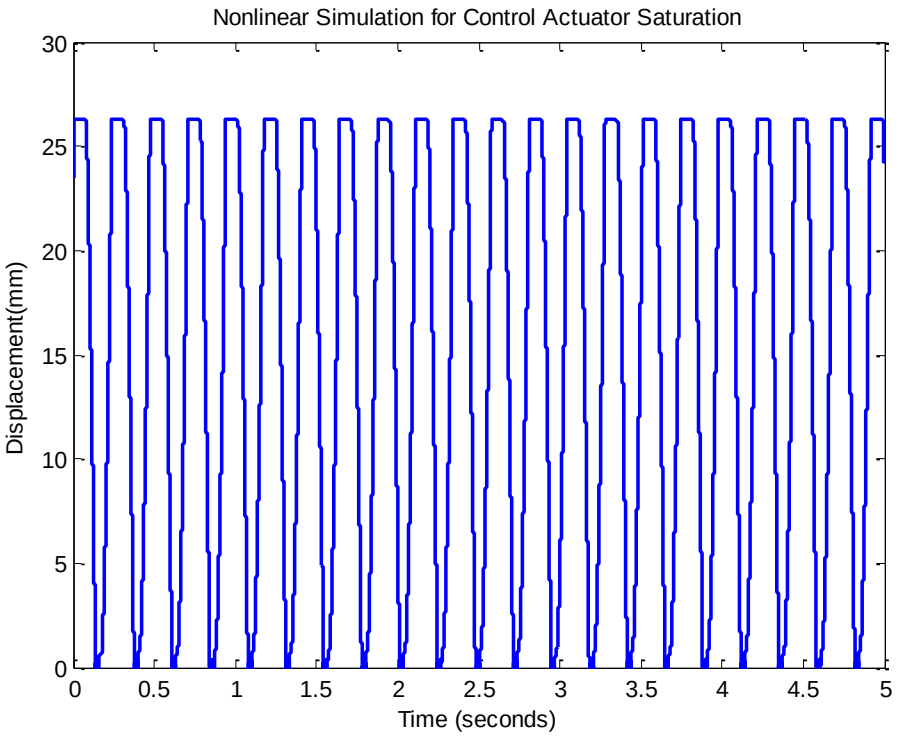

Fig. 48. Scenario 3 - NL simulation verification of describing function prediction in Fig. 47

A linear simulation was again the final verification step as is shown in Fig. 49. The linear simulation verified the predicted frequency by simulating a sinusoidal response of almost precisely 3Hz. This result clearly indicated that the control actuator saturation was the reason for the limit cycle behavior but in order to fully prove this, the PDFCV saturation case needed to be investigated as well.

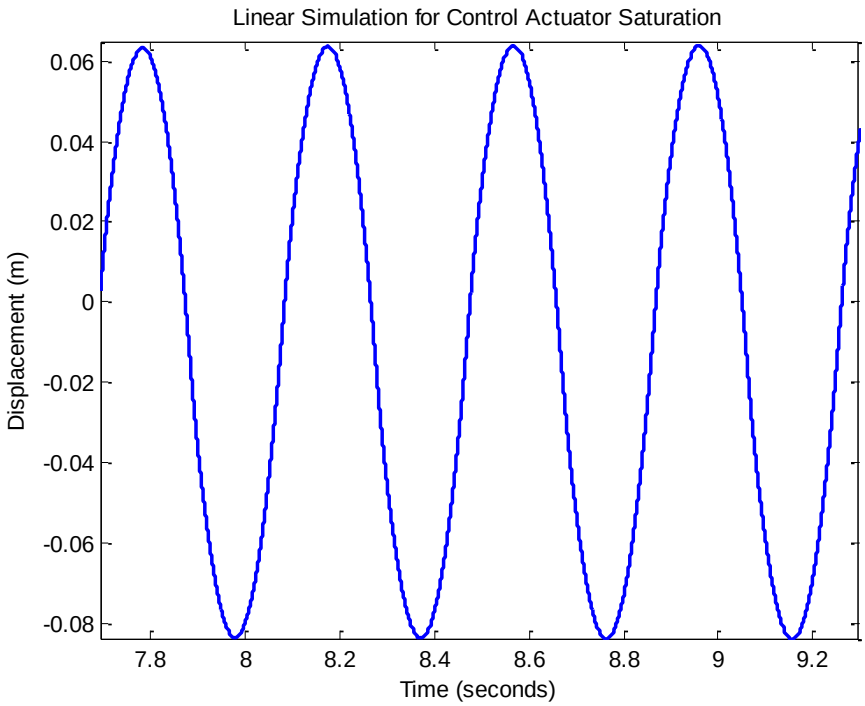

Fig. 49. Scenario 3 - Linear simulation verification of describing function prediction in Fig. 47

Due to the PDFCV also saturating, describing function analysis was also applied to the PDFCV saturation case in order to clearly identify if the control actuator saturation was causing the limit cycles within the system or if something else was happening. When describing function analysis was applied to the PDFCV saturation, no intersections were discovered in the complex plane as shown in Fig. 50. This clearly indicated that there were no limit cycles taking place due to the PDFCV saturating. Limit cycles were identified in the NL simulation of the PDFCV displacement (note this is the same NL simulation as was displayed for the control actuator displacement, just a different state) as shown in Fig. 51. The limit cycles displayed within the NL simulation of the PDFCV are believed to be sustained from the saturation of the control actuator and not the PDFCV itself.

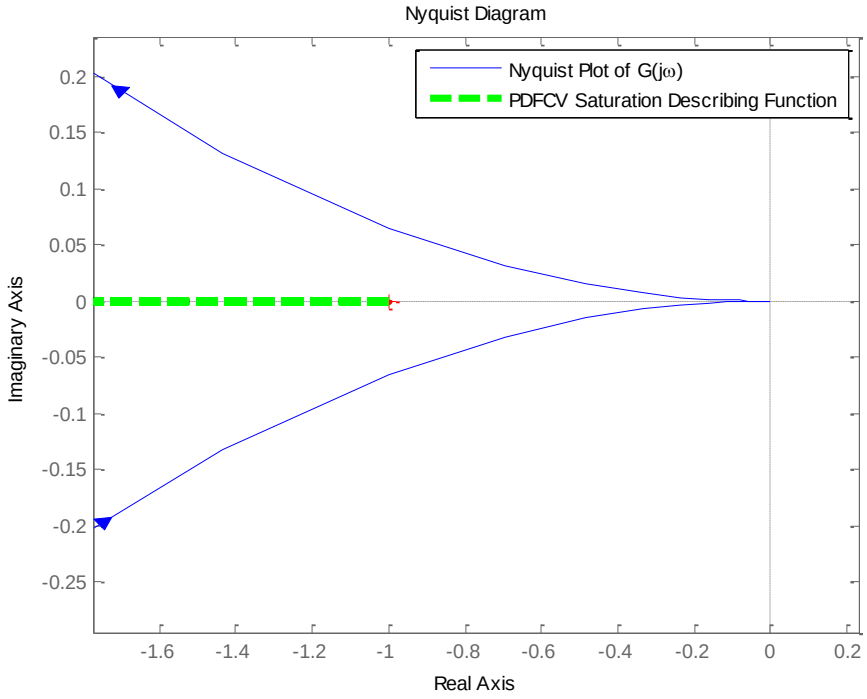

Fig. 50. Scenario 3 - Incorrect describing function prediction of no existence of limit cycles using PDFCV saturation case

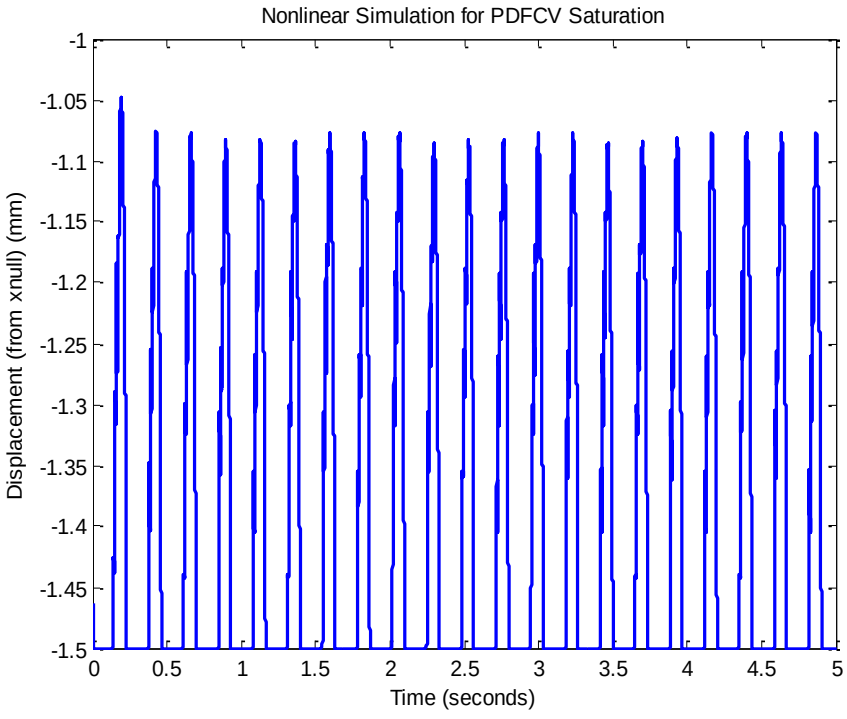

Fig. 51. Scenario 3 - NL simulation of PDFCV saturation case

In order to verify that the PDFCV saturation was not the cause of the system limit cycles and that the limit cycles within the PDFCV displacement were actually being sustained by the control actuator saturation, a linear simulation was again conducted. If the limit cycles within the PDFCV displacement response were truly self-sustaining then the linear simulation would reveal it, but as shown in Fig. 52, the response was unstable. The linear simulation along with describing function analysis proved that the saturation alone in series with the PDFCV saturation $G(s)$ was actually unstable and could not produce sustained oscillations. This also proved that the saturation of the control actuator was not only causing the limit cycles within the system but was also causing the saturation of the PDFCV and resulting limit cycles within it's response. This scenario displayed the effectiveness and advantage that describing function analysis can provide when needing to identify what nonlinearity might be causing limit cycles within the system.

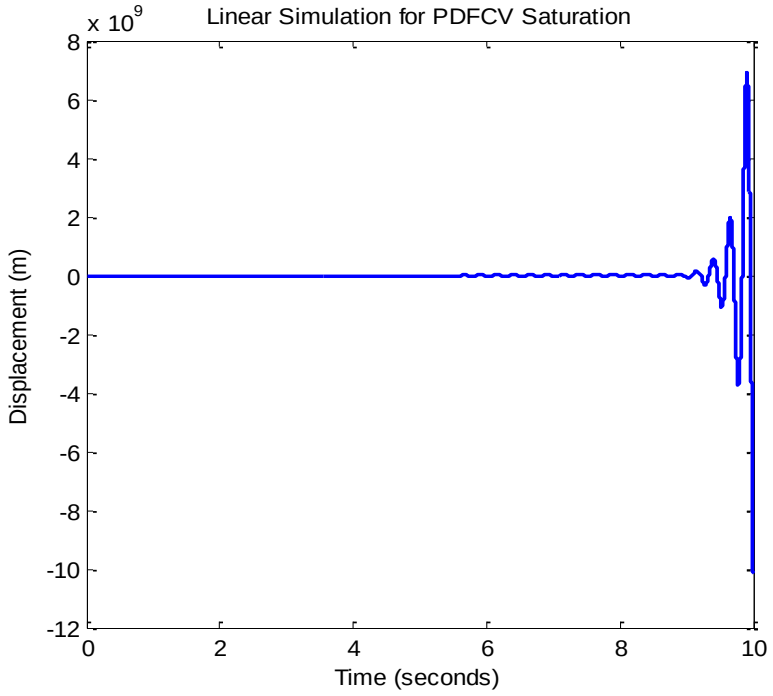

Fig. 52. Scenario 3 - Linear simulation of PDFCV saturation case

6.2. Effectiveness of Describing Function Analysis

Three scenarios were previously presented in which describing function analysis was applied to the NL hydraulic LS system. The application of describing function analysis within these three scenarios proved the effective nature that the describing function may have when applied to a LS system that suffers from limit cycles. Examples of both incorrect and correct limit cycle predictions were discovered when using describing function analysis. The stable system response in Scenario 1 was characterized correctly via the actuator saturation describing function with no intersections occurring in the complex plane. However, when using the PDFCV saturation describing function for the same stable system, limit cycles were incorrectly predicted. For Scenario 2, a system response suffering from sustained oscillations due to strictly actuator saturation was also identified correctly using the describing function along with a very accurate approximation for the frequency of oscillation. The last case, Scenario 3, investigated an additional system response suffering from both control actuator and PDFCV saturation. Using describing function analysis it was discovered that the saturation of the control actuator was the source of the limit cycle phenomena within the system response. The saturation and limit cycles within the PDFCV were believed to be a side effect of the saturation within the actuator and were actually induced by the actuator limit cycles.

Each of these scenarios proved that by using describing function analysis with respect to a LS system, the instability and limit cycles that may occur can be accurately predicted, identified, and characterized. By conducting describing function analysis on a LS hydraulic system, the effects of certain hard nonlinearities can be identified even if occurring in multiple components as proven by Scenario 3. An incorrect prediction using

describing function analysis was also encountered in Scenario 1. In this case for a stable response the PDFCV saturation case indicated limit cycles within the system response when truly there were not. A very reasonable and probable cause for this erroneous result most likely stems from a violation of the filtering hypothesis (the fundamental assumption of describing function analysis). In order to verify that this was the cause of the incorrect result, Bode diagrams were generated for both the control actuator saturation *G(s)* and the PDFCV saturation *G(s)* as is shown in Fig. 53 and Fig. 54, respectively.

By studying both frequency responses, it became clearer as to why the control actuator case correctly predicted no limit cycles within the stable system response and the PDFCV case did not. The Bode diagram for the PDFCV saturation *G(s)* displays two high frequency resonant peaks that hold a magnitude close to that of the low frequency gain. These two high frequency peaks indicate dynamics associated with higher harmonics within *G(s)* for the PDFCV saturation case. Reiterating from earlier in Chapter 5, describing function analysis requires the fundamental assumption that the linear element defining the system exhibits low-pass properties with no significant higher harmonics. This is the most likely reason behind the incorrect result from Scenario 1. Observing the Bode diagram for the control actuator saturation reveals two high frequency resonant peaks but with magnitudes much lower than the low frequency gain. This indicates the control actuator saturation *G(s)* agrees well with the filtering hypothesis and further verifies the evidence as to why the describing function analysis failed for the PDFCV saturation case. The errors that can occur from incorrect describing function analysis predictions have been noted in other research studies and are commonly discussed in nonlinear control textbooks. The error due to violation of the filtering hypothesis with high frequency resonant peaks

within the linear element is a well-known and costly mistake [27].The studies noting the limits of describing function analysis were not applied to hydraulic LS systems in specific but other certain scenarios were identified and provided a possible alternative to describing function analysis [4, 5].

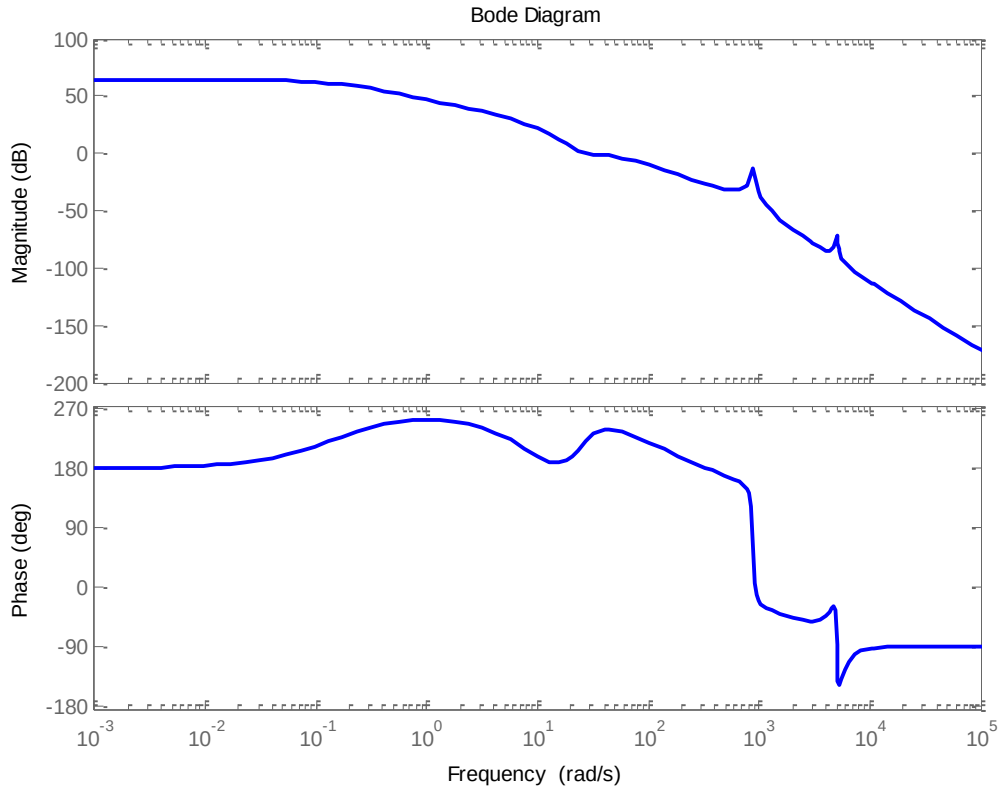

Fig. 53. Bode diagram for control actuator saturation *G(s)*

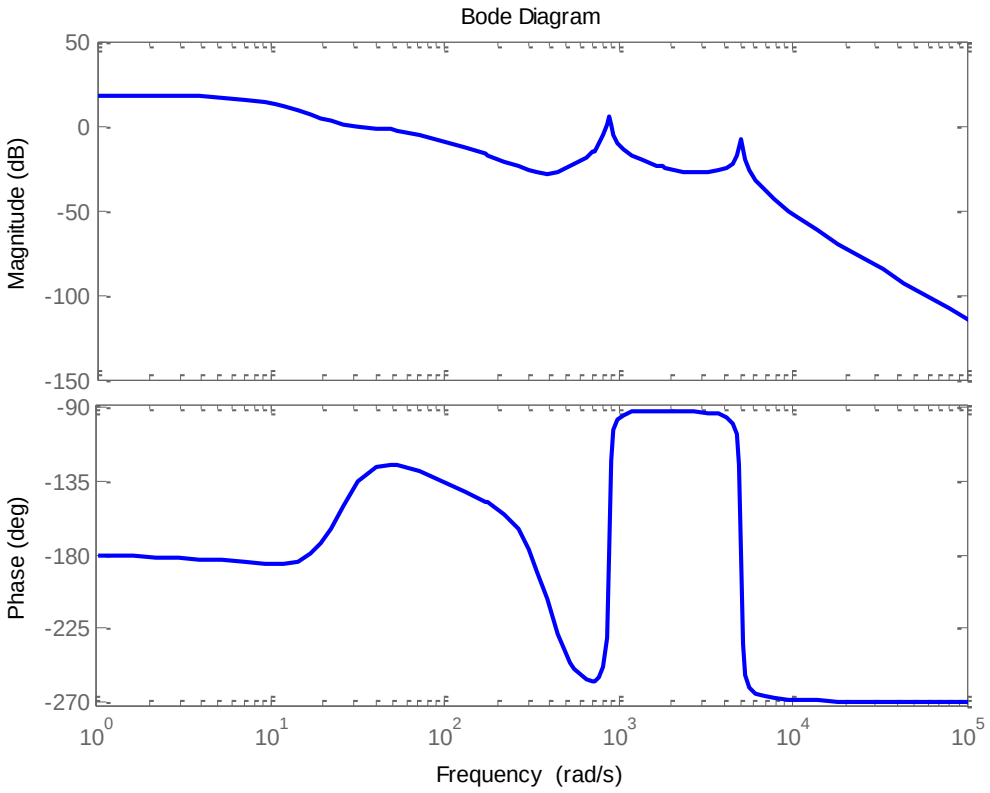

Fig. 54. Bode diagram for PDFCV saturation *G(s)*

CHAPTER 7: COMPREHENSIVE DISCUSSION OF RESULTS

This section will briefly provide and discuss a comprehensive presentation of all results that came about from this research. To begin, a NL model consisting of a LS pump, 3-way hydraulic spool valve, variable area flow control valve, and theoretical rotational motor load was defined and was then successfully simulated through MATLAB® and Simulink® with a stable response where the LS system reached an exact steady-state value for all state variables as was shown before in Fig. 16 through Fig. 20. A linear model was then successfully generated by performing a linearization based on the NL model equations that were presented in Chapter 3. The linearized model proved to match the NL model very well when within the linear operating range of the nominal state values as displayed previously in Fig 34 through Fig. 37. Slight disagreement was observed in the transient portion of the dynamic response for certain states (PDFCV and actuator velocities) but was only a difference in the amplitude of the oscillation where the frequency of oscillation still matched precisely between both the NL model and linear model.

The NL model was then appropriately validated using data acquired from an experimental test bed where the load pressure data that was acquired acted as the input to the NL model in Simulink®. The output pump discharge pressure time response data was then compared between the NL model simulation and the data obtained experimentally. The pump discharge pressure that was simulated from the model agreed very well with the pressure supplied from the actual pump in the lab, as can be seen in Fig. 25 and Fig. 28 and any error was quantified using a root mean squared error calculation with all values tabulated within Table 3 according to the specific test and the maximum, minimum, and

mean error values that were calculated. It was noticed though that primarily at the higher pressures that were tested (pressures greater than 13 MPa) the calculated error was quite high and the discharge pressure simulated by the NL model actually began to offset from the experimental data which can be seen in Fig. 30 for example. The reason for this offset was identified to be a result of the margin pressure decreasing from the desired value (approximately 2.9MPa) within the experimental set up whereas the NL model maintained a constant margin pressure across all pressures that were tested. The hypothesized reason that the NL model did not reflect this same phenomena that occurred within the experimental set up was that additional leakage that may have been occurring within certain pump components was not appropriately included in (if introduced at all) to the NL model. This offset caused the error to inappropriately reflect the accuracy of the model and so to provide further validity for the model, the Fast Fourier Transform was used to analyze the time response data within the frequency domain. The results of this analysis, displayed in Fig. 31 and Fig. 33 proved that the primary frequencies within the experimental data matched exceptionally well to the model data further verifying that the model accurately represented the physics taking place within the real system.

The linearized model that had been generated was used to assist in diagnosing the stability of the LS system. Two different SISO TF's were developed based on either saturation of the control actuator or saturation of the PDFCV and are shown in Eq. (30) and (31). These two TF's were developed from the linearized model and used to investigate how well describing function analysis would work in predicting limit cycles that might occur due to saturation within the mechanical portions of the LS system. Three scenarios were tested using describing function analysis in order to assess how effective the analysis

would be when applied to an unstable LS system. Scenario 1 tested a stable response based on NL simulations where it was expected that the describing function analysis would indicate no limit cycles within the system. This was true when the describing function analysis predicted no limit cycles for the case of the control actuator saturation, but the PDFCV saturation case falsely indicated that there were limit cycles within the system, as shown in Fig. 43. Scenarios 2 and 3 analyzed the prediction of limit cycles for each case of saturation within the mechanical components of the system. For each scenario, the describing function analysis provided excellent approximations for the frequency of oscillation for the predicted limit cycle that was simulated by both the NL and linear (saturation nonlinearity in series with TF) model. Due to a describing function being only an approximation of a nonlinearity within a system, the somewhat imprecise results for the amplitude were to be expected but these three scenarios alone provided enough information to verify that describing function analysis is an excellent tool to be used when analyzing the stability for LS systems. The final result for this research was the identification of what was believed to be the reason behind the single erroneous result indicated by the describing function analysis for Scenario 1. A Bode diagram of the PDFCV saturation *G(s)* revealed two high frequency resonant peaks and subsequently, a violation of the filtering hypothesis for describing function analysis. The significance of this result is that the fundamental assumption for a describing function states that the linear element being used to represent the system must exhibit low-pass properties. This result reveals the critical importance of not only following this fundamental assumption if accurate approximations are desired but also the importance of identifying an appropriate linear element for the PDFCV saturation case for this LS system.

CHAPTER 8: CONCLUSION

With improvements in technology and a greater demand for improved engineering systems across all fields, certain aspects of engineering are becoming even more vital to continue this technological advancement. Aspects such as system efficiency, robust operation, and stability are being pushed to the forefront more than ever. In the field of hydraulics and hydraulic control systems, it is no different. Efficiency and stability are two very important aspects of hydraulic controls. Load-sensing systems have been identified as an opportunity for great improvement in terms of efficiency. Although these systems assist in increasing the efficiency of work cycles for different types of heavy machinery, at the same time these systems have also been identified as being prone to instability and limit cycles and have carried a figurative red flag in addition to the positive characteristics they hold. For this reason, the investigation of a LS system was undertaken as a primary research focus for this thesis. The following objectives of this thesis were successfully completed:

- Complete characterization and development of a NL hydro-mechanical LS pump system model
- Accurate simulation of the NL model that obtained a stable system response
- Validation of the NL model against an experimental test bed and error quantification verified the model accurately simulated the dynamics of the real LS pump system
- Linearization of the NL model generated an SSR for the LS system and validation of the linearized model was completed through comparison simulations with the NL model

- Restructuring of the linearized SSR effectively developed two individual SISO TF's based on the two separate saturation cases present within the mechanical components of the LS system
- Utilization of the two newly developed TF's for each saturation case, allowed for stability analysis via describing functions to be conducted and to predict the existence of limit cycles within the system response
- Through multiple scenarios describing function analysis was proven to be an appropriate method to be applied to hydraulic LS systems that suffer from sustained oscillations

Both a nonlinear and linearized model were constructed and developed to aid in the accurate simulation of a LS pump's performance under various conditions and to provide a reliable dynamic model for future advancements. A better understanding of the effectiveness of describing function analysis in diagnosing and predicting the stability of a LS hydraulic system was obtained. The incorporation of describing functions in analyzing the saturation nonlinearities within the mechanical systems proved to be very effective by providing characterization of the limit cycles that might appear. Three scenarios were specifically investigated that proved the advantage describing functions provide in diagnosing the possible limit cycles within a LS system. The advantage of applying describing function analysis to LS systems would appear within the design stage for the system. The analysis would allow for detailed information to be provided (existence of limit cycles, characteristics of limit cycles if they exist, etc.) on the diagnosis of stability within the system. This research revealed that it is vital to not violate the filtering hypothesis for describing function analysis since the results of the analysis may be

inaccurate when an inappropriate linear model is utilized. It should be understood that a describing function is only an approximation of a nonlinear element within a system so there is always a chance that there will be error even with an appropriate linear model. As a result the application of describing function analysis to these systems must always be verified by simulation as was done in this research. The inaccuracies discovered from this analysis were hypothesized to be a result of high frequency resonant peaks within the specially constructed *G(s)*. In summary, this research clearly demonstrated the usefulness of describing function analysis when applied to a LS system and the insight the analysis provides when investigating potential limit cycle phenomenon.

This thesis revealed that there are several things that could be improved, expanded upon, or investigated for future research. The first would be additional investigation and possible refinement of the NL model to account for the potential leakage that may have caused the experimental test bed to decrease the margin pressure at higher pressures when the model did not reflect the same result. Additional investigation of the NL model should involve the study of the stabilizing or de-stabilizing effects that the constant orifice leakage has on the system response. Identifying how the leakage relates to saturation within the system and possible limit cycles is vital to expanding this research. The second would be model order reduction of the linear system presented in this work. If possible, by reducing the order of the system and simplifying the system, additional methods of analysis such as phase plane analysis or application of Routh-Hurwitz stability criterion would become easier to implement. Also, by attempting to remove any states that contain high frequency dynamics, an even more accurate application of describing function analysis may very well be feasible for the system. Of course simulations are essential to verify that the reduced

order model still appropriately matches the full order model. The third suggestion is actually coupled with the second and is a recommendation for further investigation into the use of describing functions for predicting limit cycles within the system with respect to the saturation cases and constant orifice leakage within this research. Specifically, a more intricate look and proper identification of the conditions requiring either the actuator saturation or the PDFCV saturation to be used (since in some scenarios both cases might be occurring). This also might mean considering other ways of formulating the linear element, *G(s)*. This could include the investigation of another possible hard nonlinearity, deadzone, in the system and the application of describing function analysis with respect to deadzone (if a closed-centered spool valve was used for example). The fourth is the expansion of the stability analysis to identify additional parameters that may cause instability since the cross-sectional areas of the actuators were the main parameter being adjusted to induce sustained oscillations. As stated before, investigation of the constant orifice leakage is vital and the effect the leakage has on the stability of the system should be the next step taken. The fifth suggestion for future research would be the investigation of additional methods of stability analysis. One possible method might be root locus analysis with varying certain system parameters such as spool valve diameter, spring rates, flow control valve area, and leakage. This method would only provide a general identification of system stability, but may also provide a better sense of the direction to take in terms of identifying which parameters to focus on for more in depth modes of stability analysis or new insight for a more accurate application of describing function analysis. Another method that was stated before which would be useful in identifying the stability of the system from a nonlinear approach would be the application of phase plane

analysis using the nonlinear equations defining the system. The difficulty here would be investigating if the system could be appropriately modeled and characterized with a 2nd order system. The sixth and final suggestion for future research would be analysis of the dynamic efficiency of the pump under certain operating conditions or work cycles. The research presented within this thesis provides a strong foundation for future work and the suggestions provided could allow for an even better understanding of the dynamics that appear within hydraulic LS systems. An improved understanding of the dynamic complexity within these hydraulic pumps and systems will only become more essential in the future as the desire for improved efficiency and stability increases.

REFERENCES

[1] Andersen, T.O., Pedersen, H.C., and Hansen, M.R. (2008) "*Controlling a Conventional LS-pump based on Electrically Measured LS-pressure"*. Proceedings of the ASME/BATH 2008 Symposium on Fluid Power and Motion Control.

[2] Burton, R., et al. (2006). *"Feasibility Study on the Use of Dynamic Neural Networks (DNN's) for Modeling a Variable Displacement Load Sensing Pump."* Proceedings of the 2006 ASME International Mechanical Engineering Congress and RD&D Expo, Paper #IMECE2006-15588.

[3] Das, A., and Bretey, E. (2014). "*Control and Stability Analysis of Practical Load-Sense Systems"*. IFPE, 2014, Paper 16.1.

[4] Engelberg, S. (2002). *"Limitations of the describing function for limit cycle prediction."* Automatic Control, IEEE Transactions on **47**(11): 1887-1890.

[5] Fadali, M. S. and N. Chachavalvoong (1995). "*Describing function analysis of uncertain nonlinear systems using the Kharitonov approach*". American Control Conference, Proceedings of the 1995.

[6] Garciano, L.O., Boylston Jr., L.E., and Cromer, S. (2014). "*Modeling, simulation, and analysis of a simple load-sense system"*. IFPE, 2014, Paper 29.1.

[7] Gopal, M. (2008). *Control Systems: Principles and Design.* New York, NY: McGraw-Hill.

[8] Heyns, L. J. and J. J. Kruger (1994). *"Describing function-based analysis of a nonlinear hydraulic transmission line."* Control Systems Technology, IEEE Transactions on **2**(1): 31-35.

[9] Jayaraman, G. P. and S. V. Lunzman (2011). "*Modeling and analysis of an electronic load sensing pump*." Control Applications (CCA), 2011 IEEE International Conference on.

[10] Kavanagh, G.P. (1987). "*The Dynamic Modelling of an Axial Piston Hydraulic Pump"*. M. Sci. Thesis, University of Saskatchewan.

[11] Kim, C.S., and Lee, C.O. (1997). *"Robust Speed Control of a Variable-Displacement Hydraulic Motor Considering Saturation Nonlinearity."* ASME J. Dyn. Sys., Meas., *Control* **122**, 196-201 (6 pages); doi:10.1115/1.482442.

[12] Krus, P. (1988). "*On Load Sensing Fluid Power Systems"*, Ph.D. thesis No.198. Linkoping University, Sweden.

[13] Lantto, B., et al. (1993). *"Dynamic Properties of Load-Sensing Systems With Interacting Complex Mechanical Loads."* Journal of Dynamic Systems, Measurement, and Control **115**(3): 525-530.

[14] Liu, S. and B. Yao (2009). *"Characterization and Attenuation of Sandwiched Deadband Problem Using Describing Function Analysis and Application to Electrohydraulic Systems Controlled by Closed-Center Valves."* Journal of Dynamic Systems, Measurement, and Control **131**(3): 031002-031002.

[15] Manring, N.D. (2013). *Fluid Power Pumps & Motors: Analysis, Design, and Control*., United States of America: McGraw-Hill Education.

[16] Manring, N.D. (2005). *Hydraulic Control Systems*. New Jersey: John Wiley and Sons.

[17] Manring, N. D. (2004). *"Modeling Spool Valve Flow Forces*," Proceedings of the 2004 ASME International Mechanical Engineering Congress and RD&D Expo, Anaheim, CA, Paper #IMECE2004-59038.

[18] Manring, N. D., and Mehta, V. S. (2011). "*Physical Limitations for the Bandwidth Frequency of a Pressure Controlled, Axial Piston Pump*." ASME J. Dyn. Syst., **133** , pp. 1–12.

[19] Manring, N.D., and Zhang, S. (2012)."*Pressure Transient Flow Forces for Hydraulic Spool Valves."* ASME J. Dyn. Sys., Meas., Control **134**, 034501 (5 pages); doi:10.1115/1.4005506.

[20] Manring, N. D. (1999). *"The Control and Containment Forces on the Swash Plate of an Axial-Piston Pump."* Journal of Dynamic Systems, Measurement, and Control **121**(4): 599-605.

[21] Manring, N. D. and F. A. Damtew (1999). "*The Control Torque on the Swash Plate of an Axial-Piston Pump Utilizing Piston-Bore Springs*". Journal of Dynamic Systems, Measurement, and Control **123**(3): 471-478.

[22] Moustafa, N. (2013). "*Robust Control Design for a Proportional Valve with Backlash Compensation"*. M. Sci. Thesis, University of Missouri.

[23] Moustafa, N. and Fales, R. (2013). "*Stability of a Proportional Valve Control System with Backlash and Saturation"*. Proceedings of the ASME/BATH 2013 Symposium on Fluid Power and Motion Control, Paper #FPMC2013-4502

[24] Roubal, J., et al. (2010). *"Linearization: Students Forget the Operating Point."* Education, IEEE Transactions on **53**(3): 413-418.

[25] Sakurai, Y. (2000). *"Calculation of dynamic overall efficiency of a load sensing hydraulic system by bondgraphs."* Industrial Electronics Society, 2000. IECON 2000. 26th Annual Conference of the IEEE.

[26] Schoenau, G. J., et al. (1990). "*Dynamic Analysis of a Variable Displacement Pump.*" Journal of Dynamic Systems, Measurement, and Control **112**(1): 122-132.

[27] Slotine, E.J.J. and Li, W. (1991). *Applied Nonlinear Control*. Englewood Cliffs, NJ: Prentice-Hall.

[28] Wu, D. (2003). *"Modeling and Experimental Evaluation of a Load-Sensing and Pressure Compensated Hydraulic System"*, Ph.D. thesis, University of Saskatchewan.

[29] Xu X. (1997). *"Experimental Modeling of a Hydraulic Load Sensing Pump using Neural Networks"*. Ph. D. Thesis, University of Saskatchewan.

[30] Zeiger, G. and A. Akers (1985). "*Torque on the Swashplate of an Axial Piston Pump*". Journal of Dynamic Systems, Measurement, and Control **107**(3): 220-226.

APPENDIX A: DESCRIBING FUNCTION DERIVATION

This entire derivation is completed by and extracted from [3], which should be investigated if additional detail is desired. The derivation is provided here for the convenience of the reader and for immediate access to the important details of the derivation.

Derivation of general describing function

Consider a sinusoidal input, $x(t) = Asin(\omega t)$, with amplitude A and frequency ω to a nonlinear element. The output, $w(t)$, typically exhibits a periodic and generally non-sinusoidal function. Using the Fourier series, $w(t)$ can be described as

$$w(t) = \frac{a_o}{2} + \sum_{n=1}^{\infty} [a_n \cos(n\omega t) + b_n \sin(n\omega t)]$$

where the Fourier coefficients, a_i's and b_i's are generally functions of the amplitude and frequency and can be described as

$$a_o = \frac{1}{\pi}\int_{-\pi}^{\pi} w(t)d(\omega t)$$

$$a_n = \frac{1}{\pi}\int_{-\pi}^{\pi} w(t)\cos(n\omega t)d(\omega t)$$

$$b_n = \frac{1}{\pi}\int_{-\pi}^{\pi} w(t)\sin(n\omega t)d(\omega t)$$

Due to the fourth assumption that is needed for the describing function method (assumption regarding symmetry of the nonlinearity relation between the input and output), $a_o = 0$. In addition to the fourth assumption, the third assumption states that only the fundamental component $w_1(t)$ described as

$$w(t) \approx w_1(t) = a_1 \cos(\omega t) + b_1 \sin(\omega t) = Msin(\omega t + \phi)$$

where

$$M(A, \omega) = \sqrt{a_1^2 + b_1^2}$$

and

$$\phi(A, \omega) = \arctan(\frac{a_1}{b_1})$$

In complex representation the fundamental component can be represented as

$$w_1 = Me^{j(\omega t + \phi)} = (b_1 + ja_1)e^{j(\omega t)}$$

A describing function of the nonlinear element is defined as the complex ratio of the fundamental component of the nonlinear element by the input sinusoid or

$$N(A,\omega) = \frac{Me^{j(\omega t+\phi)}}{Ae^{j\omega t}} = \frac{M}{A}e^{j\phi} = \frac{1}{A}(b_1 + ja_1)$$

Derivation of describing function for saturation nonlinearity

Consider the input, $x(t) = Asin(\omega t)$ with a and k representing the range and slope of the linearity. If $A \leq a$, then the input remains in the linear range, and the output is

$$w(t) = kAsin(\omega t)$$

and the describing function is simply the constant k.

Consider the case where $A > a$ and the output is symmetric over the four quarters of a period. In the first quarter, it can be expressed as

$$w(t) = \begin{cases} kAsin(\omega t), & 0 \leq \omega t \leq \gamma \\ ka, & \gamma < \omega t \leq \dfrac{\pi}{2} \end{cases}$$

where $\gamma = \sin^{-1}(\frac{a}{A})$. The odd nature of $w(t)$ implies that $a_1 = 0$ and the symmetry over the four quarters of a period implies that

$$b_1 = \frac{4}{\pi}\int_0^{\frac{\pi}{2}} w(t)\sin(\omega t)d(\omega t)$$

$$b_1 = \frac{4}{\pi}\int_0^{\gamma} kAsin^2(\omega t)d(\omega t) + \frac{4}{\pi}\int_{\gamma}^{\frac{\pi}{2}} kasin(\omega t)d(\omega t)$$

$$b_1 = \frac{2kA}{\pi}[\gamma + \frac{a}{A}\sqrt{1 - \frac{a^2}{A^2}}]$$

Therefore, the describing function for saturation is

$$N(A) = \frac{b_1}{A} = \frac{2k}{\pi}[\sin^{-1}\frac{a}{A} + \frac{a}{A}\sqrt{1 - \frac{a^2}{A^2}}]$$

APPENDIX B: LINEARIZED SYSTEM PARTIAL DERIVATIVES

Presented here are the individual partial derivatives of each state variable with respect to each NL equation used in the NL model presented in Chapter 3 of this thesis. Note that two different linearizations were completed due to the system having two possible operating points dependent on the position of the PDFCV ($x4_o > x_{null}, x4_o < x_{null}$). *During simulations the system primarily reached steady-state when* $x4_o > x_{null}$ *which allowed pressure to reach the control actuator and de-stroke the pump. The partial derivatives that are presented here represent that case*. The variables x_{1_o} through x_{8_o} represent the stable nominal operating points for each state variable and are tabulated at the end of the appendix. Partial derivatives of state variables x_1 through x_8 with respect to:

f_1	f_2
$\frac{\partial f_1}{\partial x_1} = -\frac{\sqrt{2}A\beta C_d}{2V_{pd}\rho\sqrt{\frac{x_{1_o} - x_{3_o}}{\rho}}}$	$\frac{\partial f_2}{\partial x_1} = \frac{\sqrt{2}\,(\pi d x_{4_o})\beta C_d}{2\,V_c\rho\sqrt{\frac{x_{1_o} - x_{2_o}}{\rho}}}$
$\frac{\partial f_1}{\partial x_2} = 0$	$\frac{\partial f_2}{\partial x_2} = -\frac{\sqrt{2}\beta C_d}{2V_c\rho}\left(\frac{(\pi d x_{4_o})}{\sqrt{\frac{x_{1_o} - x_{2_o}}{\rho}}} + \frac{K_{SVA}}{\sqrt{\frac{x_{2_o}}{\rho}}}\right)$
$\frac{\partial f_1}{\partial x_3} = \frac{\sqrt{2}A\beta C_d}{2V_{pd}\rho\sqrt{\frac{x_{1_o} - x_{3_o}}{\rho}}}$	$\frac{\partial f_2}{\partial x_3} = 0$
$\frac{\partial f_1}{\partial x_4} = 0$	$\frac{\partial f_2}{\partial x_4} = \frac{\sqrt{2}\beta C_d\,(\pi d)\sqrt{\frac{x_{1_o} - x_{2_o}}{\rho}}}{V_c}$
$\frac{\partial f_1}{\partial x_5} = 0$	$\frac{\partial f_2}{\partial x_5} = 0$
$\frac{\partial f_1}{\partial x_6} = -\frac{\beta V_d w_p}{L\,V_{pd}\alpha_{max}\left(\frac{\left(x_{6_o} - y_{max}\right)^2}{L^2} + 1\right)}$	$\frac{\partial f_2}{\partial x_6} = 0$
$\frac{\partial f_1}{\partial x_7} = -\frac{A_1\beta}{V_{pd}}$	$\frac{\partial f_2}{\partial x_7} = -\frac{A_2\beta}{V_c}$
$\frac{\partial f_1}{\partial x_8} = 0$	$\frac{\partial f_2}{\partial x_8} = 0$

f_3	f_4
$\frac{\partial f_3}{\partial x_1} = \frac{\sqrt{2}A\beta C_d}{2V_L\rho\sqrt{\frac{x_{1_o} - x_{3_o}}{\rho}}}$	$\frac{\partial f_4}{\partial x_1} = 0$
$\frac{\partial f_3}{\partial x_2} = 0$	$\frac{\partial f_4}{\partial x_2} = 0$
$\frac{\partial f_3}{\partial x_3} = -\frac{\sqrt{2}A\beta C_d}{2V_L\rho\sqrt{\frac{x_{1_o} - x_{3_o}}{\rho}}}$	$\frac{\partial f_4}{\partial x_3} = 0$
$\frac{\partial f_3}{\partial x_4} = 0$	$\frac{\partial f_4}{\partial x_4} = 0$
$\frac{\partial f_3}{\partial x_5} = 0$	$\frac{\partial f_4}{\partial x_5} = 1$
$\frac{\partial f_3}{\partial x_6} = 0$	$\frac{\partial f_4}{\partial x_6} = 0$
$\frac{\partial f_3}{\partial x_7} = 0$	$\frac{\partial f_4}{\partial x_7} = 0$
$\frac{\partial f_3}{\partial x_8} = -\frac{V_m\beta}{V_L}$	$\frac{\partial f_4}{\partial x_8} = 0$

f_5	f_6
$\frac{\partial f_5}{\partial x_1} = \frac{A_A}{m_{spool}} - \frac{2C_d^2 \cos(\theta)(2K_{SVA} + \pi d x_{4_o})}{C_C m_{spool}}$	$\frac{\partial f_6}{\partial x_1} = 0$
$\frac{\partial f_5}{\partial x_2} = -\frac{2C_d^2 \cos(\theta)(2K_{SVA} + \pi d x_{4_o})}{C_C m_{spool}}$	$\frac{\partial f_6}{\partial x_2} = 0$
$\frac{\partial f_5}{\partial x_3} = -\frac{A_A}{m_{spool}}$	$\frac{\partial f_6}{\partial x_3} = 0$
$\frac{\partial f_5}{\partial x_4} = -\frac{2(\pi d)C_d^2 \cos(\theta)(x_{1_o} - x_{2_o})}{C_C m_{spool}} - \frac{k_{spool}}{m_{spool}}$	$\frac{\partial f_6}{\partial x_4} = 0$
$\frac{\partial f_5}{\partial x_5} = -\frac{K_{SV}}{m_{spool}}$	$\frac{\partial f_6}{\partial x_5} = 0$
$\frac{\partial f_5}{\partial x_6} = 0$	$\frac{\partial f_6}{\partial x_6} = 0$
$\frac{\partial f_5}{\partial x_7} = 0$	$\frac{\partial f_6}{\partial x_7} = 1$
$\frac{\partial f_5}{\partial x_8} = 0$	$\frac{\partial f_6}{\partial x_8} = 0$

f_7	f_8
$\frac{\partial f_7}{\partial x_1} = -\frac{A_1}{(m_1+m_2)} + \frac{C_p}{(m_1+m_2)L}$	$\frac{\partial f_8}{\partial x_1} = 0$
$\frac{\partial f_7}{\partial x_2} = \frac{A_2}{(m_1+m_2)}$	$\frac{\partial f_8}{\partial x_2} = 0$
$\frac{\partial f_7}{\partial x_3} = 0$	$\frac{\partial f_8}{\partial x_3} = \frac{V_m}{J_m}$
$\frac{\partial f_7}{\partial x_4} = 0$	$\frac{\partial f_8}{\partial x_4} = 0$
$\frac{\partial f_7}{\partial x_5} = 0$	$\frac{\partial f_8}{\partial x_5} = 0$
$\frac{\partial f_7}{\partial x_6} = -\frac{k_1}{(m_1+m_2)} + \frac{C_i}{(m_1+m_2)\left(L^2\left(\frac{\left(x_{6_o}-y_{max}\right)^2}{L^2}+1\right)\right)}$	$\frac{\partial f_8}{\partial x_6} = 0$
$\frac{\partial f_7}{\partial x_7} = -\frac{K_{AG}}{(m_1+m_2)}$	$\frac{\partial f_8}{\partial x_7} = 0$
$\frac{\partial f_7}{\partial x_8} = 0$	$\frac{\partial f_8}{\partial x_8} = -\frac{b_m}{J_m}$

x_{1_o}	$1.2307\ x\ 10^7\ Pascals$
x_{2_o}	$1.1879\ x\ 10^6\ Pascals$
x_{3_o}	$1.0086\ x\ 10^7\ Pascals$
$x_{4_o}\ (x_{null} = -5.6944\ x\ 10^{-4}\ m)$	$-5.3267\ x\ 10^{-4}\ meters$
x_{5_o}	$-2.2630\ x\ 10^{-9}\ meters/sec$
x_{6_o}	$1.1866\ x\ 10^{-2}\ meters$
x_{7_o}	$-2.3402x10^{-8} meters/sec$
x_{8_o}	$33.619\ rad/sec$

APPENDIX C: MODEL SIMULATION VALUES (NOT USED FOR MODEL VALIDATION SIMULATIONS)

Model Parameter	***Numerical Value***	***Unit (Metric)***
Spool Valve Diameter	0.007	m
Spring Rate for Bias Spring	4,671.5	N/m
Spring Rate for PDFCV Spring	16,800	N/m
Control Actuator Diameter	0.02965	m
Bias Actuator Diameter	0.01398	m
Piston /Slipper Area	4.15×10^{-4}	m^2
Piston Pitch Radius	0.0469	m
PDFCV Mass	0.005	kg
Control Actuator Mass	0.3452	kg
Bias Actuator Mass	0.1452	kg
Piston Mass	0.1605	kg
Pump Speed	1800 (188.49)	rpm (rad/s)
Moment Arm Distance for Actuator	.087	m
Maximum Swash plate Angle	16.83 (0.2937)	deg (rad)
Number of Pistons within pump	9	
Fluid Bulk Modulus (Oil)	4×10^{8}	Pa
Fluid Density (Oil)	850	kg/m^3
Pump Discharge Pressure Volume	0.01	m^3
Control Pressure Discharge Volume	0.0005	m^3
Pressure Carryover Angle	20 (0.3491)	deg (rad)
FCV Area	3.75×10^{-5}	m^2
Discharge Coefficient	0.62	
Contraction Coefficient	0.61	
Jet Angle for Flow Forces	69 (1.2043)	deg (rad)
Pump Volumetric Displacement	1.5915×10^{-5} ($\approx$100)	m^3/rad (cc/rev)
Spool Valve Leakage Area	2.474×10^{-6}	m^2
Actuator Viscous Damping Coeff.	1	N-s/m
PDFCV Viscous Damping Coeff.	1	N-s/m
Desired Margin Pressure	2.1×10^{6}	Pa
Maximum Actuator Displacement	0.0263	m
PDFCV Spring Pre-Load Distance	0.00538	m
Load Pressure Discharge Volume	0.0002	m^3
Motor Volumetric Displacement	5×10^{-5}	m^3/rad
Motor Load Viscous Damping Gain	15	N-m-s
Motor Load Mass Moment of Inertia	1	kg-m^2

APPENDIX D: EXAMPLES OF SIMULINK® MODEL SUBSYSTEMS USED FOR NL MODEL SIMULATIONS

Pump Discharge Pressure Dynamics

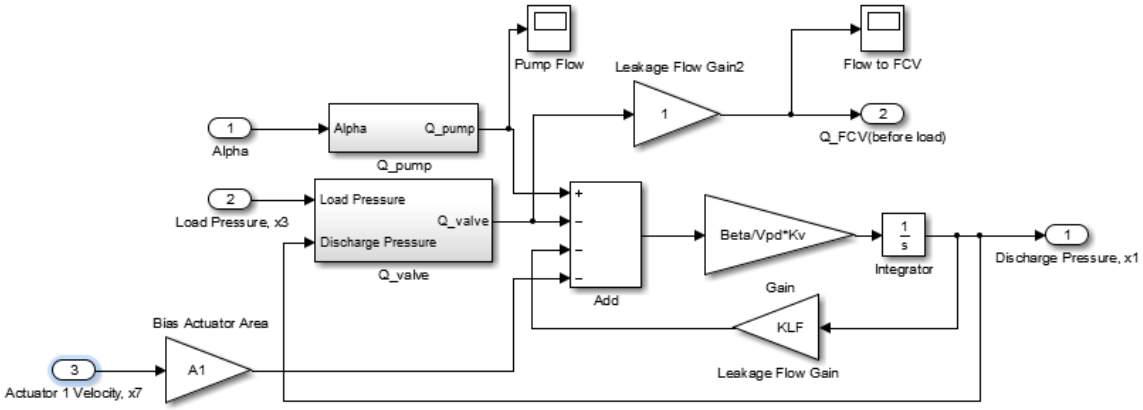

Control Pressure Dynamics

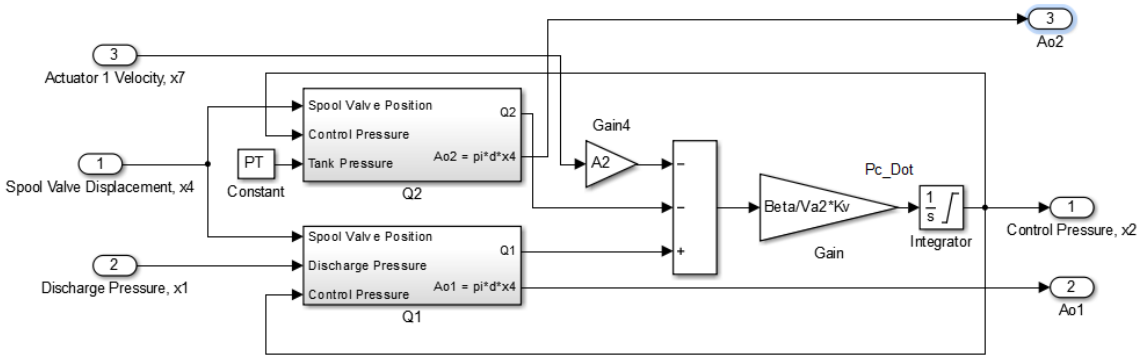

Swash plate/ Actuator System Dynamics

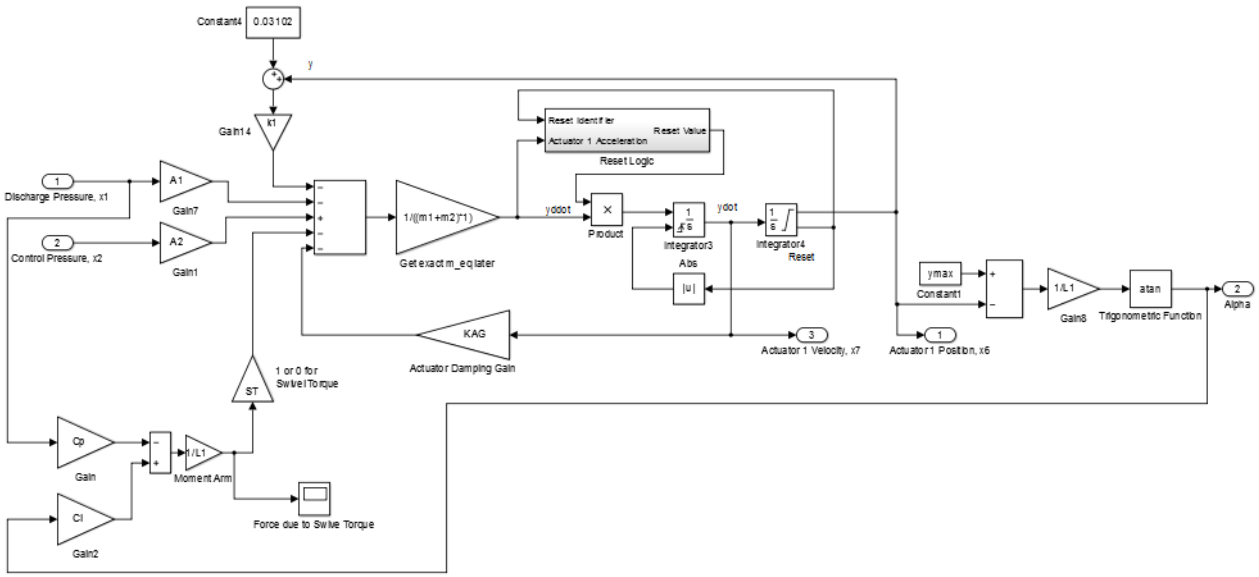

PDFCV Dynamics